Stability of Periodic Surface Gravity Water Waves

Katie Oliveras

A dissertation submitted in partial fulfillment of
the requirements for the degree of

Doctor of Philosophy

University of Washington

2009

Program Authorized to Offer Degree: Applied Mathematics

University of Washington
Graduate School

This is to certify that I have examined this copy of a doctoral dissertation by

Katie Oliveras

and have found that it is complete and satisfactory in all respects,
and that any and all revisions required by the final
examining committee have been made.

Chair of the Supervisory Committee:

_____

Bernard Deconinck

Reading Committee:

_____

Bernard Deconinck

_____

J. Nathan Kutz

_____

Robert E. O'Malley, Jr.

_____

Kristi A. Morgansen

Date: _____

In presenting this dissertation in partial fulfillment of the requirements for the doctoral degree at the University of Washington, I agree that the Library shall make its copies freely available for inspection. I further agree that extensive copying of this dissertation is allowable only for scholarly purposes, consistent with "fair use" as prescribed in the U.S. Copyright Law. Requests for copying or reproduction of this dissertation may be referred to Proquest Information and Learning, 300 North Zeeb Road, Ann Arbor, MI 48106-1346, 1-800-521-0600, to whom the author has granted "the right to reproduce and sell (a) copies of the manuscript in microform and/or (b) printed copies of the manuscript made from microform."

Signature_____

Date_____

University of Washington

Abstract

Stability of Periodic Surface Gravity Water Waves

Katie Oliveras

Chair of the Supervisory Committee:
Professor Bernard Deconinck
Applied Mathematics

Euler's equations describe the dynamics of gravity waves on the surface of an ideal fluid with arbitrary depth. In this dissertation, we discuss the stability of traveling wave solutions to the full set of nonlinear equations via a non-local formulation of the water wave problem in two-dimensions. We demonstrate that this new non-local formulation is equivalent to the original formulation of Euler's equations using an extension of the results of Ablowitz and Haut. Transforming the non-local formulation into a traveling coordinate frame, we obtain a new equation for the stationary solutions in the traveling reference frame as a single equation for the surface in physical coordinates. Using this new equation, we develop a numerical scheme to determine traveling wave solutions by exploiting the bifurcation structure of the non-trivial periodic solutions. Finally, we numerically determine the spectral stability for the periodic traveling wave solution by extending Fourier-Floquet analysis to apply to the non-local problem. The full spectra for various traveling wave solutions is generated. In addition to recovering past well-known results such as the Benjamin-Feir instability for deep water, the presence of high-frequency instabilities in shallow water is confirmed. Additionally, new instability regions are found that appear unpublished in the literature.

Table of Contents

List of Figures

List of Tables

Acknowledgments

There have been several people that have helped me through my time in graduate school and without their support, I would have not completed this dissertation. Foremost, I must thank my advisor, Bernard Deconinck who consistently gave me guidance and encouragement throughout the whole process. I am also grateful to my committee members for their feedback regarding the content and organization of this dissertation. Outside of faculty support, I must thank all of my friends that I have made during my time in graduate school. Without the laughter, I would have probably been a bit grumpier and not have gotten anything done! And finally, I must thank Jeremy Caney. He has put up with me throughout my time in graduate school, and all of the while has been very supportive.

Dedication

To everyone who believed in me even when I did not.

Chapter 1

Introduction

Euler's equations for fluid motion are a set of nonlinear partial differential equations of order two that describe surface gravity and capillary waves of an ideal fluid with arbitrary depth. A large class of commonly used mathematical models for ocean waves have been derived from these equations as approximations; examples include the Korteweg–de–Vries equation (in the case of shallow water) and the Nonlinear Schrödinger equation (in the case of deep water). While we can analytically determine solutions to some of the approximate equations, analytical solutions to the original Euler's equations are unknown. Thus we rely on alternative methods to determine information about the qualitative behavior of solutions to the full equations such as stability analysis of stationary solutions. The goal of this dissertation is to numerically determine solutions to Euler's equations using a new non-local formulation and to investigate their stability.

1.1 History

The quest for a mathematical description of surface waves has a rich history that dates back to the 17th century when Newton first derived a relationship between the frequency and "breath" of a wave on deep water [19]. Approximately seventy years later, the governing equations of motion for an ideal fluid were derived by Euler [19]. In this section we give a brief historical account of the equations of motion, their solutions, and stability.

In 1847 G.G. Stokes [56] published his theory on oscillatory surface waves in deep water in an attempt to determine if waves of permanent form, as observed by Russell, were supported by the mathematical theory. Several years earlier, Russell had published a series of wave observations in various bodies of water. One of his observations was a single solitary wave traveling with an unchanging shape in a canal at constant speed. This observation seemed impossible to the fluids

community at the time, and generally, the existence of a solution that remained of a permanent shape was dismissed.

To investigate this phenomena, Stokes introduced a power series expansion for the surface elevation as a function of the wave amplitude. Stokes' series solution for the surface elevation demonstrated that permanent periodic solutions could exist in terms of the theory, but not as a single wave. In other words, the conclusion from Stokes was that these stationary solutions do exist, but not as a single wave with a single frequency; instead, the solutions are a sum of infinitely many periodic waves with different frequencies[1]. Additionally, Stokes showed that as the amplitude of the solution becomes larger, the solutions become more elliptic until they form crests at a 120^o angle, corresponding to a maximal wave height.

The convergence of the series representation was the cause of much discussion and research for the following 70 years. It was not until the 1920s that the question of existence and convergence of these series solution was answered. Nekrasov in 1921 [44] and Levi-Civita [33] in 1925 independently proved the existence of Stokes' wave solutions and the convergence of the series representation by mapping the problem from the unknown physical domain to a fixed domain in the complex plane. Struik [57] extended these results to the case of finite depth using the same methods. According to Stoker in the 1950s, [55] these proofs of the existence of periodic traveling waves were the only progress made towards solving or determining solutions to Euler's equations for surface waves to that point.

Due to the complicated nature of the equations of interest, researchers turned to experimentation and perturbation analysis to determine the general behavior of these traveling wave solutions. During the next forty years, the question of stability of these Stokes' waves remained unexamined. In fact, no researchers until the 1960s had even "suspected ... that [their] equilibrium ... is in fact unstable" [6,28]. According to a historical account given in [28], by the 1960s, researchers had already conducted several experiments in the wave tank on interactions between waves of different frequencies and wave lengths. Furthermore, some of these experiments demonstrated that finite-amplitude pure oscillations would break down into higher and lower harmonics [28]. These experiments raised the question: *is there some perturbation of a periodic wave with another periodic wave that could result in the growth of such harmonics? If so, would the growth rate of the harmonics be exponential?*

The most celebrated answers to this question came independently from Benjamin and Feir [6, 7] and Whitham [61]. However, the experiments and analysis leading up to the discovery of what is now known as the Benjamin-Feir instability began several years earlier. In 1963, according to a historical account given by Hunt [28], Benjamin and his research student Feir were conducting experiments in the new wave tank in Cambridge's engineering department, when they noticed a peculiar phenomena. What started out as a regular train of periodic waves near the wave maker with constant frequency and wavelength began to form into groups of waves with different frequencies and wave-lengths.

[1]The conclusion drawn by Stokes is incorrect since he only considered periodic solutions to Euler's equations. There are indeed solitary wave solutions to Euler's equations. For a summary of results, see [55]

Their experiments showed that there was an exponentially growing amplitude modulation. Another interesting observation was that the exponential growth ceased at certain values of the wave slope. Originally, they suspected a problem with the experimental apparatus. However, they soon replicated their results at the National Physics Lab near London [28].

It was at this time that Benjamin examined the Fourier mode expansion of Stokes' wave solutions perturbed by two sidebands. With this perturbation analysis, Benjamin [6] determined that for waves with the minimal period of 2π and dimensionless depth $kh > 1.363$, periodic waves are unstable.

Additionally, Benjamin found relationships between the uniform wave train with amplitude a_0, wave number k_0 and frequency ω_0 corresponding to stability and instability of waves to certain classes of perturbations. In the same year these results were published, Whitham independently produced the same result using averaged Lagrangians [61]. A detailed explanation of this derivation can be found in Whitham's book [62].

This new insight (that periodic waves are indeed modulationally unstable) led to the question of how these instabilities played out over long propagation times. All analysis until this point was only valid for the initial transient growth rates. As summarized in [65], over the next five years, numerous researchers worked to answer the question of how the modulational perturbations would behave over time. Using various methods, researchers agreed that the approximate equations describing the evolution of wave-trains on deep water was the Nonlinear Schrödinger equation for the complex wave-train envelope $A(x,t) = a(x,t)e^{i\theta(x,t)}$ where

$$i\left(A_t + \frac{\omega_0}{2k_0}A_x\right) - \frac{\omega_0}{8k_0^2}A_{xx} - \frac{1}{2}\omega_0 k_0^2|A|^2 A = 0, \tag{1.1}$$

and $\theta_t = \omega_0 - \omega$, $\theta_x = k - k_0$ and the free surface elevation $\eta(x,t)$ is given by

$$\eta(x,t) = \mathcal{R}\left(Ae^{i(k_0 x - \omega_0 t)}\right),$$

which is the one-dimensional version of the equation presented by Zakharov in 1968 [66]. While use of the Nonlinear Schrödinger (NLS) equation as an approximation to phenomena in deep water did not answer all of the questions regarding the long time behavior of solutions, it did support experimental evidence that the unstable modulations grew to a maximum and then abated. Furthermore, experimental and numerical evidence seems to suggest that, without dissipation, there were no steady-state solutions. Instead, a series of modulation and demodulation cycles occur, also known as the Fermi-Pasta-Ulam recurrence phenomenon [65].

Simultaneous to the investigation of stability, Zakharov had shown that the Euler equations for surface gravity waves are Hamiltonian [66]. Though the Hamiltonian contained a complicated term which required the integration of the velocity potential over an unknown domain, it has since become a basis for a large amount of analytic study of the water wave problem.

The first full numerical analysis of the stability of waves to the fully nonlinear set of equations was conducted by Longuet-Higgins. In 1978, Longuet-Higgins [35, 36] numerically investigated the stability of water waves to the full original set of Euler's equations in two-dimensions. He considered

surface elevation profiles of the form

$$\bar{\eta}(x,t) = \sum_{n=0}^{\infty} A_n \cos\left[nk_0(x-ct)\right],$$

and perturbations of the form $\eta(x,t) = \bar{\eta}(x,t) + \eta_1(x,t)$ where $Z(x,t)$ has the form

$$\eta_1(x,t) = \exp\left[i\left(pk_0(x-ct)\right) + \lambda t\right] \sum_{n=-\infty}^{\infty} a_n \exp\left[ink_0(x-ct)\right] + c.c.\ ,$$

p represents some perturbation parameter, and $c.c.$ represents the complex conjugate expression. As formulated, instability corresponds to $\mathcal{R}(\lambda) > 0$ which, due to the Hamiltonian nature of the system, is the same as saying that $\mathcal{R}(\lambda) \neq 0$. By writing the problem for the spectrum as an eigenvalue problem for λ, Longuet-Higgins calculated the growth rates of Stokes' waves on deep water numerically. Using a limited number of modes in his perturbation, he was able to recover the Benjamin-Feir instability. Additionally, he found new classes of instabilities corresponding to large amplitude waves. Around the same time, Bryant [9,10] investigated the instabilities in shallow water and determined that weakly nonlinear waves in depths below the critical Benjamin-Feir depth were marginally stable. In his approach, Bryant restricted his investigations to a truncated version of Euler's equations.

Throughout the 1980s as computers became more readily available, researches began to investigate numerically the stability of solutions to a broad array of perturbations. McLean [42] extended the results of Longuet-Higgins by investigating three-dimensional instabilities of water waves over finite depth. He considered two-dimensional solutions of the form

$$\bar{\eta}(x,t) = \sum_{n=0}^{\infty} A_n cos\left[nk_0(x-ct)\right],$$

and three-dimensional perturbations of the form $\eta(x,y,t) = \bar{\eta}(x,t) + \eta_1(x,y,t)$ where $Z(x,y,t)$ is given by

$$Z(x,y,t) = \exp\left[i\left(pk_0(x-ct) + qk_0y\right) + \lambda t\right] \sum_{n=-\infty}^{\infty} a_n \exp\left[ink_0(x-ct)\right] + c.c.$$

In the above perturbation, p and q are arbitrary real numbers, and $c.c.$ represents the complex conjugate. In the case where $q = 0$, the problem reduces to the two dimensional problem. For various one-dimensional waves, McLean numerically determined the values of p and q which corresponded to instabilities. McLean showed that the Benjamin-Feir instability (a two-dimensional instability) dominates for small amplitude waves, but as the amplitude of the wave increases, three-dimensional effects are more dominant and they result in larger growth rates. He was able to determine the stability of solutions with amplitude of up to 90% of the maximal wave height predicted by Stokes.

In the mid 1980s the movement of eigenvalues on the imaginary axis was examined. In particular, it was recognized that as the amplitude of the solution increases, the eigenvalues associated with the linearized problem move along the imaginary axis. In 1986, MacKay and Saffman [41] showed that a

necessary condition for the eigenvalues to move off the imaginary axis is for two or more eigenvalues to collide with opposite Krein signatures. Thus if two eigenvalues with opposite Krein signatures collide, an instability could arise.

Within the last fifteen years, there have been a large number of advancements towards understanding solutions of Euler's equations. Perhaps one of the biggest advancements is a reformulation of the Hamiltonian equation given by Craig and Sulem in 1993 [18]. This formulation eliminated the velocity potential integrated over the vertical variable in the formulation given by Zakharov and replaced it with a new operator $G(\eta)$ which we will discuss in more detail later. Additionally, in their formulation, Craig and Sulem demonstrated that this operator could be calculated as a power-series in the surface elevation, and gave a recursive formulation to determine the higher-order coefficients in the power series as a function of the lower order terms. This formulation has been used to numerically investigate the solutions of the water wave problem, as well as to provide a basis for the analytic investigation of solution properties. For example, this new formulation was a basis for the investigation of the existence of solutions [17] as the solution to a Lyapunov-Schmidt reduction.

Additionally, the investigation of the stability of solutions to Euler's equation is still an area of active research. Only in 1995 was there a rigorous proof for the Benjamin-Feir instability given by Bridges and Mielke in [8]. They used the Hamiltonian structure and a center manifold reduction to show that for $h > 1.363$ and for small amplitude solutions, the spectra near the origin developed positive real parts and, thus, the solution was unstable. As recently as 2006, Francius and Kharif made note of the lack of study of the stability of solutions in shallow water [25] and proceeded to begin an investigation of stability of the full equations in shallow water. Specifically, they determined that there was a narrow band of wavelengths to which the solutions in shallow water were unstable. Most recently, Nicholls [46] demonstrated the analytic dependence of the spectrum on the amplitude of the solution about which the problem is linearized. This allows him to determine how individual eigenvalues move in the complex plane as the amplitude of the solution is increased.

Despite the large amount of history discussed in this section, this is by no means a comprehensive summary of results, but more of a sampling of important breakthroughs and methodology. Even with many researchers working on the problem of stability of solutions to Euler's equations over the past 50 years, there are still a large number of questions unanswered.

First, to the best of our knowledge, there have been no publications or results demonstrating the full spectrum associated with the linearized problem[2]. Previous numerical calculations were limited to a small number of Fourier modes and a small class of perturbations. Additionally, for depths smaller than the critical threshold given by Benjamin-Feir and Whitham, there has been little discussion of stability or instability with the exception of the work by Francius and Kharif [25].

---

[2]A recent paper by Nicholls [47] earlier this year presented a method for determining the full spectrum of the linearized water wave problem. His method relies on the analytic dependence of the spectra on the amplitude of the solution. However, the results presented in his paper only demonstrate the location of eigenvalue collisions in the complex plane which is a necessary but not sufficient condition for instability.

1.2 Overview of The Dissertation

As mentioned in the previous section, there has been a large amount of research and investigation into the stability of these traveling wave solutions. This field continues to be an active field of research with many different classes of investigation of stability. The main objective of this dissertation is to continue the investigation of the stability of periodic traveling surface gravity waves by focusing on spectral stability of traveling wave solutions. We consider a broad range of periodic traveling wave solutions for both finite and infinite depth. We determine the associated growth rates corresponding to all bounded two- and three-dimensional perturbations. This dissertation is broken down into three main section; (i) formulation of the equations of motion, (ii) determination of the traveling wave solutions, and (iii) stability analysis of the traveling wave solutions to two- and three- dimensional perturbations.

Chapters 2 and 3 focus on the equations of motion, and discusses a reformulation of the set of partial differential equations describing the surface elevation into a new non-local formulation. Next, we consider the equations of motion in a traveling coordinate frame, and introduce a single equation for the surface elevation that to the best of our knowledge, is completely new. We conclude the discussion of the equation of motion by discussing the existence of solutions to the traveling wave problem in terms of a bifurcation problem. Chapter 4 discusses the new equation for the surface elevation and outlines a method to determine the solutions numerically. We conclude the Chapter by discussing the accuracy of our method and producing plots of surface elevations for various parameter values. The last two chapters are dedicated to determining the stability of the calculated traveling wave solutions. In Chapter 5, we discuss a method for determining the spectra of linear operators with periodic coefficients referred to as Hill's method. We proceed to extend this method for our non-local problem in order to determine the associated growth rates of our traveling wave solution to the class of all bounded perturbations. We conclude chapter 5 by calculating the spectra associated with several traveling wave solutions and discuss the stability or instability of each solution with respect to two-dimensional perturbations. Chapter 6 repeats the analysis with three-dimensional perturbations of the two-dimensional solutions obtained in Chapter 4. Our results are in good general agreement with previous results published in [9, 10, 25, 35, 36, 42]. However, we obtain more accurate results with a faster computation scheme.

Chapter 2

Equations of Motion

In this chapter, we derive Euler's equations for invicid, irrotational fluid flow under the influence of gravity. These equations present a large number of difficulties both analytically and numerically. For completeness, we review several equivalent formulations and discuss the advantages and disadvantages of each. Finally, we conclude with a non-local formulation of the water wave problem due to Ablowitz, Fokas, and Musslimani [1], extended to the case of periodic boundary conditions, and demonstrate their equivalence to the original equations of motion.

2.1 Original Formulation

The equations of motion that we plan to derive in the current section are the equations for a fluid with a free boundary at the surface with periodic boundary conditions. This process will be divided into two main steps. First, we plan to discuss the model for a fluid under the effects of gravity without boundary conditions. Then, we investigate the effects at the boundary of appending appropriate boundary conditions for our model.

2.1.1 Derivation of Euler's Equations without Boundary Conditions

We begin our derivation by starting with our assumption that we are modeling an ideal fluid. An ideal fluid is a fluid that is (i) incompressible, (ii) has constant density, and (iii) exerts no tangential forces across the fluid element boundaries (no viscous forces). While, in practice, ideal fluids do not exist, the effects of compressibility, stratification, and viscosity are typically small enough to justify neglecting them in the final equations.

The derivation for the governing equations can be found in most introductory books on fluid

dynamics [4,21,30,32,54]. Following the formulation given by Shen [54], and Kundu and Cohen [32], let $\mathbf{u}$ be the vector valued function in the (x, z) plane such that $\mathbf{u} = [u \quad w]'$, ρ be the density, p the pressure, and g the force due to gravity. If we consider a fluid element, the equation for conservation of mass and conservation of momentum can be written as follows:

$$\nabla \cdot \mathbf{u} = 0 \tag{2.1}$$

$$\frac{D\mathbf{u}}{Dt} = \mathbf{u}_t + (\mathbf{u} \cdot \nabla)\mathbf{u} = -\frac{1}{\rho}\nabla p - g\mathbf{j}. \tag{2.2}$$

In the above equation, $\mathbf{j}$ is the unit vector in the z direction, so gravity g is only acting in the vertical direction. The above equations are referred to as Euler's equations. The only assumptions that we have made so far is that the fluid is ideal. If we define the vorticity ω as

$$\omega = \nabla \times \mathbf{u},$$

we can rewrite the equation for conservation of momentum as

$$\frac{D}{Dt}\omega = \omega \cdot \mathbf{u}.$$

At this point, we assume that the flow is irrotational[1]. This implies that the velocity field $\mathbf{u}$ satisfies the no-vorticity condition. Since the curl of the velocity potential is zero, there exists a potential ϕ such that $\mathbf{u} = \nabla\phi$ can be substituted into (2.1). This substitution yields the relationship that the velocity potential ϕ must satisfy Laplace's equation

$$\nabla^2\phi = 0.$$

Before we consider the effects at the free surface and other boundaries, we need to define precisely the fluid domain that described by the boundaries. Consider the diagram of the two dimensional water wave problem (one dimensional surface) given in Figure 2.1.

The fluid domain D is defined as the region bounded above by the free surface at $z = \eta(x, t)$, bounded below by the bottom (which we treat as flat), and periodic boundary conditions. Formally, we can define this region as

$$D = \{(x, z) \mid 0 \leq x < L, \ -h < z < \eta(x, t)\}$$

From the above derivation, we know that inside the fluid domain D, the velocity potential ϕ must satisfy Laplace's equation. Additionally, since the flow is irrotational inside the domain D, the equation for conservation of momentum is satisfied automatically and need not be taken into account at this point.

[1]Since our final goal is to investigate the stability of traveling wave solutions, we briefly justify assuming that the flow is irrotational. When solving the stability problem, we can split the perturbation into a rotational and irrotational component. Linearizing about a steady flow, it can be shown that the rotational component does not change in time. In the general case, Colin [14] showed that in the case of long-wave perturbations of general nonlinear waves, the equations governing the stability for the rotational component are indeed the same as the equations governing the stability for the irrotational component. In these cases, the stability does not depend explicitly on the portion of the perturbation due to rotation.

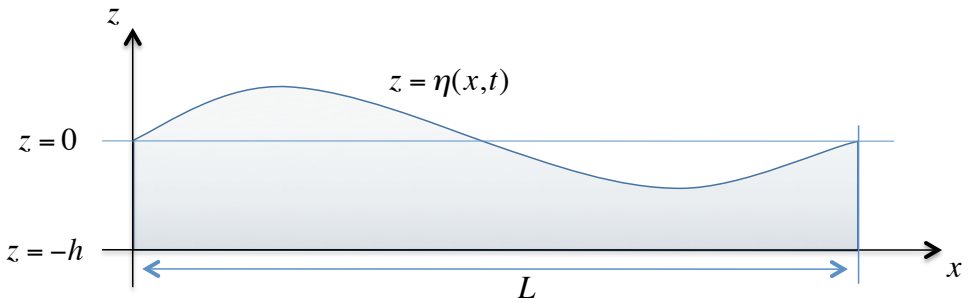

Figure 2.1: Schematic of the water wave problem in two dimensions.

2.1.2 Boundary Conditions

As seen in Figure 2.1, there are three interfaces where we need to define boundary conditions. For periodic surface gravity waves, the three boundaries to be taken into account are:

- periodicity in x,

- effects at the bottom assuming constant bathymetry,

- and effects at the free surface $\eta(x,t)$ which is itself an unknown.

The periodic boundary conditions are simply the conditions that the surface elevation and velocity potential at $x = 0$ are equal to the surface elevation and velocity potential at $x = L$. The condition at the bottom surface, $z = -h$, is that the boundary is impermeable, or $w = 0$ at $z = -h$.

These constraints can be written as

$$\begin{aligned}
&\phi_z = 0 \text{ at } z = -h,\\
&\eta(0,t) = \eta(L,t),\\
&\phi(0,z,t) = \phi(L,z,t).
\end{aligned}$$

Additionally, we require that the derivatives (through second order) at the boundaries are periodic as well. The final boundary conditions are those that are imposed at the free surface $z = \eta(x,t)$. There are two boundary conditions that need to be taken into account at the free surface:

1. *The Dynamic Boundary Condition* - The boundary condition that takes into account the forces acting on the free surface. Typical examples include gravity, surface tension, pressure balance, etc.

- *The Kinematic Boundary Condition* - The condition that particles on the surface remain on the surface.

We now derive the effects of each of the above conditions at the free surface.

The Dynamic Boundary Condition

Using various vector calculus identities, we rewrite the equations for the conservation of momentum inside the fluid domain D as

$$\mathbf{u}_t + \frac{1}{2}\nabla(\mathbf{u}\cdot\mathbf{u}) = -\nabla\left(\int^p \frac{dp}{\rho} + gz\right),$$

where $\mathbf{a}\cdot\mathbf{b}$ is the dot product of two vectors. If we define the quantity $H = \int^p \frac{dp}{\rho} + gz + \frac{1}{2}(\mathbf{u}\cdot\mathbf{u})$, we can rewrite the above equation as

$$\mathbf{u}_t + \nabla H = 0.$$

Using this information, the equations for the conservation of momentum become

$$\nabla(\phi_t + H) = 0 \qquad \longrightarrow \qquad \phi_t + \frac{p}{\rho} + \frac{1}{2}|\nabla\phi|^2 + gz = C(t).$$

Due to the irrotational flow assumption made earlier, we know that this rewriting of the conservation of momentum equation is already valid inside the fluid domain D. We only need to check its' validity at the top surface. Noting that the pressure at the surface is simply a constant $p = p_0$, we can define $C(t)$ (a constant due to integration) to be p_0/ρ. Simplifying yields the dynamic boundary condition at the surface

$$\phi_t + \frac{1}{2}|\nabla\phi|^2 + g\eta = 0 \text{ at } z = \eta(x,t).$$

The Kinematic Boundary Condition

The final boundary condition that we need to derive is the kinematic boundary condition. This condition states that a particle on the surface remains on the surface for all time. To determine this boundary condition, consider the vertical distance from the surface at some point x

$$P(x,z,t) = z - \eta(x,t).$$

For a particle on the surface, we know $(x, z = \eta(x,t))$, $P(x,\eta,t)$ as well as its total derivative[2] are equal to zero. Thus, we know

$$\begin{aligned}\frac{DP}{Dt} &= P_t + \mathbf{u}\cdot\nabla P \\ &= -\eta_t - \phi_x\eta_x + \phi_z.\end{aligned}$$

Evaluating the total derivative at the surface the kinematic boundary condition is simply

$$\eta_t + \phi_x\eta_x = \phi_z \text{ at } z = \eta(x,t). \tag{2.3}$$

[2]The total derivative of a quantity is the derivative of the quantity taken along a path moving with velocity $\mathbf{u}$. This derivative is typically denoted as $\frac{DP}{Dt}$. The statement $\frac{DP}{Dt}$ can be interpreted as the rate of change in time of the distance of some fluid particle from the surface as it moves with the flow.

2.1.3 Equations of Motion

Combining Euler's equations with the boundary conditions for the free surface, bathymetry, and periodicity, we obtain Euler's equations for periodic surface gravity waves:

$$\phi_{xx} + \phi_{zz} = 0, \qquad (x,z) \in D, \tag{2.4}$$

$$\phi_z = 0, \qquad z = -h, \tag{2.5}$$

$$\eta_t + \eta_x \phi_x = \phi_z, \qquad z = \eta(x,z,t), \tag{2.6}$$

$$\phi_t + \frac{1}{2}\left(\phi_x^2 + \phi_z^2\right) + g\eta = 0, \qquad z = \eta(x,t), \tag{2.7}$$

$$\phi(x,z,t) = \phi(x+L,z,t), \qquad \eta(x,t) = \eta(x+L,t), \tag{2.8}$$

where g is the acceleration due to gravity, h is the constant depth of the fluid when at a state of rest, and L is the period in the x direction.

Remark 1. *If we include the effect of surface tension, the equations and derivation remain the same with the addition of a term in the dynamic boundary condition. In this case, (2.7) becomes*

$$\phi_t + \frac{1}{2}\left(\phi_x^2 + \phi_z^2\right) + g\eta = \sigma \frac{\eta_{xx}}{(1+\eta_x^2)^{3/2}}, \qquad z = \eta(x,t),$$

where σ is the coefficient of surface tension.

2.2 Alternative Formulations

One of the major difficulties of investigating Euler's equations is the inclusion of nonlinear boundary conditions defined at the free surface which is an unknown variable in our problem. Therefore, when most researchers approach this problem, they typically use an alternative formulation that eliminates the vertical variable and casts the problem in such a way that there is no need to solve Laplace's equation inside an unknown domain. In this section, we address briefly the various reformulations of Euler's equations and discuss their strengths and weaknesses.

2.2.1 Conformal Mapping

The use of conformal mappings as a method for reformulating Euler's equations for the free-boundary problem has a rich history, and was at the heart of the first analytical progress made towards finding and describing solutions to the fully nonlinear equations. As mentioned in the introduction, after Stokes published his series expansion of the surface elevation in 1847 [56] there was much debate regarding the convergence of the series, and whether or not solutions described by Stokes' series actually existed. It took almost 70 years before progress was made in this area. In 1921 and 1925, Nekrasov [44] and Levi-Civita [33] both proved the existence of periodic traveling wave solutions in infinite depth for a one dimensional surface by using conformal mappings. Several years later, Struik extended this result to finite depth using the same method.

The benefit of using conformal mappings is that the mapping casts the problem from one defined on the unknown domain $D \in \mathbb{R}\times\mathbb{R}$ to one defined in $\mathbb{C}$ on a fixed domain. For Nekrasov, Levi-Civita, and Struik, this reduced the problem to proving the existence of a solution in the complex domain which is much easier. The main advantage of this approach is that in the mapped formulation one can take full advantage of large amount of tools available in complex analysis. However, there are two disadvantages. First, the problem is written in coordinates and boundary conditions that are not physically intuitive. When working with the conformal mapping formulation, it is difficult to grasp the physical interpretation of the equations or any results obtained using the formulation. One would have to invert the conformal mapping to determine the relevance to the physical coordinates. The second disadvantage, and perhaps the most important, is that the formulation cannot be extended to higher dimensions. Thus, any result obtained with this formulation would only be applicable to the one-dimensional surface problem.

2.2.2 Hamiltonian Formulation

In 1968, Zakharov [66] discovered that Euler's equations for the free-boundary problem are Hamiltonian. He defined a new variable $q(x,t)$ that represents the velocity potential at the surface, i.e. $q(x,t) = \phi(x,\eta(x,t),t)$ and showed that the equations of motion could be written as

$$\eta_t = \frac{\delta H}{\delta q}, \tag{2.9}$$

$$q_t = -\frac{\delta H}{\delta \eta}, \tag{2.10}$$

where $\frac{\delta H}{\delta q}$ is the variational derivative of H with respect to q. The Hamiltonian H is given in canonical variables $\eta(x,t)$ and $q(x,t)$ by

$$H = \frac{1}{2}\int_D \Big(\int_{-h}^{\eta(x,t)} |\nabla\phi|^2\, dz + g\eta^2\Big) dx. \tag{2.11}$$

This formulation has an advantage over the conformal mapping formulation in that it is easily extended to higher dimensions. However, the velocity potential throughout the entire fluid is still a part of the equation, and we are required to integrate over the unknown range $[-h,\eta(x,t)]$ in z. Nevertheless, the discovery of the Hamiltonian structure was a huge breakthrough in the area of nonlinear waves, and has been the basis of much study.

2.2.3 Dirichlet-to-Neumann Formulation

In 1993, Craig and Sulem [18] determined that the integral term $\int_{-h}^{\eta(x,t)} |\nabla\phi|^2\, dz$ in Zakharov's Hamiltonian formulation could be simplified by introducing a Dirichlet-to-Neumann operator (DNO) $G(\eta)$ which represents the normal derivative of the velocity potential calculated at the surface by realizing that the integral was simply a map of Dirichlet data to Neumann data. In other words, we can define the operator $G(\eta)$ acting on the velocity potential ϕ at the surface by the normal

derivative of the velocity potential at the surface

$$G(\eta)\phi = \frac{\partial \phi}{\partial z} - \eta_x \frac{\partial \phi}{\partial x} \text{ at } z = \eta.$$

If we let $\phi = \cosh(k(z+h))\, e^{ikx}$, then ϕ is a solution to Laplace's equation, which also satisfies the boundary condition at the bottom surface, and the periodic boundary conditions imposed at $x = 0$ and $x = L$[3]. Substituting ϕ into the expression for the normal derivative and expanding both sides as a Taylor series in η, Craig and Sulem showed that the operator $G(\eta)$ could be expressed as a power series in the surface elevation η for small amplitude solutions $G(\eta) = \sum_l G^{(l)}(\eta)$ where $G^{(l)}(\eta)$ is of order l in η. Additionally $G^{(l)}(\eta)$ can be calculated recursively in terms of $G^{(j)}(\eta)$ for $j = 0, \ldots, l-1$ with $G^{(0)}(\eta) = -i\partial_x \tanh(-ih\partial_x)$ which makes the operator $G(\eta)$ easy to calculate numerically. Substituting this form into the Hamiltonian formulation given by Zakharov, Craig and Sulem obtained a new Hamiltonian formulation with Hamiltonian

$$H = \frac{1}{2}\int_D \left(qG(\eta)q + g\eta^2\right)dx, \tag{2.12}$$

which eliminates the vertical variable completely from the Hamiltonian formulation. With this new Hamiltonian, the corresponding equations of motion become

$$\eta_t = G(\eta)q, \tag{2.13}$$

$$q_t + \tfrac{1}{2}q_x^2 + g\eta - \frac{1}{2}\frac{\left(G(\eta)q + q_x\eta_x\right)^2}{1+\eta_x^2} = 0. \tag{2.14}$$

This formulation addresses all the problems that we have encountered so far with any formulation of Euler's equations. It eliminates the vertical variable from the formulation, is written directly in physically intuitive coordinates, and the formulation can easily be extended to higher dimensions. The only disadvantage of this formulation is that the convergence of the series expansion of the operator $G(\eta)$ depends on the amplitude of the solution.

2.3 Non-local Formulation

In the previous section, we discussed various formulations of the water-wave problem and discussed some of the advantages and disadvantages of each. We conclude this chapter with an examination of a new nonlocal formulation for periodic waves which is an extension of the formulation due to Ablowitz, Fokas, and Musslimani (AFM) [1]. Some of the benefits of this formulation are:

- The vertical variable is completely eliminated from the formulation.

- The equations are presented in the same canonical variables as the Hamiltonian and Dirichlet-to-Neumann operator (DNO) formulation.

---

[3]The periodic boundary conditions imply that $k = \frac{2n\pi}{L}$ for all $n \in \mathbb{Z}$.

- The equations are valid for both one and two dimensional surfaces (two and three spatial variables).

- The equations do not rely on a small amplitude assumption.

We proceed to derive the non-local description for the periodic problem following the formulation of AFM starting from the original equations of motion given in equations 2.4 - 2.7. The derivation is broken down into two parts; (i) derivation of a local equation and (ii) derivation of an integro-differential equation.

2.3.1 Local Equation

Let $q(x,t)$ represent the velocity potential at the surface $\eta(x,t)$

$$q(x,t) = \phi(x, \eta(x,t), t).$$

This the same canonical variable used by Zakharov. By using the chain rule, we can represent the velocity potential at the surface in terms of the canonical variables η and q. First, we calculate the derivative of the potential at the surface:

$$q_x = \phi_x + \phi_z \eta_x.$$

Combining the above with equation (2.6), we have

$$\phi_z = \eta_t + \eta_x \left(q_x - \phi_z \eta_x\right)$$

This allows us to solve directly for ϕ_x, ϕ_z, and ϕ_t in terms of η and q

$$\phi_x = \frac{q_x - \eta_x \eta_t}{1+\eta_x^2}, \qquad \phi_z = \frac{\eta_t + \eta_x q_x}{1+\eta_x^2}, \qquad \phi_t = q_t - \frac{\eta_t\left(\eta_t + \eta_x q_x\right)}{1+\eta_x^2}. \tag{2.15}$$

By substituting the resulting expressions into the dynamic boundary conditions equation (2.7), we reduce (2.6)-(2.7) to a single equation given by:

$$q_t + \frac{1}{2}q_x^2 + g\eta - \frac{1}{2}\frac{\left(\eta_t + q_x\eta_x\right)^2}{1+\eta_x^2} = 0.$$

This is one equation for two unknowns $q(x,t)$ and $\eta(x,t)$ that is completely free of the vertical variable.

Remark 2. *When the effects of surface tension are included, the local equation becomes*

$$q_t + \frac{1}{2}q_x^2 + g\eta - \frac{1}{2}\cdot\frac{\left(\eta_t + q_x\eta_x\right)^2}{1+\eta_x^2} = \sigma\frac{\eta_{xx}}{(1+\eta_x^2)^{3/2}}.$$

2.3.2 Non-local Equation

To determine a second equation, we consider two separate periodic harmonic functions $\phi(x,z,t)$ and $\psi(x,z,t)$ in the domain of the fluid such that

$$\phi(x,z,t) = \phi(x+L,z,t), \qquad \psi(x,z,t) = \psi(x+L,z,t).$$

Since both functions are harmonic, they satisfy Laplace's equation:

$$\phi_{xx} + \phi_{zz} = 0, \qquad \psi_{xx} + \psi_{zz} = 0,$$

and can be combined in the following way to create the identity

$$\phi_z\left(\psi_{xx} + \psi_{zz}\right) + \psi_z\left(\phi_{xx} + \phi_{zz}\right) = 0.$$

This identity is rewritten as

$$\left(\phi_z\psi_x + \psi_z\phi_x\right)_x + \left(\phi_z\psi_z - \phi_x\psi_x\right)_z = 0. \tag{2.16}$$

Let $\psi(x,z,t) = \exp\left[i(k_x x) + k_z z\right]$ where, in order to maintain the periodic boundary conditions and consistency with Laplace's equation, we have

$$k_x = \frac{2n\pi}{L}, \quad k_x = \pm k_z.$$

Thus, (2.16) becomes

$$\left(\phi_z k_x\psi + k_z\psi\phi_x\right)_x + \left(k_z\phi\psi_z - k_x\phi_x\psi\right)_z = 0.$$

Since this equation holds for all x, z inside the fluid domain D, we can integrate both sides of the above equation over the entire fluid domain D.

$$\int_D \left(ik_z\phi_z\psi + k_z\psi\phi_x\right)_x + \left(k_z\phi\psi_z - ik_x\phi_x\psi\right)_z dA = 0.$$

Using Stokes' Theorem, we can replace the integral over the interior of the domain with an integral along the boundary of the domain:

$$\int_{\partial D} \psi\big(\left(k_z\phi_y - ik_x\phi_x\right)dx - \left(ik_x\phi_y + k_z\phi_x\right)dz\big) = 0.$$

By transforming our integral from one over the domain D to one along the boundary ∂D, we can use the boundary conditions to simplify the integrand. With the aid of Figure 2.2 we calculate the integrals along the four main path segments labeled I - IV, oriented in a positive (counter-clockwise) direction.

The various integrals are

- **Path I**

$$\int_0^L e^{ik_x x - k_z h}\left(ik_x\ \phi_x|_{z=-h}\right)dx,$$

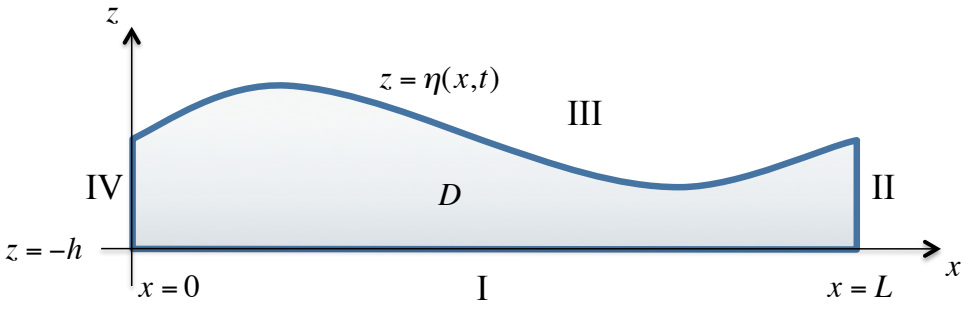

Figure 2.2: Indication of the various path integrals

- **Path II**

$$\int_{-h}^{\eta(L,t)} e^{ik_x L + k_z z} \left(ik_x \phi_z + k_z \phi_x\right) dy,$$

- **Path III**

$$\int_{L}^{0} e^{ik_x x - k_z \eta} \left(ik_x \phi_x - k_z \phi_z + ik\phi_z \eta_x + k_z \phi_z \eta_x\right) dx,$$

- **Path IV**

$$\int_{\eta(0,t)}^{-h} e^{k_z y} \left(ik_x \phi_z + k_z \phi_x\right) dz.$$

Using the relationships given in (2.15), and the periodicity of $\eta(x,t)$ and $q(x,t)$, we can add the integrals calculated along paths I-IV to obtain an expression for the total integral along the boundary of the fluid domain:

$$\int_0^L e^{ik_x x} \left(ie^{-k_z h} k_x \ \phi_x|_{z=-h} + e^{k_z \eta} \left(-k_z \eta_t + ik_x q_x\right)\right) dx = 0$$

Remark 3. *It is important to note that the above equation is identically satisfied with* $k_x = 0$.

We have not completely eliminated the vertical variable from this equation. However, we do know that the above equation is valid for $k_z = k_x$ and $k_z = -k_x$. This allows us to subtract the equations resulting from each case, and simplify to obtain a single equations eliminating the velocity at the bottom of the surface. Let $k = k_x$ and let Λ represent the dual lattice. Thus, $\Lambda = \{\frac{2n\pi}{L} \| n \in \mathbb{Z} - \{0\}\}$. For the case of finite depth, the resulting equation becomes

$$\int_0^L e^{-ikx} \Big(\eta_t \cosh(k(h+\eta)) - iq_x \sinh(k(h+\eta))\Big) dx = 0, \quad \forall k \in \Lambda \tag{2.17}$$

Remark 4. *We refer to the above equation as the non-local spectral equation in the AFM formulation. We call this the spectral representation because of its similarity to the calculation of a Fourier coefficient. This equation is defined over k space. At times, we will want an equation defined over x. We can multiply the non-local spectral equation by e^{ikx} and sum over all $k \in \Lambda$. Doing this, we obtain what we refer to as the nonlocal equation*

$$\sum_{k\in\Lambda} e^{ikx} \int_0^L e^{-ikx}\Big(\eta_t \cosh(k(h+\eta)) - iq_x \sinh(k(h+\eta))\Big)dx = 0.$$

Remark 5. *While the above equation assume finite depth, we can consider the deep water limit $h \to \infty$. Taking limits appropriately, we obtain the following non-local equation for the case of infinite depth: In the case of infinite depth ($h \to \infty$), the non-local spectral equation is:*

$$\int_0^L e^{-ikx} e^{|k|\eta} \left(\eta_t - i\ sign(k) q_x\right) dx = 0, \quad \forall k \in \Lambda, \tag{2.18}$$

and similarly, the non-local equation is

$$\sum_{k\in\Lambda} e^{ikx} \int_0^L e^{-ikx} e^{|k|\eta} \left(\eta_t - i\ sign(k) q_x\right) dx = 0, \quad \forall k \in \Lambda, \tag{2.19}$$

2.4 Equivalence of Formulations

One of the first questions one should ask when examining this new nonlocal formulation is whether or not the nonlocal equations are equivalence to the traditional formulation. It is obvious that a solution to the original formulation solves the new nonlocal formulation. However, along the way, we did several operations that might break the equivalence and thus solutions to the AFM formulation might not solve the original equations. In the following section, we determine the equivalence of the two formulations by examining the dual problem as defined by the adjoint. By showing that the dual formulation is related to the DNO formulation discussed earlier, we conclude that solutions to the periodic form of AFM are indeed solutions to the DNO formulation, and thus, to the full water wave problem. This question has already been answered for the case of the full line by Ablowitz and Haut [2]. Following their formulation and by adding an explicit proof of invertibility, we proceed to extend their results explicitly for the periodic case.

2.4.1 Preliminaries

We begin by comparing the DNO and AFM formulations. Both formulations have the same equation for the time evolution of the velocity potential at the surface. This means that the problem of demonstrating equivalence is reduced to showing that there is an equivalence between the AFM non-local equation and the time-evolution of the surface as given in the DNO formulation.

Following the work and notation of Ablowitz and Haut, we rewrite the non-local equation as given by AFM in operator form

$$A(\eta)\eta_t = B(\eta)q,$$

where

$$A(\eta)g = \sum_{k\in\Lambda} e^{ikx}\int_0^L e^{-ikx}\cosh(k(h+\eta))g dx, \tag{2.20}$$

$$B(\eta)g = i\sum_{k\in\Lambda} e^{ikx}\int_0^L e^{-ikx}\sinh(k(h+\eta))\partial_x g dx. \tag{2.21}$$

Adjoint Formulation

We use the standard definition of the inner-product over the space of square integrable L-periodic functions

$$\langle f, g\rangle = \int_0^L \bar{f} g dx,$$

to determine the adjoint of our operators $A(\eta)$ and $B(\eta)$ where $(\bar{f})$ is the complex-conjugate of the function f.

The adjoint of the operator $A(\eta)$ is determined by the following calculation

$$\begin{aligned}
< f, A(\eta)g > &= \int_0^L \bar{f}(x)\sum_{k\in\Lambda} e^{ikx}\int_0^L e^{-iky}\left(g(y)\cosh(k(h+\eta))\right)dydx \\
&= \sum_{k\in\Lambda}\int_0^L e^{-iky}\left(g(y)\cosh(k(h+\eta))\right)dy\int_0^L \bar{f}(x)e^{ikx}dx \\
&= \sum_{k\in\Lambda}\bar{\hat{f}}_k\int_0^L e^{-iky}\left(g(y)\cosh(k(h+\eta))\right)dy \\
&= \int_0^L g(x)\sum_{k\in\Lambda}\bar{\hat{f}}_k e^{-ikx}\cosh(k(h+\eta))dx \\
&= \overline{\int_0^L \bar{g}(x)\sum_{k\in\Lambda}\hat{f}_k e^{ikx}\cosh(k(h+\eta))dx} \\
&= \overline{\langle g, A^\dagger(\eta)f\rangle}.
\end{aligned}$$

Thus, we have found the adjoint of $A(\eta)$ defined as

$$A^\dagger(\eta)f = \sum_{k\in\Lambda}\hat{f}_k e^{ikx}\cosh(k(h+\eta)). \tag{2.22}$$

Likewise, for the operator $B(\eta)$ we have

$$
\begin{aligned}
< f, B(\eta)g > &= i\int_0^L \bar{f}(x)\sum_{k\in\Lambda} e^{ikx}\int_0^L e^{-iky}\left(g_y\sinh(k(h+\eta))\right)dydx \\
&= \sum_{k\in\Lambda}\int_0^L e^{-iky}\left(g(y)k\left(-i\sinh(k(h+\eta))+\eta_x\cosh(k(h+\eta))\right)\right)dy\int_0^L \bar{f}(x)e^{ikx}dx \\
&= \sum_{k\in\Lambda}\bar{\hat{f}}_k\int_0^L \left(g(y)k\left(-i\sinh(k(h+\eta))+\eta_x\cosh(k(h+\eta))\right)\right)dy \\
&= \int_0^L g(x)\sum_{k\in\Lambda}\bar{\hat{f}}_k e^{-ikx}k\left(-i\sinh(k(h+\eta))+\eta_x\cosh(k(h+\eta))\right)dx \\
&= \overline{\int_0^L \bar{g}(x)\sum_{k\in\Lambda}\hat{f}_k e^{ikx}k\left(-i\sinh(k(h+\eta))+\eta_x\cosh(k(h+\eta))\right)dx} \\
&= \overline{\langle g, B^\dagger(\eta)f\rangle}.
\end{aligned}
$$

Thus, we have found the adjoint of $B(\eta)$ defined as

$$
\begin{aligned}
B^\dagger(\eta)f &= \sum_{k\in\Lambda} k\left(i\sinh(k(h+\eta))+\eta_x\cosh(k(h+\eta))\right)\hat{f}_k e^{ikx} \\
&= \partial_x\sum_{k\in\Lambda} e^{ikx}\sinh(k(\eta+h))\hat{f}_k. \qquad (2.23)
\end{aligned}
$$

Dual Formulation

In preparation for the proof of the equivalence of the two formulations, it is useful to introduce a dual formulation of the equations. We plan on taking the adjoint of the non-local equation, and showing a similarity to the DNO formulation.

To begin, we consider the DNO and AFM formulation simultaneously:

$$\eta_t = G(\eta)q \qquad\qquad A(\eta)\eta_t = B(\eta)q.$$

Applying the operator $A(\eta)$ to both sides of the DNO formulation yields:

$$A(\eta)\eta_t = A(\eta)G(\eta)q \longrightarrow B(\eta)q = A(\eta)G(\eta)q.$$

If we can show that that $B(\eta) = A(\eta)G(\eta)$, then we can demonstrate equivalence of the two formulations. Taking the adjoint of the above equation, and noting that the operator $G(\eta)$ as defined by Craig and Sulem [18] is self-adjoint, yields

$$G^\dagger(\eta)A^\dagger(\eta) = B^\dagger(\eta) \rightarrow G(\eta)A^\dagger(\eta) = B^\dagger(\eta).$$

Now, we rephrase the statement of equivalence: *Can we find a function $\xi(x,t)$ such that $A^\dagger(\eta)\xi(x,t) = q(x,t)$. If so, we then have*

$$\eta_t = G(\eta)q = G(\eta)A^\dagger(\eta)\xi = B^\dagger(\eta)\xi,$$

or in other words, we have the dual formulation

$$\eta_t = B^\dagger(\eta)\xi,$$

subject to ξ satisfying $A^\dagger(\eta)\xi(x,t) = q(x,t)$. This problem can be addressed by proving the invertibility of the operator $A^\dagger(\eta)$. If $A^\dagger(\eta)$ is invertible, then it is possible to find a function ξ such that $A^\dagger(\eta)\xi(x,t) = q(x,t)$ is satisfied.

Invertibility of the $A^\dagger(\eta)$ operator

As mentioned earlier, if the operator $A^\dagger(\eta)$ is invertible, we can proceed to show that the two formulations are equivalent. For the whole line, the invertibility of the operator $A(\eta)$ was shown to be invertible by Craig *et. al* [16].

Proposition 1. *The inverse $C(\eta)$ of the operator $A^\dagger(\eta)$ is well-defined.*

Proof. Modifying Craig's proof, we reformulate the problem of determining the invertibility of the operator $A^\dagger(\eta)$ by considering the following problem for $w(x,z)$

$$\nabla^2 w = 0, \qquad (x,z) \in D, \tag{2.24}$$

$$w_z = 0, \qquad z = -h, \tag{2.25}$$

$$w = p(x), \qquad z = \eta, \tag{2.26}$$

$$w(0,x) = w(L,x), \tag{2.27}$$

where $p(x)$ is a known arbitrary periodic function with period L. Without loss of generality, assume that $L = 2\pi$.

We begin by considering Laplace's equation for the function $w(x,z)$, and represent $w(x,z)$ by a Fourier series $w(x,z) = \sum_k e^{ikx}\hat{w}_k$ where

$$\hat{w}_k = \hat{w}_k(k,y) = \int_0^{2\pi} e^{ikx} w(k)dk.$$

Substituting this into Laplace's equation results in the need to solve

$$k^2\hat{w}_k = \hat{w}_{k,zz} \qquad \hat{w}_{k,z}(x,-h) = 0.$$

This equation has the solution $\hat{w}_k = \xi_k \cosh(k(z+h))$ and thus, $w(x,z) = \sum_k e^{ikx}\xi_k \cosh(k(z+h))$. Checking the final boundary condition at $z = \eta$, we have

$$p(x) = \sum_k e^{ikx}\xi_k \cosh(k(\eta+h))$$

which can be rewritten as $p(x) = A(\eta)\xi(x)$. This demonstrates that proving the existence and uniqueness of a solution to the above potential problem is equivalent to demonstrating that the inverse of the operator $A(\eta)$ is well-defined.

We can prescribe arbitrary boundary conditions at $x = 0$ and $x = 2\pi$ in the form $w(0, z) = w(2\pi, z) = g(z)$ such that $g_z(-h) = 0$ and $g(\eta) = p(0) = p(2\pi)$. In other words, we choose boundary conditions at $x = 0$ and $x = L$ such that the function value along the boundary of the domain is continuous. Thus, we have a problem of the form

$$w_{xx} + w_{zz} = 0, \qquad w = r \text{ for } (x, z) \in \partial D,$$

where r is a continuous function defined along the boundary and D is the domain of our problem. We know from the min-max principle, there is at most one solution to the problem [24]. Thus, if we can show that a solutions exists, we are guaranteed uniqueness. Since the domain is simply connected and bounded, there exists a solution $w(x, z)$. Thus there is a unique solution $w(x, z)$ for our problem (for complete reference, see Chapters 6 and 7 of [24]). This implies that our operator $A^\dagger$ is invertible. □

2.4.2 Equivalence Statements

Now that we have established that the operator $A^\dagger(\eta)$ is invertible, we proceed to demonstrate that the DNO and AFM formulations are equivalent.

Theorem 1. *The AFM and DNO formulations of the water-wave problem over a periodic domain are equivalent and thus, a solution of one formulation is a solution to the other.*

Proof. It is obvious that solutions to Euler's equations in the original formulation are indeed solutions to the AFM formulation. We now prove the converse of this statement by making use of the DNO formulation. Specifically, re-write the DNO formulation as

$$\eta_t = G(\eta)q, \tag{2.28}$$

$$q_t + \frac{1}{2}q_x^2 + g\eta - \frac{1}{2} \cdot \frac{(\eta_t + q_x\eta_x)^2}{1 + \eta_x^2} = 0. \tag{2.29}$$

The second equation of the DNO formulation is identical to the local equation of the AFM formulation. Thus, if we can show that

$$A(\eta)\eta_t = B(\eta) \longrightarrow \eta_t = G(\eta)q,$$

then we know that any solution to either formulation will indeed solve the alternative formulation and the AFM formulation and DNO formulation are equivalent.

Following the method of Ablowitz and Haut, we start by considering an arbitrary real valued periodic function $p(x)$ such that $p(x) = p(x + L)$. Additionally, we introduce a harmonic function $w(x, z, t)$ such that

$$w_{xx} + w_{zz} = 0, \qquad z \in (-h, \eta(x, t), \tag{2.30}$$

$$w_z = 0, \qquad z = -h, \tag{2.31}$$

$$w = p(x), \qquad z = \eta(x, t). \tag{2.32}$$

Using the fact that $A^*(\eta)$ is invertible (as demonstrated in the previous section), it is possible to find $\xi(x)$ such that

$$p(x) = \sum_{n\in\mathbb{Z}-0} e^{inx}\cosh\left(n(\eta+h)\right)\hat{\xi}_n$$

where $\hat{\xi}_n = \int_0^L e^{-ikn}\xi(x)dx$.

Returning to the nonlocal equation, taking the complex conjugate, and using integration by parts, we rewrite it as

$$\int_0^L e^{ikx}\Big(\eta_t\cosh(k(h+\eta)) - iq\big(ik\sinh(k(h+\eta)) - k\eta_x\cosh(k(\eta+h))\big)\Big)dx = 0, \quad \forall k\neq 0.$$

We now multiply both sides by $\hat{\xi}_k$ and sum over all $k\in\Lambda$. This yields

$$\begin{aligned}&\sum_{k\in\Lambda}\hat{\xi}_k\int_0^L e^{ikx}\Big(\eta_t\cosh(k(h+\eta))\\ &-iq\big(ik\sinh(k(h+\eta)) - k\eta_x\cosh(k(\eta+h))\big)\Big)dx = 0.\end{aligned}$$

If we assume that both the integral and the sum converge (this is equivalent to saying that the Fourier coefficients decay sufficiently fast or that we have smooth C^∞ functions), we can interchange the order of integration to get

$$\begin{aligned}&\int_0^L \eta_t\sum_{k\in\Lambda}\hat{\xi}_k e^{ikx}\cosh(k(h+\eta))dx\\ &-i\int_0^L q\sum_{k\in\Lambda}\hat{\xi}_k e^{ikx}\big(ik\sinh(k(h+\eta)) - k\eta_x\cosh(k(\eta+h))\big)dx = 0.\end{aligned}$$

Using the relations

$$p(x) = \sum_{k\in\Lambda}\hat{\xi}_k e^{ikx}\cosh(k(h+\eta)), \text{ and } G(\eta)p = B^\dagger(\eta)\xi,$$

we can replace terms in the above equation by their relationship to the arbitrary periodic function $p(x)$ to simplify the above to

$$\int_0^L \eta_t p dx - \int_0^L qG(\eta)pdx = 0 \qquad \langle\eta_t, p\rangle = \langle q, G(\eta)p\rangle\,.$$

Using the fact that $G(\eta)$ is self-adjoint, we have

$$\langle\eta_t, p\rangle = \langle G(\eta)q, p\rangle\,,$$

which is true for any periodic function $p(x)$. This implies that $\eta_t = G(\eta)q$ and thus, by starting with the AFM formulation and using the invertibility of the operator $A(\eta)$, we have shown that the two formulation are indeed equivalent. □

A consequence of this proof is that the AFM formulation inherits all of the analytical results determined for the general water-wave problem.

Chapter 3

Periodic Traveling Waves in One Spatial Dimension

In this chapter, we transform the AFM formulation into a reference frame moving with the periodic wave of speed c. By looking for stationary solutions, we are able to reduce the equations for a one dimensional surface from a system of two equations to a single integro-differential equation. We conclude the chapter by discussing results regarding the existence of solutions via the Lyapunov-Schmidt method.

3.1 Traveling Wave Coordinate System and the Resulting Reduction

In order to move into a traveling coordinate system moving with speed c, we must transform the variables in the following way

$$(x', t) \to (x - ct, t).$$

By changing the coordinates and using the chain rule when differentiating with respect to time t, we obtain the AFM formulation in a coordinate system moving in time t with speed c. The system of equations we obtain by moving to the translating coordinates are

$$q_t - cq_x + \frac{1}{2}q_x^2 + g\eta - \frac{1}{2}\cdot\frac{(\eta_t - c\eta_x + q_x\eta_x)^2}{1+\eta_x^2} = 0, \tag{3.1}$$

$$\sum_{k\in\Lambda} e^{ik(x-ct)} \int_{ct}^{L+ct} e^{-ik(x-ct)}\Big((\eta_t - c\eta_x)\cosh\left(k\left(h+\eta\right)\right) - iq_x \sinh\left(k\left(h+\eta\right)\right)\Big)dx = 0. \tag{3.2}$$

Using the periodic boundary conditions, we can simplify equation (3.2) to the following integral over the fundamental period.

$$\sum_{k\in\Lambda} e^{ikx} \int_{0}^{L} e^{-ikx}\Big((\eta_t - c\eta_x)\cosh\left(k\left(h+\eta\right)\right) - iq_x \sinh\left(k\left(h+\eta\right)\right)\Big)dx = 0. \tag{3.3}$$

Equations 3.1 and 3.3 are thereby the AFM formulation of Euler's equations in a traveling coordinate system.

Stationary Solutions

Periodic traveling waves are solutions that are stationary in a traveling coordinate system. In other words, in the moving coordinate system, the solution does not change in time and so any derivitives with respect to time t are zero. The resulting stationary equations in a moving frame are

$$-cq_x + \frac{1}{2}q_x^2 + g\eta - \frac{1}{2}\cdot\frac{\eta_x^2(q_x-c)^2}{1+\eta_x^2} = 0, \tag{3.4}$$

$$\sum_{k\in\Lambda} e^{ikx}\int_0^L e^{-ikx}\Big(-c\eta_x\cosh\left(k\left(h+\eta\right)\right) - iq_x\sinh\left(k\left(h+\eta\right)\right)\Big)dx = 0. \tag{3.5}$$

Even though our primary interest is to determine the surface elevation η, in the above formulation we must solve two equations for both unknowns η and q in order to determine the surface elevation. This problem can be simplified further by noting that (3.4)'s dependence on the velocity potential is quadratic in q_x. This allows us to solve equation (3.4) for q_x in order to determine the velocity potential at the surface explicitly in terms of the surface elevation η. We find that

$$q_x(x-ct,t) = c \pm \sqrt{\left(1+\eta_x^2\right)\left(c^2-2g\eta\right)}. \tag{3.6}$$

Remark 6. *We should note here that the induced flow created by moving to a traveling coordinate frame. Once we transformed the problem to the traveling wave coordinate frame, we induced a mean flow such that $q(x,t) \longrightarrow q(x-ct,t)-cx$. One could change the problem to eliminate this unbounded growth of the velocity potential in the traveling frame by introducing a new velocity potential at the surface $\tilde{q}(x-ct,t) = q(x-ct,t)-cx$, such that $\tilde{q}$ is bounded for all time. This new velocity potential $\tilde{q}$ has the representation*

$$\tilde{q}_x = \pm\sqrt{\left(1+\eta_x^2\right)\left(c^2-2g\eta\right)}.$$

By introducing $\hat{q}_x$, the meaning of the plus/minus sign become clear. This $\pm$ simply refers to right and left traveling waves. For simplicity, we will choose the plus sign. However, we note that there are no differences between the two cases.

Now that we have an expression for the velocity potential at the surface in terms of the surface elevation, we can substitute (3.6) into (3.5). Integrating by parts and simplifying, we obtain the following single spectral equation for the surface elevation η.

$$\int_0^L e^{-ikx}\sqrt{\left(1+\eta_x^2\right)\left(c^2-2g\eta\right)}\sinh\left(k(\eta+h)\right)dx = 0. \tag{3.7}$$

Similarly, for the case of infinite depth, we have

$$\sum_{k\in\Lambda} e^{ikx}\int_0^L e^{-ikx}e^{|k|\eta}\sqrt{(1+\eta_x^2)\,(c^2-2g\eta)}dx = 0. \tag{3.8}$$

To the best of our knowledge, this is the first time that the equations for stationary surface gravity waves have been written as a single equation for the surface elevation in physical coordinates. The beauty of this single equation is that it is easy to write down, it is written in physically intuitive variables, and it only requires solving for the one unknown of interest, η. Once a solution η is determined, the velocity potential at the surface is obtained directly by substituting η into (3.6).

Using the above formulation, we immediately draw some conclusions about the solutions. For example, at the crest and trough of a periodic solution, the surface elevation is at a maximum or minimum, respectively, and thus $\eta_x = 0$. Substituting this into the equation for the velocity potential $\tilde{q}$, we have

$$\tilde{q}_x = \sqrt{c^2 - 2g\eta}.$$

At the crest and trough, the velocity of a fluid partical in the x direction is given by the value of q_x. This can be seen by recalling that we earlier defined $\tilde{q}$ in such a way that that $q_x = \phi_x + \phi_y\eta_x$ where ϕ_x and ϕ_y are the velocities in the horizontal and vertical directions. Since we are only considering the crest and trough (where $\eta_x = 0$), q_x reduces to the velocity in the x direction. Without loss of generality, we assume that the surface elevation η has zero average and that $\eta_{crest} > 0 > \eta_{trough}$ (we eliminate the trivial solution from consideration). It's easy to see with this formulation that the velocity at the crest is smaller than the velocity at the trough.

Another interesting fact that we can determine from this formulation is that there is an upper limit to the maximal amplitude in the traveling coordinate frame for a given velocity. To see this, let a represent the maximal positive displacement of the surface elevation above $z = 0$ ($\eta_{\max} = a$). From this viewpoint, it is easy to see that in order for the velocity at the surface to remain real valued, we require that the quantity under the radical be positive. This condition is satisfied by requiring that the amplitude a and wave speed c satisfy the inequality $c^2 - 2ga > 0$, hence $a < c^2/(2g)$. This fact will be useful later during the numerical implementation of the algorithm.

Inclusion of Surface Tension

Finally, we note a generalization of (3.7)'s simplification is also valid when including surface tension. This is easily seen since the surface tension term in the local equation depends only on the curvature of the surface and not on the velocity potential. The resulting equations are

$$q_x = c \pm \sqrt{(1+\eta_x^2)\left(c^2 - 2g\eta + \frac{2\sigma\eta_{xx}}{(1+\eta_x^2)^{3/2}}\right)},$$

$$\int_0^{2\pi} \sqrt{(1+\eta_x^2)\left(c^2 - 2g\eta + \frac{2\sigma\eta_{xx}}{(1+\eta_x^2)^{3/2}}\right)}\sinh\left(k(\eta+h)\right)dx = 0.$$

We draw similar conclusions as before. For example, if we consider the velocity at the crests and troughs, we find that the crest is traveling slower than the trough. Additionally, the differences are larger since the elevation is being amplified by the presence of surface tension.

3.1.1 Existence of a Branch of Solutions

Before we continue with the numerical calculation of solutions, we make note of the results regarding the existence of stationary periodic traveling wave soltuions to Euler's equations. The conclusions drawn from previous work will aid us when choosing initial guesses for the surface elevation and wave speed in our numerical implementation.

The existence of traveling wave solutions with periodic boundary conditions had been established in the 1920's. Originally solutions were treated as small amplitude perturbations for the flat surface. Existence of the periodic solutions was then proved by demonstrating the convergence of such series. For the numerical method we shall introduce in the next chapter, it is beneficial to consider the existence of solutions in terms of solutions to a bifurcation problem where for a fixed period, there is a specific relationship between the amplitude of the solution a and the wave speed c. This problem has been investigated both numerically [13, 17, 45] and analytically [5, 11, 12, 17, 45] by many researchers. We choose to summarize the results obtained by Nicholls in 1998 [45]. Using a Lyapunov-Schmidt reduction, Nicholls proved the existence of periodic traveling wave solutions for one and two dimensional surfaces in the DNO formulation of the water wave problem. While we do not attempt to repeat the Lyapunov-Schmidt reduction for the AFM formulation, it is a useful result that the bifurcation of the non-trivial branch of solutions from the trivial branch occurs at the singular values of the linearized about the trivial solution. For completeness, we show that the singular values and null space of the linearization equation (3.7) are the same as those obtained by Nicholls. To begin, we consider the linear problem associated with the linearization about ($\eta = 0$, c). To leading order, the spectral problem becomes

$$\left(c^2 k - g \tanh kh\right) \int_0^L e^{-ikx} \eta dx = 0 \longrightarrow \left(c^2 k - g \tanh kh\right) \hat{\eta}_k e^{ikx}. \tag{3.9}$$

In the linearization, it is easy to see that the singular values obtained from our linearization are the values of wave speeds c_k such that

$$c_k = \sqrt{\frac{g \tanh(hk)}{k}}.$$

This implies that the null space of the linearization is given by the functions such that $\hat{\eta_k} = \hat{\eta}_{-k} = 0$. Furthermore, there is a two dimensional null space given by

$$\eta^{(1)}(x) = \cos(kx), \quad \text{and} \quad \eta^{(2)}(x) = \sin(kx).$$

These are the same singular values and null-space obtained by Nicholls in the DNO formulation [45]. There are a countably infinite number of bifurcation branches; one for each k value. In general,

we fix the period to be 2π and only consider the first bifurcation branch corresponding to $k = 1$. Additionally, since the null space is two dimensional, we choose to follow the branch associated with $\cos(x)$ so that the solutions we obtain are even functions of x. This means that for small amplitude perturbations from the zero solution, the leading order approximation of the solution will be

$$c \approx \sqrt{g \tanh(h)}, \eta \approx \epsilon \cos(x), \text{ and } \epsilon \ll 1.$$

This approximate solution and bifurcation points will be exploited in the next chapter as we determine numeric solutions to (3.7).

Remark 7. *As we mentioned above, there are two branches that we could follow (the sine or cosine branch) and we have made the choice to follow the cosine branch. In Section 4.3.1, we will comment on the sine branch of solutions and justify our choice of following the cosine branch numerically.*

Chapter 4

Numerical Computation of Periodic Traveling Waves in One Spatial Dimension

In this chapter, we develop a numerical scheme to determine periodic traveling wave solutions to Euler's equations using the AFM formulation described in the previous chapter. Specifically, we address some of the complexities when using this formulation. Finally, we conclude with numerical solutions for the traveling wave problem and compare the results with solutions of limiting equations.

Remark 8. *For the remainder of the dissertation, we will let $g = 1$. Further, we look only for solutions with minimal period $L = 2\pi$.*

4.1 Numerical Formulation

As mentioned earlier, we consider the problem of finding solution to the traveling wave problem as a bifurcation problem from the trivial solution $\eta = q = 0$. Recall that the null-space of the linear problem corresponds to values of c and η that satisfy

$$c_k = \pm\sqrt{\frac{g\tanh(hk)}{k}}, \qquad \eta = a\cos(kx),$$

and that at these values, a branch of a solutions bifurcates from the trivial solution. We consider the amplitude of our solution, a, to be our perturbation parameter away from the zero solution where increasing the amplitude a is equivalent to increasing the nonlinearity of the solution. In parameter space, there is a continuous curve describing the dependence of a on the speed of the solution c. Since we do not know the expression for the continuous curve analytically, we determine it numerically. This sort of bifurcation problem is ideally set up for a numerical continuation method. Such methods

applied to the DNO formulation have been explored by [17, 45]. However, we hope to investigate alternative solution techniques that rely on the bifurcation structure without needing to preform numerical continuation explicitly.

To implement our numerical method, we first discretize our problem using a spectral collocation method. Since we have fixed the period of our problem to 2π, it is natural to choose a projection of our solution onto a truncated Fourier series representation with N Fourier modes resulting in $2N+1$ Fourier coefficients. Using these coefficients to represent our solution, we discretize the interval on the real line into $2N+1$ equally spaced collocation points in x so that $x_j = \frac{2\pi(j-1)}{2N+1}$ for $j = 1 \dots 2N+1$. This gives us an approximation for η at x_j as

$$\eta(x_j) \approx \sum_{n=-N}^{N} \hat{\eta}_n e^{inx_j},$$

where $\hat{\eta}_n$ is the n-th Fourier coefficient calculated by a discrete Fourier transform. Our goal is to solve for the $2N+1$ unknown Fourier coefficients representing our solution η.

Remark 9. *For our implementation, we calculate derivatives with spectral accuracy in Fourier space by multiplying $\hat{\eta}_n$ by the ik and revert back to the physical domain via the Fast Fourier Transform (FFT). We perform multiplication and other nonlinear functions in the physical domain point wise. For example, when we need to calculate nonlinear quantities such as $(1+\eta_x^2)(c^2-2g\eta)$, we first calculate the derivative in the Fourier domain, transform to the real line by means of the FFT, and then calculate the square and multiplication point wise in the physical domain.*

Given the $2N+1$ unknowns we need to determine the appropriate $2N+1$ equations to solve. Since our nonlocal spectral equation

$$\int_0^{2\pi} e^{-ikx} \sqrt{(1+\eta_x^2)\,(c^2-2g\eta)} \sinh\left(k(\eta+h)\right) dx = 0 \quad \forall k \in \Lambda, \tag{4.1}$$

is valid for all $k \in \Lambda$ where $\Lambda = \{\frac{2n\pi}{L} \mid n \in \mathbb{Z} - \{0\}\}$, it makes sense to take the $2N$ equations corresponding to $n = -N, \dots, -1, 1, \dots, N$. Thus, at this point, we have $2N$ equations for $2N+1$ unknowns. We can reduce the number of unknowns by noting that the average value of the surface elevation can be made zero without loss of generality. This allows us to choose the zeroth Fourier coefficient of the surface elevation. For simplicity, we let $\hat{\eta}_0 = 0$. Thus, we have $2N$ equations for $2N$ unknowns.

Since we are looking at this problem as a bifurcation problem in a (the amplitude parameter), we know that there are specific values of c for which periodic solutions exist. Specifically we are seeking to determine how c changes as a function of the amplitude. In order to solve for the new unknown c, we introduce a new equation constraining the amplitude of the surface elevation η_{max} to a fixed value a which we shall choose ahead of time. This increases the number of equations/unknowns to $2N+1$ equations for $2N+1$ unknowns. We are now charged with solving the following $2N+1$ equations given by:

$$\int_0^{2\pi} e^{-ikx}\sqrt{(1+\eta_x^2)\,(c^2-2g\eta)}\sinh\left(k(\eta+h)\right)dx = 0 \quad k \in \{\pm 1, \pm 2, \ldots, \pm N\},$$

$$||\eta||_\infty = a,$$

for the $2N+1$ unknowns c and $\hat{\eta}_n$ for $n = -N, \ldots, -1, 1, \ldots N$.

Before we proceed to discuss the method we use to solve the above system, we address the problem of $\sinh(n(\eta+h))$ being unbounded for large values of n. Leaving this unchecked could present difficulties when computing solutions on fine grids since $\sinh(n) \to \infty$ as $n \to \infty$. This problem can be eliminated by rewriting $\sinh(n(\eta+h))$ as

$$\sinh(n(\eta+h)) = \sinh(n\eta)\cosh(nh) + \cosh(n\eta)\sinh(nh)$$

Substituting this into the traveling wave nonlocal spectral equation and dividing through by $\cosh(nh)$ removes the exponential growth rate in nh,

$$\int_0^{2\pi} e^{-inx}\sqrt{(1+\eta_x^2)\,(c^2-2g\eta)}\left(\sinh(n\eta)+\cosh(n\eta)\tanh(nh)\right)dx = 0 \quad n = -N, \ldots, -1, 1, \ldots N \tag{4.2}$$

by recasting the dependence on nh through $\cosh(nh)$ and $\sinh(nh)$ with the bounded function $\tanh(nh)$.

Remark 10. *Exponential growth is still possible through the terms* $\sinh(n\eta)$ *and* $\cosh(n\eta)$*. We could bound this in theory by recalling that a necessary condition for real-valued solutions is that the amplitude of the solution is bounded by* $a < \frac{c^2}{2g}$*. We can then divide the nonlocal spectral equation by* $\cosh\left(n\frac{c^2}{2g}\right)$ *and obtain*

$$\int_0^{2\pi} e^{-inx}\sqrt{(1+\eta_x^2)\,(c^2-2g\eta)}\left[\frac{\sinh(n\eta)+\cosh(n\eta)\tanh(nh)}{\cosh\left(n\frac{c^2}{2g}\right)}\right]dx = 0 \quad \forall n \in \Lambda \tag{4.3}$$

While this is bounded, it can present numerical difficulty since we are evaluating a large number divided by another large number (as n becomes larger).

4.2 Numerical Implementation

As mentioned earlier, it is very useful to consider the non-trivial solutions as solutions to a bifurcation problem away from the trivial solution. For numerical purposes, we begin our numerical scheme by considering a small amplitude cosine wave as our initial guess. Correcting this approximation with our numerical method, we proceed to obtain a higher amplitude solution using the new corrected solution as our initial guess. We continue in this manner until we have reached the critical amplitude $a = .14\pi\tanh(kh)$ as given by [43]. We now formally outline the procedure that we use:

- Start with a small amplitude initial guess η_0 and an appropriate corresponding initial speed c_0 where

$$\eta_0 = a_1 \cos(x), \qquad c_0 = \sqrt{\tanh(h)}, \qquad a_1 << 1.$$

- Use a numerical nonlinear solver to determine a solution for the unknowns $\hat{\eta}_j$ and c for the given amplitude a_1. This determines a new small amplitude solution set (η_1, c_1) with amplitude a_1.

- Proceed to calculate higher amplitude solutions by rescaling η_1 to a new amplitude a_2 slightly larger than a_1. Estimate a new initial guess for c_2 based on the previously solved for value of c_1. The rescaled surface elevation and estimated wave speed will serve as the new initial guess.

- Solve the nonlinear equations numerically again to determine a new solution set (η_2, c_2) with amplitude a_2.

- Repeat this process, increasing the amplitude each time until the critical wave height $a = .14\pi \tanh(h)$ is reached.

4.2.1 Methods of Solving the Nonlinear Problem

The most crucial part of our algorithm is solving the $2N + 1$ nonlinear equations for the $2N + 1$ unknowns. In the current implementation, we use Newton's method to determine the solution to our nonlinear set of equations[1]. One of the disadvantages to using Newton's method is that the initial guess needs to be relatively close to the actual solution in order to guarantee convergence. As the amplitudes become larger, the solutions become inherently more nonlinear and thus, Newton's method becomes more sensitive to initial guess choices. However, in our numerical scheme, we have developed a method to predict good initial guesses by following the bifurcation curve in parameter space. As we travel higher up the branch, we use polynomial interpolation to predict better initial guesses.

In general, this method works well for a small number of unknowns (coarse grid resolution). However, as the size of our problem becomes larger (and our grid becomes finer), the method becomes slow and unreliable. Our original goal was to develop an iterative method to determine the solution at higher resolutions with relatively small computation time and reasonable stability properties. For a decaying boundary condition at $\pm\infty$, there are several methods that work reliably well. We attempted to modify these methods for the periodic case. Throughout the remainder of this subsection, we briefly discuss some of the methods, describe their implementations and periodic extensions, and conjecture why the methods failed to consistently converge for our problem.

---

[1]For a complete reference on Newton's method, see [50]).

Petviashvilli and Spectral Renormalization

Our initial first choice of numerical methods was that which was presented by Petviashvili in 1976 upon the discovery of soliton solutions to the modified KdV equation [53]. Petviashvili's method is an iterative scheme based on the separation of the linear and nonlinear terms. We introduce the method by working through the example for the KdV equation.

Consider the traveling wave problem associated with KdV. This equation and its' integrated counterpart are given below

$$-cu_x + u_{xxx} + u_x u = 0, \text{ and } -cu + u_{xx} + \frac{1}{2}u^2 = d.$$

In this formulation, the parameter d is a constant due to integration. For radially decaying boundary conditions ($u(x) \to 0$ as $|x| \to \infty$), the constant d is identically zero ($d = 0$). Following the general idea of separating linear and nonlinear parts, we can rewrite the equation as

$$(c - \partial_x^2)u = \frac{1}{2}u^2.$$

Taking the Fourier transform on both side yields

$$(c + k^2)\hat{u}(k) = \frac{1}{2}\mathcal{F}\left(u^2\right),$$

where

$$\mathcal{F}(u) = \hat{u}(k) = \int_{-\infty}^{\infty} e^{-ikx}u(x)dx, \qquad u(x) = \frac{1}{2\pi}\int_{-\infty}^{\infty} e^{ikx}\hat{u}(k)dk.$$

Naively, one can consider the iterative algorithm given by

$$\hat{u}_{n+1}(k) = \frac{\mathcal{F}\left(u_n^2\right)}{2(c + k^2)},$$

such that future approximations of the solution are based on the nonlinearity. Starting with an initial guess $\hat{u}_0$, the above problem is iterated until $u_{n+1} \approx u_n$, or, in other words, a fixed point was found. This method typically diverges even if there is a fixed point to the original problem. The Petviashvili method addresses this divergence problem by introducing an acceleration and stabilizing operator M_n such that as $u_{n+1} \to u_n$, $M_n \to 1$. For the case of KdV the operator M_n is chosen as

$$M_n = \frac{\left\langle (c + k^2)\hat{u}_n(k), \hat{u}_n(k)\right\rangle}{\left\langle \hat{u}_n(k), \hat{u^2}_n(k)\right\rangle}.$$

By simple inspection, it is obvious that as $||u_{n+1} - u_n|| \to 0$, $M_n \to 1$. Finally, the iterative method becomes

$$\hat{u}_{n+1}(k) = M_n^{\gamma}\frac{\mathcal{F}\left(u_n^2\right)}{2(c + k^2)}.$$

The parameter γ is a number chosen to accelerates the convergence of the iterative method. For KdV, Petviashvili determined heuristically that the best choice of γ is $\gamma = 2$.

This method has been shown to be convergent for the generalized KdV equation

$$-cu + u_{xx} + \frac{1}{p}u^p = 0.$$

by Pelinovski and Stephyants [51]. Additionally, they showed analytically that Petviashvili's estimate for $\gamma = \frac{p}{p-1}$ was the appropriate choice of γ to ensure the optimal convergence rate.

The correct choice of the M_n operator is critical to ensure rapid convergence to the solution. For a general nonlinear problem, finding the correct acceleration operator could become an issue of trial and error for any given problem. However, Ablowitz and Musslimani [3] proposed a method to determine the correct acceleration operator. They noticed that in general (as mentioned above), when one considers solutions to a nonlinear problem as a naive fixed point iteration scheme, the solution either converged to the trivial solution or diverged. To prevent divergence, they introduced a new scaled variable $v(x)$ with scaling parameter α such that $u(x) = \alpha v(x)$. This new parameter α is also iterated with the solution so that instead of considering $u_n(x)$, we consider α_n and $v_n(x)$ at each iteration step n. By introducing this new scaling factor α and variable $v(x)$, the KdV iteration equation is transformed into solving

$$\hat{v}_{n+1}(k) = \alpha_n \frac{\mathcal{F}\left(v_n^2\right)}{2(c+k^2)}.$$

They choose to solve for α by taking the inner product of both sides with $v_n(x)$ and letting $v_{n+1}(x) = v_n(x)$. This can be thought of as looking for the correct value of α to minimize the norm of the difference between the old solution and the updated one.

In the formulation for KdV that we have been working with, we can solve for α_n to find that at each iteration α_n is the same as the above acceleration operator M_n where $\gamma = 1$, and that as $v_{n+1} \to v_n$, v_n converges to a solution $u(x)$ of the original problem. This example was meant to demonstrate the equivalence of the two formulations. However, the spectral renormalization algorithm is more general. Typically, in highly nonlinear problems, one cannot find an analytic expression for the acceleration operator α_n, since it might show up in nonlinearly. For example, when this method is applied to the AFM formulation on the whole line [1], a Newton solver must be used to obtain an approximation for the acceleration operator α_n at each iteration. Thus, even through the spectral renormalization method is an iterative method for the solution, at each iteration, a nonlinear problem must be solved.

Our initial approach to solving the nonlinear periodic problem was to extend this method to the case of periodic boundary conditions. By using a Fourier series representation of the solution instead of a Fourier transform, we hoped to determine a periodic analogue to the method previously outlined. We conjecture that this attempt was unsuccessful for two main reasons. First, this method fails to take into account the relationship between the wave speed c and the amplitude of the solution a. As demonstrated earlier, if we fix the period of the solution we are looking for (as we would do if we chose a specific Fourier Series representation), there are specific wave speeds c corresponding to specific solution amplitudes a. In other words, there is a very specific curve in parameter space that relates

the amplitude of the solution to the wave speed. In this scheme, it seems most straightforward to pick a valid wave speed c and let the method determine the solution with the correct corresponding amplitude. For such problems, the solution might never converge if it shoots from point to point along or nearby the bifurcation branch in parameter space. This seems to be the largest difficulty that we have with our problem. The method tends to converge for a small times to $||u_{n+1} - u_n|| \approx \mathcal{O}(10^{-3})$, well above our error tolerance. Then, depending on the initial guess, the method will rapidly converge to zero or diverge completely. It thus appears as though the method has found a local minimum which is not a solution of the problem, and overshoot the solution on the bifurcation curve to only diverge or converge to the zero solution. Secondly, there are documented problems with fixed point algorithms when the solutions have multiple zero crossings. This shortcoming not only apply to periodic solutions, but also for solutions on the whole line that are in excited states (a localized solution with oscillatory tails) . These two shortcomings are addressed by the next method we investigated.

Imaginary Time Step Methods

A second class of iterative methods we hoped to extend to the periodic case are Imaginary Time Evolution Methods (ITEM). ITEM are methods to determine the solution to a nonlinear differential equation by rewriting the problem as a time-dependent evolution equation [64]. For example, consider the general differential equation

$$\mathcal{L}u = f(u, u_x, u_{xx}, \ldots) = 0.$$

ITEM proposes that the problem should be written as

$$u_t = \mathcal{L}(u). \tag{4.4}$$

If we can find a steady-state solution to the with equation with $u_t = 0$, then we have found the solution to our nonlinear differential equation. In other words, ITEM poses the problem in the following way: *Can we find a steady state solution so that as $t \to \infty$, $u_t = 0$.*

Remark 11. *It is important to note that using an imaginary time in this scenario does not refer to introducing a complex number into the problem. Instead, it simply refers to the introduction of the time evolution, and looking for the solution of the differential equation as a steady-state solutions to the time dependent problem. As we will show shortly, the time evolution simply aids us in developing an iterative scheme.*

By posing the problem in this manner, one can use any timestepping method to determine the approximation for $u(x, t + \Delta t)$ in terms of previous solution $u(x, t)$. For example, by approximating the derivative as

$$u_t \approx \frac{u_(x, t + \Delta t) - u(x, t)}{\Delta t} = \frac{u_{n+1} - u_n}{\Delta t},$$

we can use a forward Euler method to write the iteration scheme as

$$u_{n+1} = u_n + \Delta t \mathcal{L} u_n.$$

As with the previous methods, this method will typically diverge unless there is a steady state solution for the problem (4.4). However, when rewriting the problem as an evolution problem, we are free to pre-multiply the operator $\mathcal{L}$ by any operator $\mathcal{M}$ we choose as long as the operator has a trivial null-space. In other words, $\mathcal{M}u = 0$ can only have the trivial solution which implies that the operator $\mathcal{M}$ is definite.

Remark 12. *For stability purposes, we require $\mathcal{ML}$ to be negative definite. This implies that there exists a steady state solution to the problem $u_t = \mathcal{ML}u$.*

With the introduction of the operator $\mathcal{M}$, the iteration scheme becomes

$$u_{n+1} = u_n + \Delta t \mathcal{M}\mathcal{L} u_n$$

For KdV, an appropriate choice of $\mathcal{M}$ is the inverse of the linear operator, i.e. $\mathcal{M} = -(c - \partial_x^2)^{-1}$. Thus ITEM applied to KdV is simply

$$u_{n+1} = u_t - \Delta t (c - \partial_x^2)^{-1} u_n^2,$$

where $(c + \partial_x^2)^{-1}$ is calculated in Fourier space as $(c + k^2)^{-1}$. Since the operator $\mathcal{M}$ is negative definite, and $\mathcal{ML}$ is also negative definite, the evolution equation has a steady state solution, and ITEM will converge for an appropriate choice of Δt.

For more general nonlinear equations, this method is highly effective and easy to implement on the whole line. However, as stated above, there are still numerous problem with convergence when the solutions have multiple zero crossing or are in excited states; the same category as the periodic solutions we are attempting to find. To combat the problems associated with multiple zero crossings on the whole line, Yang and Lakoba [64] introduced a new acceleration operator $\mathcal{M} = \mathcal{A}^{-1}\mathcal{L}_1^\dagger \mathcal{A}$ where $\mathcal{L}_1^\dagger$ is the adjoint of the linearized operator about the trivial solution, and $\mathcal{A}$ is some definite operator that accelerates the convergence. For example, when $\mathcal{A} = 1$ the problem becomes $u_t = \mathcal{L}_1^\dagger \mathcal{L}$. Thus the linear portion of the operator $\mathcal{L}$ is squared by the algorithm. We refer to this method as the Squared Operator Method (SOM). SOM eliminates some of the difficulties with multiple zero crossings. Additionally, Yang provided an algorithmic method to incorporate constraints based on problem parameters such as conservation laws. For example, when there are propagation constants, Yang developed an iterative method to determine the free parameter so that a constraint was satisfied. For example, consider the operator

$$\mathcal{L}_0 u + \mu u = 0$$

where μ is a free parameter. In this problem, the parameter shows up linearly, and the operator $\mathcal{L}_0$ is independent of μ. If one is interested in conserving the 2-norm of the solution

$$\langle u(x), u(x) \rangle = \int_{-\infty}^{\infty} u^2(x) dx = E,$$

the iterative method can be posed as[2]

$$u_{n+1} = \left[\frac{E}{\langle \tilde{u}_n, \tilde{u}_n \rangle}\right]^{\frac{1}{2}} \tilde{u}_{n+1},$$

where

$$\tilde{u}_{n+1} = u_n - \Delta t \left[\mathcal{L}_1^\dagger \mathcal{L} u - \gamma u\right]_{u=u_n, \mu=\mu_n},$$

and

$$\gamma = \frac{\left\langle u, \mathcal{L}_1^\dagger \mathcal{L} u \right\rangle}{\langle u, u \rangle}, \quad \mu_n = \frac{\langle u, \mathcal{L}_0 u \rangle}{\langle u, u \rangle}.$$

The advantages of SOM when compared to the Petviashvili and spectral renormalization methods presented earlier is that (i) the method already takes into account the possibility of zero crossings, and (ii) includes a power-conserving scheme to determine the appropriate values of parameters that correspond to the conserved norm. Again, we planned to use Fourier series representations to extend this method to the periodic case. However, our problem is more complicated than the examples where the method has been proven to converge. For example, in the SOM scheme with a constraint, we hoped to use our wave-speed c as a free-parameter, and fix an appropriate norm of our solution. For the AFM formulation, the parameter c shows up in our integral equation in a highly nonlinear way, and so any update via iteration on c would not occur at the proper order. By determining an improper wave speed c, the amplitude of the solution is then adjusted. Likewise the problem repeats itself until the solution has converged to the trivial solution, and the wave speed has diverged.

Poincaré-Lindstedt Methods

The Poincaré-Lindstedt method is a perturbation scheme used to find periodic solutions to nonlinear differential equations when the period of the solution is unknown. In general, this method generates periodic solution by rescaling the independent variables and perturbing both the solution and the period of the solution. Viswanath [60] adapted this method to a numerical scheme that is highly accurate and converges quadratically. This numerical scheme is best presented through the example of a general ordinary differential equation of the form

$$\frac{dy}{d\tau} = f(y).$$

We begin by rescaling τ ($\omega\tau = t$) so that the unknown periodic solution with unknown period L is now periodic with period 2π, and $\omega L = 2\pi$. Substituting this new scaling into the differential equation yields:

$$\omega \frac{dx}{dt} = f(x)$$

where $x(t) = y(\omega\tau)$. At this point, we perturb x and ω by letting $x = x_0 + \epsilon x_1 + \ldots$ and $\omega = \omega_0 + \epsilon\omega_1 + \ldots$ where $\epsilon << 1$. We can think of this as correcting an initial guess solution set (x_0, ω_0)

[2]For simplicity, we do not include the acceleration operators in this formulation. Regardless, the proof of convergence given in [64] does not depend on the operator $\mathcal{A}$.

by a small amount given by (x_1, ω_1). Substituting the perturbation into the rescaled differential equation and keeping only terms through $\mathcal{O}(\epsilon)$, we have the following equation where we have now set $\epsilon = 1$:

$$\omega_0 \dot{x}_1 = f'(x_0)x_1 + f(x_0) - \omega_0 \dot{x}_0 - \omega_1 \dot{x}_0. \tag{4.5}$$

where we have dropped the ϵ's. Given some initial guess (x_0, ω_0), we want to find both x_1 and ω_1. We start this process by noting that equation (4.5) can be written in the general form

$$\dot{x}_1 = A(t)x_1 + b(t) + \omega_1 c(t).$$

We break down the solution so that $x_1 = f_1(t) + \omega_1 f_2(t)$. This allows us to solve for both $f_1(t)$ and $f_2(t)$ using any numerical differential equation solver with any initial condition of our choice. The only unknown remaining is ω_1. To solve for ω_1, we require that our correction be 2π periodic. In other words, $f_1(0) + \omega_1 f_2(0) - (f_1(2\pi) + \omega_1 f_2(2\pi)) = 0$. Additionally, we require that our correction moves perpendicular to the flow along the initial guess. In other words, in phase space, our correction moves in a direction normal to the initial guess. Thus, we have two equations for one unknown x_1. We can use least squares approximations to determine ω_1. Once we determine ω_1, the correction is simply $x_1(t) = f_1(t) + \omega_1 f_2(t)$, and our corrected solution is $x(t) = x_0(t) + x_1(t)$ with corrected period estimate $\omega = \omega_0 + \omega_1$. Using the corrected solution as a new initial guess, this method can be iterated until the correction term satisties $\omega_1 < \epsilon_{tol}$. Viswanath showed that this method converges quadratically [60].

This is the first method that we attempted that was specifically developed to find period solutions, so an extension to the periodic case was not necessary. However, because we are not dealing with a differential equation, we must still adapt the method quite a bit. In the previous sections, we fixed the period and then determined the corresponding amplitudes and wave speeds. However, in this case, we assume that the wavelength is unknown, so while we still have a bifurcation problem, we are now considering a different parameter space. It seems logical that for this method, we would pick a wave-speed c, and determine the corresponding period for the solution. We should still have a one parameter family of solutions. In other words, if we only fix the wave-speed c, there is still a one-parameter family of solutions for a given amplitude a and the corresponding wave length L. However, regardless of the wavelength, we know that $c^2 - 2ga \geq 0$, so we should be able to pick any speed and amplitude that satisfies this condition. Also, we must keep in mind the fact that the maximal amplitude is related to the depth as given in [43].

We begin with the equations for arbitrary wave-length given in (3.7). Rescaling $x \to \omega x$ so that the problem is 2π periodic, we have the new nonlocal spectral equation

$$\int_0^{2\pi} e^{-inx} \sqrt{(1 + \omega^2 \eta_x^2)\,(c^2 - 2g\eta)} \sinh\left(\omega n(\eta + h)\right) dx = 0, \quad n \in \mathbb{Z} - \{0\}.$$

We proceed in the same typical way by perturbing both η and ω by letting $\eta = \eta_0 + \epsilon\eta_1$ and $\omega = \omega_0 + \epsilon\eta_1$ and keeping terms through order ϵ. As before, we will drop the ϵ's. If we expand the

nonlocal equation by substituting Fourier series for η_0 and η_1, we can write the infinite dimensional linear system for the Fourier coefficients of η_1 in the following form:

$$\hat{A}(\omega_0, \eta_0)\hat{N} = \hat{B}(\omega_0, \eta_0) + \omega_1 \hat{C}(\omega_0, \eta_0).$$

At this point, we could guess an initial solution η_0 and ω_0 and iterate as before to determine the corrections ω_1 and η_1. Since we are already using Fourier series, the corrected solution is automatically 2π periodic. We still need an additional constraint to solve for the period update ω_1. For this additional constraint, we force the correction to be perpendicular to the previous residual from the integral equation. What this means is that if we consider the original equation, we want the new solution to be perpendicular to the error. In other words, $\langle \eta_{1,1}(x) + \omega_1 \eta_{1,2}, \mathcal{N}(\eta_0) \rangle = 0$. Using the new value of ω_1, we update the solution function η. We repeat this process until the solution converges to ϵ_{tol}. With the current implementation, the solutions tended only to converge when the initial guess was a very small amplitude periodic function. However. there is no constraint to determine larger amplitude solutions. This is due to the fact that there is still a one-parameter family of solutions corresponding to valid amplitudes a. Since we pick the wave-speed at the initial part of the iteration scheme, it stands to reason that at each iteration, we could over-determine the system of equations for ω_1 by adding the additional constraint that $||\eta_0 + \eta_1\omega_1||_\infty = a$ for some fixed appropriate α. However, when we add this additional constraint, the value of the period update ω_1 diverges rapidly.

A final adaptation to the Poincaré-Lindstedt method is to combine the idea of renormalization. At each iteration, we renormalize the solution to a desired amplitude a enforcing that $||\eta||_\infty = a$. By so enforcing the amplitude, we can use the same pseudo-continuation method as described for Newton's method. While we believe that the development of this numerical method is an important step, at this point we still find Newton's method more robust for the solutions that we intend to calculate[3].

4.2.2 Other Numerical Schemes

There are several other approaches for solving this problem which we shall not address here. However, as an important example, we have already mentioned that continuation is ideally set up to determine solutions for bifurcation problems of this nature. Specifically, packages such as AUTO or MATCONT are ideal programs for the differential equation counterpart of this problem. However, since our equations is written as an integral equation, it does not fit into any of the standard packages and would require reformulation in order to be applied to the AFM formulation.

---

[3]For additional information regarding the Poincaré-Lindstedt iteration method applied to Euler's equation, refer to appendix A.

4.3 Numerical Convergence and Stability

Before we proceed to the numerical solutions obtained with this method, we should discuss convergence and stability of the algorithm. Given the current numerical scheme, we do not attempt to prove convergence analytically. However, we can demonstrate that as we increase the number of Fourier modes used to approximate the surface elevation, the Fourier coefficients of each successive approximation converge towards the same solution. This idea is referred to as numerical Cauchy convergence which we now define.

Definition 1 (Numerical Cauchy Convergence)**.** *A series e_n is said to be* Cauchy Convergent *if and only if for each $\epsilon > \epsilon_{tol}$, there exists a $N(\epsilon)$ such that $||e_n - e_m|| < \epsilon$ for all $n, m \geq N(\epsilon)$ where ϵ_{tol} is our maximal allowable error (for instance, $\epsilon = \epsilon_{mach}$ where ϵ_{mach} is machine precision).*

Let η_N represent the solution η computed with N Fourier modes (i.e. $2N+1$ collocation points), and the error e_N represent

$$e_N = ||\eta_N - \eta_{N-1}||_2$$

We can demonstrate Cauchy convergence by showing that we can pick any $\epsilon > \epsilon_{\text{tol}}$ and show that as we take the size of our truncation large enough, the difference in the approximation of the eigenvalues converges to ϵ_{tol}. For several amplitudes and depths, we calculated the Cauchy error as a function of the number of Fourier modes used in the approximation of the solution. The results are shown in the Table 4.1, as well as in the Figure 4.1. As can be seen clearly in Figure 4.1, the Cauchy error decreases linearly on a logarithmic scale which demonstrates spectral accuracy. We also keep track of the residuals of our solutions as calculated when our solution set (η, c) is substituted back into equation (4.2). These numbers can be seen in Table 4.2 and Figure 4.2. It is important to note that as the amplitude of the solution increases (and consequently the nonlinearity of the solution), it is necessary to take a larger number of Fourier modes to reach Cauchy convergence.

Table 4.1: The Cauchy error e_N for solutions of various amplitudes a and depths h.

	$h = .5$		$h = \infty$	
N	$a = .01$	$a = .05$	$a = .1$	$a = .2$
6	6.05e-07	7.84e-04	3.94e-05	1.15e-03
8	7.43e-09	3.88e-05	8.30e-07	7.55e-05
10	3.58e-09	2.53e-06	2.50e-08	6.93e-06
12	4.34e-09	1.96e-07	1.18e-09	7.86e-07
14	9.83e-10	1.68e-08	1.90e-10	1.04e-07
16	2.22e-16	1.57e-09	2.22e-16	1.58e-08
18	2.22e-16	8.57e-10	2.22e-16	2.84e-12
20	2.22e-16	5.11e-10	2.22e-16	3.05e-12
22	2.22e-16	8.33e-10	2.22e-16	3.16e-12
24	2.22e-16	5.84e-11	2.22e-16	3.31e-12
26	2.22e-16	2.22e-16	2.22e-16	3.48e-12
28	2.22e-16	2.22e-16	2.22e-16	3.74e-12
30	2.22e-16	2.22e-16	2.22e-16	3.93e-12
32	2.22e-16	2.22e-16	2.22e-16	4.10e-12

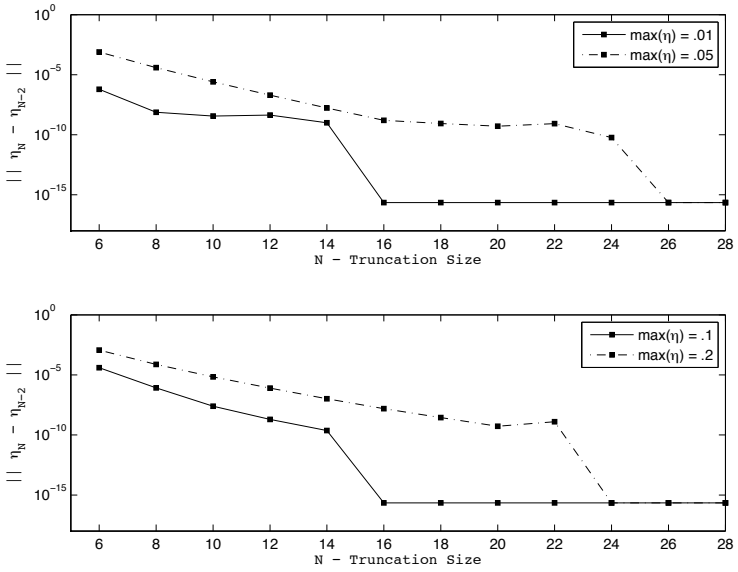

Figure 4.1: Semilog plot of the Cauchy Error for various depths ($h = .5$ and $h = \infty$) with various amplitudes.

Table 4.2: The residual error e_N for solutions of various amplitudes a and depths h.

	$h = .5$		$h = \infty$	
N	$a = .01$	$a = .05$	$a = .1$	$a = .2$
4	7.75e-17	6.20e-16	2.29e-13	2.45e-12
6	3.76e-16	1.32e-12	3.22e-16	8.59e-11
8	1.23e-16	1.22e-09	3.22e-13	4.10e-16
10	2.66e-16	1.35e-11	5.31e-16	4.40e-13
12	3.35e-16	7.25e-16	2.01e-15	1.45e-15
14	2.65e-16	3.37e-15	2.60e-15	3.14e-12
16	6.43e-15	2.20e-15	1.63e-11	1.96e-14
18	5.58e-15	1.36e-15	1.64e-11	6.55e-11
20	6.43e-15	6.64e-16	1.64e-11	1.88e-11
22	4.11e-15	1.71e-15	1.64e-11	4.45e-10
24	5.77e-15	1.79e-15	1.64e-11	4.68e-13
26	7.55e-15	2.11e-13	1.64e-11	2.75e-13
28	4.33e-15	2.26e-13	1.64e-11	2.39e-12
30	6.05e-15	2.19e-13	1.64e-11	8.09e-12
32	9.94e-15	2.23e-13	1.64e-11	2.90e-12
34	1.29e-14	2.17e-13	1.64e-11	2.77e-13
36	1.09e-14	2.13e-13	1.64e-11	4.71e-14
38	5.11e-15	2.15e-13	1.64e-11	1.55e-13
40	4.47e-15	2.15e-13	1.64e-11	1.75e-12

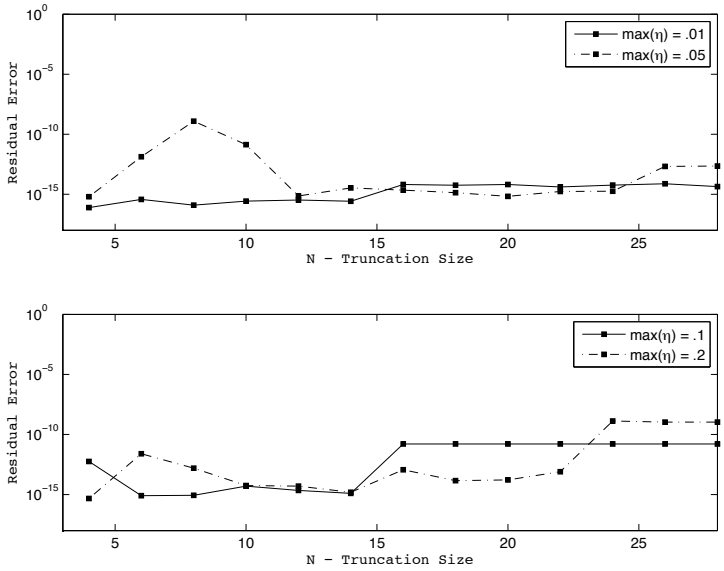

Figure 4.2: Semilog plot of the Residual error for various depths ($h = .5$ and $h = \infty$) with various amplitudes.

4.4 Numerical Results

Finding numerical traveling wave solutions to the surface gravity wave problem is not a new task. Many researchers have calculated periodic traveling wave solutions for waves of various amplitudes, from small amplitude waves to waves near and at the Stokes' limiting wave with a 120^o crest.

Solutions were calculated for a variety of depths and amplitudes. We include several example of periodic solutions for four sample depths: $kh = .1$, $kh = .5$, $kh = 1.5$ and finally, $kh = \infty$. Additionally, along with each solution, we show a picture of the bifurcation curve in parameter space, and an indicator of where the displayed solutions lie on the curve.

Remark 13. *Before we present the remaining results, we briefly justify our choice of following the cosine branch by showing several solutions generated by following the cosine and side branch. We compare the cosine solution branch shifted by $\pi/2$ with the sine solution branch in Figure 4.3. The results are very convincing that the solutions obtained by following the sine branch are simply a $\pi/2$ shift of the cosine branch. One of the main advantages of following the cosine branch is the symmetry inside the periodic cell.*

Our numerical solutions demonstrate the phenomena that we expect. As the amplitude of the solution increases, the solutions becomre more elliptic. In other words, the troughs become wider and the crests become sharper. We are able to calculate solutions with high degrees of accuracy

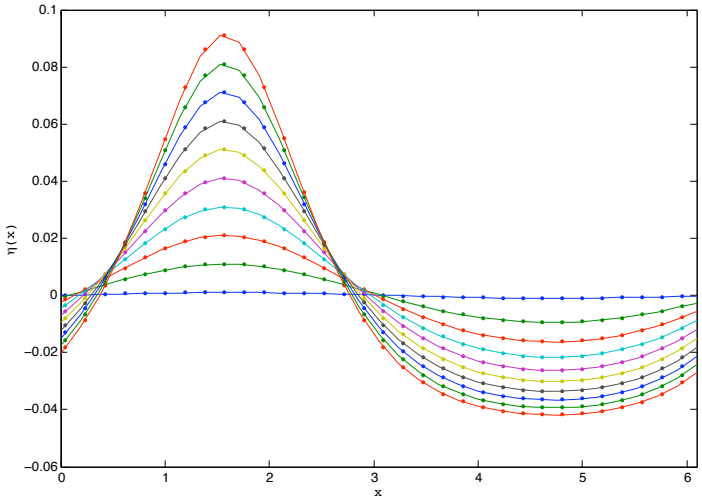

Figure 4.3: Solutions for $h = .5$ with various amplitudes. The solid lines correspond to the solution obtained by following the sine branch, and the dots correspond to the solution obtained by following the cosine branch shifted by $\pi/2$.

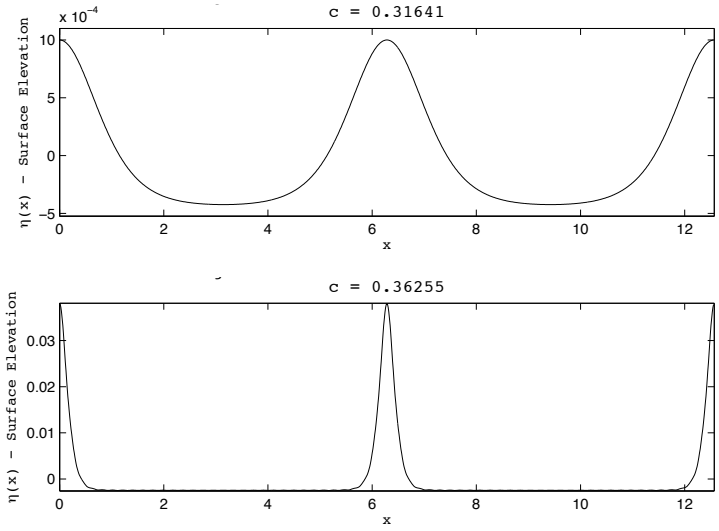

Figure 4.4: Solutions for $h = .1$ with amplitudes $a = .001$ (top) and $a = .038$ (bottom). Both solutions are calculated with $N = 64$ Fourier modes. The residual error for both approximations was less than 10^{-14}. Corresponding wave speeds and norms are marked on the bifurcation curve shown in Figure 4.5

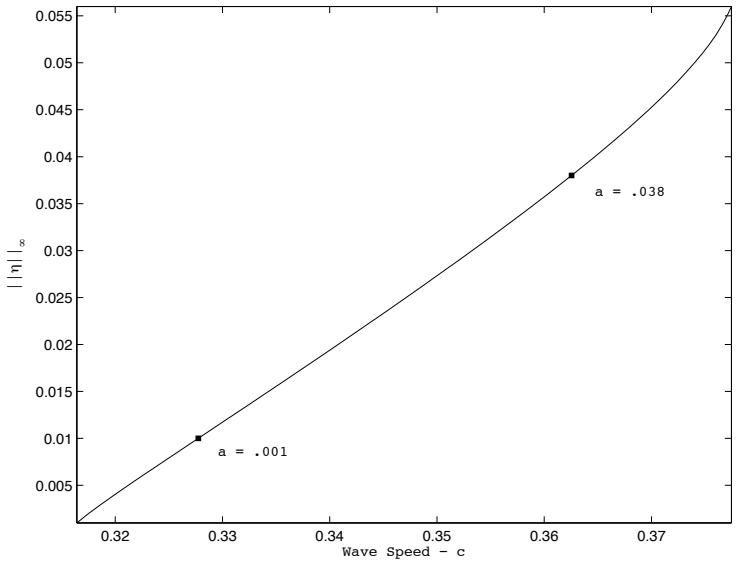

Figure 4.5: Bifurcation curve of amplitude vs. wave speed for $h = .1$.

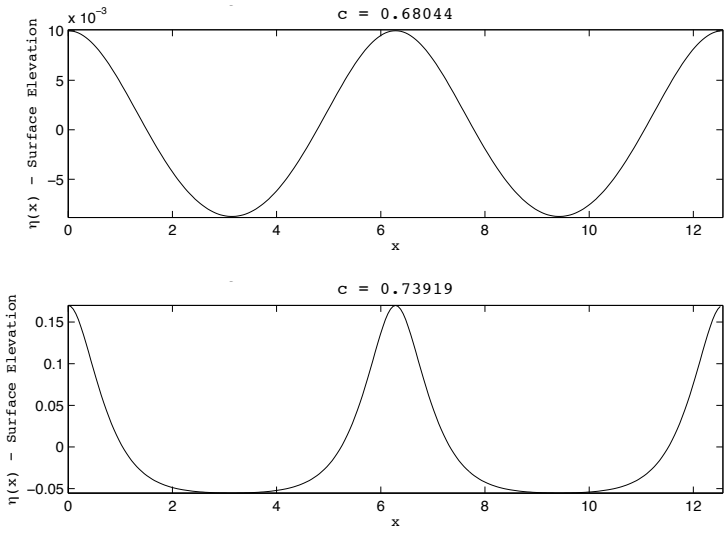

Figure 4.6: Solutions for $h = .5$ with amplitudes $a = .01$ (top) and $a = .17$ (bottom). Both solutions are calculated with $N = 64$ Fourier modes. The residual error for both approximations was less than 10^{-14}. Corresponding wave speeds and norms are marked on the bifurcation curve shown in Figure 4.7

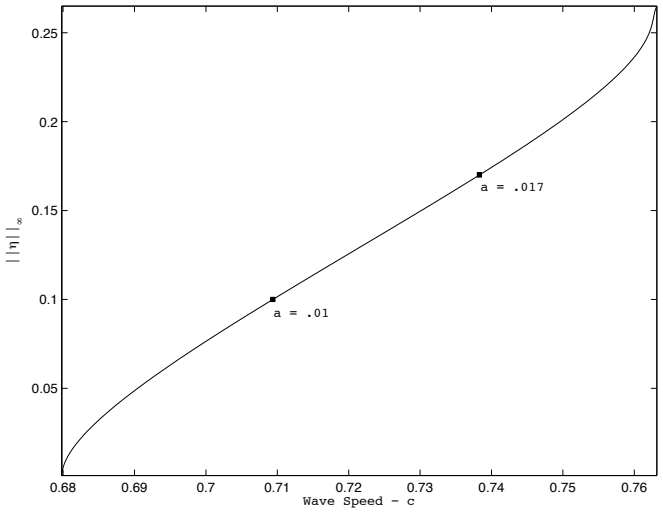

Figure 4.7: Bifurcation curve of amplitude vs. wave speed for $h = .5$.

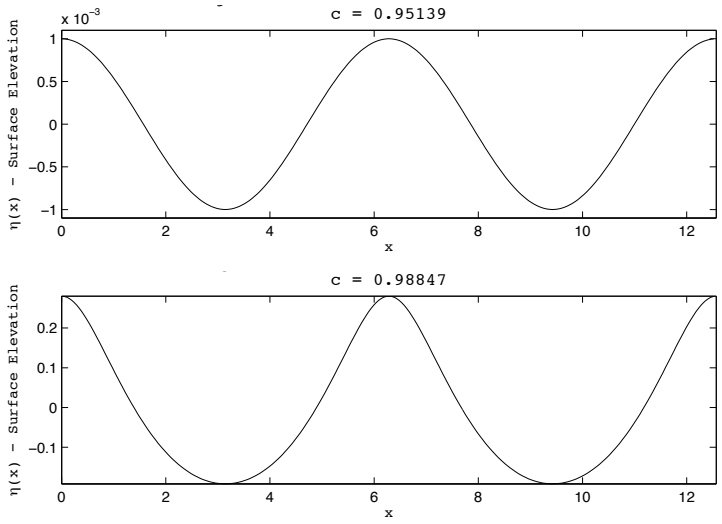

Figure 4.8: Solutions for $h = 1.5$ with amplitudes $a = .001$ (top) and $a = .28$ (bottom). Both solutions are calculated with $N = 64$ Fourier modes. The residual error for both approximations was less than 10^{-13}. Corresponding wave speeds and norms are marked on the bifurcation curve shown in Figure 4.9

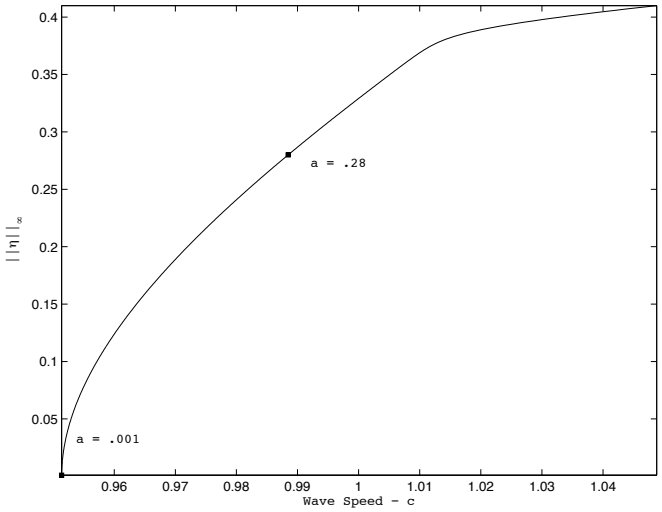

Figure 4.9: Bifurcation curve of amplitude vs. wave speed for $h = 1.5$.

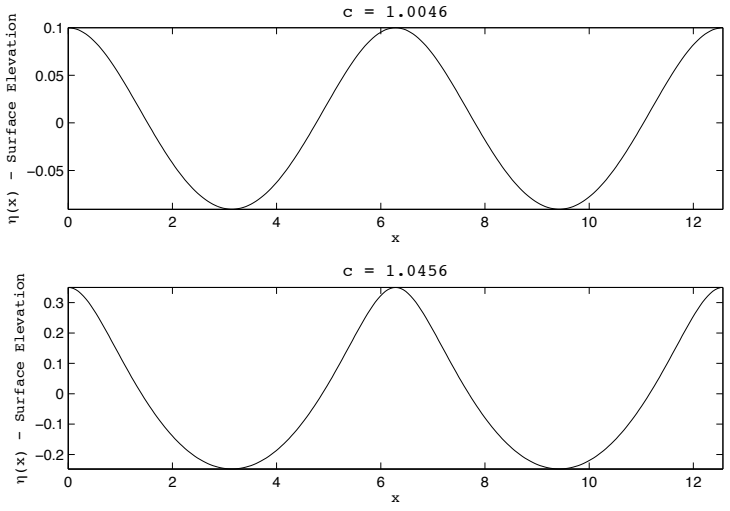

Figure 4.10: Solutions for $h = \infty$ with amplitudes $a = .1$ (top) and $a = .35$ (bottom). Both solutions are calculated with $N = 64$ Fourier modes. The residual error for both approximations was less than 10^{-14}. Corresponding wave speeds and norms are marked on the bifurcation curve shown in Figure 4.11

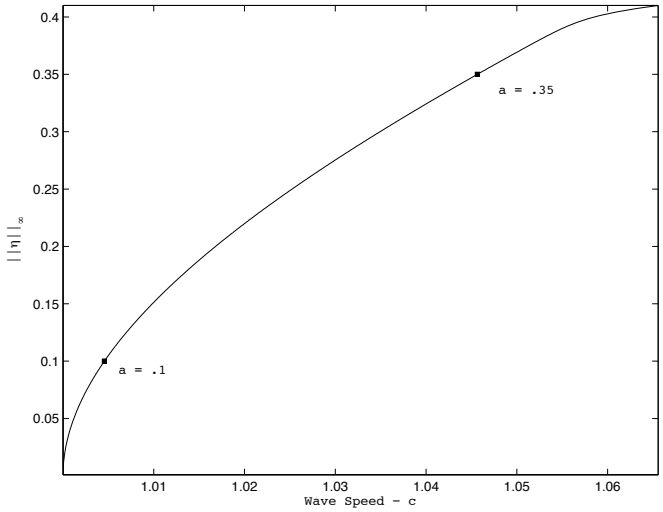

Figure 4.11: Bifurcation curve of amplitude vs. wave speed for $h = \infty$.

to approximately 99% of the maximal wave height. However, since we are using Fourier series to determine solutions numerically, it is expected that our method would break down near the limiting wave.

Chapter 5

Stability of Traveling Wave Solutions in One Spatial Dimension

In this chapter, the stability of periodic traveling wave solutions to Euler's equations is determined using Hill's Method. We first introduce the concepts of stability, and explain Hill's Method applied to a general nonlinear evolution equation. Next, we will adapt the method for the non-local formulation of Euler's equations so that Hill's Method can be applied to the equations in order to determine the stability of the traveling wave solutions. Finally, we discuss the numerical implementation and stability results.

5.1 Stability of Traveling Wave Solutions

The problem we aim to consider is a reformulation of a set of partial differential equations. Before we discuss the method we use to determine stability, we define the concept of stability for partial differential equations and how it relates to the long-time behavior of solutions.

5.1.1 Stability of Solutions to Partial Differential Equations

Consider the evolutionary partial differential equation

$$u_t = \mathcal{N}u,$$

where $\mathcal{N}$ is a nonlinear operator of u and all of its x derivatives. We linearize about a stationary solution u_0[1] by letting $u(x,t) = u_0(x) + \epsilon u_1(x,t) + \mathcal{O}(\epsilon^2)$ where $\epsilon << 1$. To leading order, all terms vanish since $u_0(x)$ is a stationary solution. We drop terms of order ϵ^2 and higher leaving us with

[1] A stationary solution $u_0(x,)$ is a solution that does not depend on time. In other words, $u_0(x)$ satisfies $\mathcal{L}u_0 = 0$.

the linear evolution equation

$$u_{1,t} = \mathcal{L}(u_0)u_1,$$

at order ϵ where $\mathcal{L}$ is a linear operator of x-derivatives with variable coefficients that are functions of the stationary solution $u_0(x)$. Our aim is to determine the growth rates in time, so we can use separation of variables to separate the time dependent and time independent parts since the equation does not depend explicitly on t. Let $u_1(x,t) = U(x)T(t)$. Substituting this into the above linear evolution equation yields

$$T'(t)U(x) = T(t)\mathcal{L}(u_0)U(x),$$

where $T(t)$ can be pulled outside of the operator $\mathcal{L}$ since it has no effect on the time dependent portion of the dynamics. Dividing both sides of the equation by $T(t)$ and $U(x)$ gives

$$\frac{T'(t)}{T(t)} = \frac{\mathcal{L}(u_0)U(x)}{U(x)}.$$

Since the left hand side of the above equation depends only on t and the right hand side depends only on x, both the left and right hand sides of the above equation must be equal to some constant λ. Therefore, $T(t) = e^{\lambda t}$. This yields the following eigenvalue problem for $U(x)$

$$\lambda U(x) = \mathcal{L}U(x).$$

The time dependence of these product solutions is exponentially dependent on λ. If λ has a positive real part, the linear approximation of the solution will grow in time and thus the perturbed solution will exponentially diverge from the stationary solution in the linear approximation. With this intuition in mind, we now define the concept of spectral stability.

Definition 2 (Spectral Stability)**.** *An equilibrium solution $u_0(x)$ of a dynamical system $u_t = \mathcal{N}(x, u, u_x, \ldots)$ is spectrally stable if the spectrum of the linear operator obtained by linearizing $\mathcal{N}$ around $u_0(x)$ has no strictly positive real part.*

In order to use this definition, we need to define the spectrum of a linear operator.

Definition 3 (Spectrum of a Linear Operator)**.** *The spectrum of the linearized operator $\mathcal{L}$ is given by*

$$\sigma(\mathcal{L}) = \{\lambda \in \mathbb{C} : ||v(x)|| < \infty\}, \tag{5.1}$$

where v satisfies $\lambda v = \mathcal{L}v$.

The spectra is the set of all λ values so that $v(x)$ is a bounded solution to $\mathcal{L}v = \lambda v$. Once we have determined the spectrum, we can conclude spectral instability if any of the elements of $\sigma(\mathcal{L})$ have positive real parts.

Remark 14. *Before we proceed to discuss our method of determining spectral stability, we remark about the classes of stability. In the grand scheme of proving stability of an equilibrium solution to a nonlinear evolution equation, there are three main classes of stability. They are*

- *spectral stability*

- *linear stability*

- *nonlinear stability*

Spectral stability is by far the weakest form of stability. It simply states that there are no exponentially growing instabilities for local perturbations. Linear stability takes this a step further and states that there are also no algebraically growing instabilities for local perturbations. The strongest form of stability for stationary solutions of evolution equation is orbital stability which explicitly shows that in some appropriate norm, the perturbed solution remains "close" to the original solution. Due to the complicated nature of the equations we are planning to investigate, we restrict ourselves to examining spectral stability as it is the easiest of the three to examine.

5.2 A Method for Determining the Spectral Stability of Periodic Stationary Solutions

Hill's method is a method for numerically determining the spectral stability of periodic stationary solutions. It starts with the linearization of the nonlinear operator $\mathcal{N}$ about a stationary periodic solution. At the heart of this method is the exploitation of the periodic structure of the resulting linearized operator $\mathcal{L}$. This allow use of Floquet's theorem to further decompose the class of perturbations into a periodic part and a part that is quasi-periodic with respect to the period of the stationary solution. Using a Fourier decomposition, the problem is further decomposed to generate a bi-infinite eigenvalue problem. By the inherent nature of the Fourier decomposition, this formulation of the stability problem has the distinct advantage of being easily programmed in a spectrally convergent manner. This method is discussed in great detail in [20, 22], however, for completeness, we present it again here.

5.2.1 Problem Formulation

Our main interest is to consider the stability of a periodic stationary solution $u_0(x)$ with period L which solves the evolution equation

$$u_t = \mathcal{N}(x, u, u_x, u_{xx}, \ldots), \qquad u(0,t) = u(L,t), \qquad u \in \mathbb{R}^n. \tag{5.2}$$

In order to determine the spectral stability of the solution u_0, one needs to determine the spectrum of the associated linear operator $\mathcal{L}(u_0)$ obtained by linearizing about the solution u_0. Proceeding as we did in the previous section, the spectrum is determined by the eigenvalue problem for the time-independent portion of the solution

$$\lambda U(x) = \mathcal{L}(u_0)U(x). \tag{5.3}$$

Remark 15. *Since the solution we are linearizing about is a periodic solution with minimal period L, the variable coefficient functions of the linearized operator $\mathcal{L}(u_0)$ will also be periodic with the same period.*

In order to conclude spectral stability/instability, we need to determine the spectrum associated with the linearized operator. By definition of the spectrum, we are only interested in bounded eigenfunctions $U(x)$. Thus, we need to determine the values of λ that yield bounded periodic solutions $U(x)$. Since coefficients of the differential equation (5.3) are periodic with period L, we can decompose the solution $U(x)$ even further by use of Floquet's Theorem as found in [52].

Theorem 2 (Floquet's Theorem)**.** *Consider the linear homogeneous differential equation*

$$y' = A(x)y,$$

for some square matrix $A(x)$ of complex continuous functions such that $A(x) = A(x+L)$. Then any fundamental matrix of the system $\Phi(x)$ can be decomposed as

$$\Phi(x) = \hat{\Phi}(x)e^{Rx},$$

where $\hat{\Phi}(x) = \hat{\Phi}(x+L)$, $\hat{\Phi}(x)$ is non-singular, and R is a constant matrix.

Based on this theorem, we know that $U(x)$ is of the form

$$U(x) = e^{Rx}v(x),$$

where $v(x)$ is periodic with period L.

Since the spectrum is defined by the set of all λ values so that (5.3) has bounded solutions $U(x)$, the problem can be reduced to examining the relationship between λ and R as $U(x)$ is the product of a periodic bounded function and an exponential function dependent on R. The only condition that results in bounded solutions for all $x \in \mathbb{R}$ is that the Floquet exponents (the eigenvalues of R) are purely imaginary. Thus every bounded solution of (5.3) is of the form

$$U(x) = e^{i\mu x}v(x),$$

where $v(x)$ is periodic with period L, $\mu \in \left[-\frac{\pi}{L}, \frac{\pi}{L}\right)$.

Using the above decomposition of $U(x)$, (5.3) becomes

$$\lambda v(x) = \mathcal{L}_1(u_0)v(x), \tag{5.4}$$

where

$$\mathcal{L}_1 = \sum_{j=0}^{M} f_j(u_0)\left(\partial_x + i\mu\right)^j.$$

5.2.2 Fourier Decomposition

Since $v(x)$ and $f_j(u_0)$ for $j \in \{0, \ldots, N\}$ are periodic with the same period L, they can be expanded in Fourier Series with the same period L. In other words, given a function $g(x)$ that is periodic with period L, the Fourier series representation is given as

$$g(x) = \sum_{j=-\infty}^{\infty} \hat{g}_j e^{2i\pi jx/L},$$

where the jth Fourier coefficient is

$$\hat{g}_j = \int_0^L e^{-2i\pi jx/L} g(x) dx.$$

Taking the nth Fourier coefficient of each side of (5.4) yields:

$$\begin{aligned}
\lambda \hat{v}_n &= \int_0^L e^{-2i\pi nx/L} \mathcal{L}_1(u_0) v(x) dx \\
&= \int_0^L e^{-inx/L} \sum_{j=0}^{N} f_j(u_0) \left(\partial_x + i\mu\right)^j dx \\
&= \sum_{j=0}^{N} \sum_{k=-\infty}^{\infty} \sum_{l=-\infty}^{\infty} \hat{f}_{j,n-k} \left(\frac{2i\pi n}{L} + i\mu\right)^j \hat{v}_k \int_0^L e^{-2i\pi nx/L} e^{2i\pi kx/L} e^{2i\pi lx/L} dx.
\end{aligned}$$

Thus, for all $n \in \mathbb{Z}$, we have

$$\lambda \hat{v}_n = \sum_{k=-\infty}^{\infty} \sum_{j=0}^{N} \hat{f}_{j,n-k} \left(\frac{2i\pi n}{L} + i\mu\right)^j \hat{v}_k \quad \forall n \in \mathbb{Z}. \tag{5.5}$$

Let $\hat{V}$ be defined as $[\ldots, \hat{v}_{-2}, \hat{v}_{-1}, \hat{v}_0, \hat{v}_1, \hat{v}_2, \ldots]^T$ and $\hat{\mathcal{L}}$ be the bi-infinite matrix defined as

$$\hat{\mathcal{L}}(\mu)_{n,m} = \sum_{j=0}^{M} \hat{f}_{j,n-k} \left(\frac{2i\pi nx}{L} + i\mu\right)^j.$$

Using this notation, the original eigenvalue problem (5.3) is expressed as the following bi-infinite matrix eigenvalue problem

$$\lambda V = \hat{\mathcal{L}}(\mu) V. \tag{5.6}$$

5.2.3 Truncation of the Bi-infinite Problem

Finding an analytic expression for λ in terms of the solution u_0 is often a very difficult task even incorporating both formulations given by (5.3) and (5.4). In cases where the spectrum is not known analytically, numerical methods are typically used. However, in order to numerically determine eigenvalues λ, we need to truncate the bi-infinite systems of equations to a finite number of Fourier

modes N. This is equivalent to looking at the Fourier coefficients $\hat{v}_j$ for $j \in [-N, N]$ and $\hat{V}_N \in \mathbb{R}^{2N+1}$. Thus, we are only interested in the finite matrix eigenvalue problem

$$\lambda_N \hat{V}_N = \hat{\mathcal{L}}_N(\mu)\hat{V}_n$$

where the N subscript represents the size of the truncated matrix.

Justification for the Truncation and Convergence to the Full Spectrum

The first question one might ask is regarding the convergence of the eigenvalues to the spectrum σ. In other words, in the limit as $N \to \infty$, does $\lambda_N \to \sigma(\mathcal{L})$? This problem was addressed in a recent paper by Deconinck and Curtis [20]. They proved that for linear operators of the form

$$\mathcal{L}u = \partial_x^p u + \sum_{n=0}^{\infty} f_n(x)\partial_x^n u$$

where all of the $f_j(x)$ are smooth periodic functions, Hill's method will converge. Specifically, as the size of the truncated problem becomes larger, (i) the method only produces eigenvalues that are in the spectrum of $\mathcal{L}$ and (ii) in the case where $\mathcal{L}$ is self adjoint, the method produces the full spectrum. Likewise, in the case where $\mathcal{L}$ is self-adjoint, the convergence rate of the eigenvalues is faster than$\mathcal{O}(N^{-q})$ for all $q \geq 1$. Thus, we have confidence in the numerical method to produce no spurious modes, and in the case of self-adjoint operators, Hill's method will converge to the full spectrum at a rate beyond all orders of $1/N$.

5.2.4 Numerical Implementation

In order to compute the spectrum numerically using this algorithm, we decompose the method into the following steps:

- Determine a stationary solution.
- Linearize the nonlinear operator about this solution and determine the appropriate eigenvalue problem.
- Fix a series of Floquet Parameters μ_j such that $\mu_j \in \left[\frac{-\pi}{L}, \frac{\pi}{L}\right)$.
- Expand $v(x)$ in a Fourier Series truncated after N modes.
- Compute the eigenvalues λ_j for each μ_j.

The set of all eigenvalues is our numerical approximation to the spectrum of the operator linearized about the stationary solution. In certain scenarios, we can reduce the number of computations necessary to calculate the full spectra by a factor of two with the same resolution in μ. If in our linearization the function $f_j(u_0)$ are strictly real valued, we can reduce the range of Floquet exponents μ_j by half as stated in the following theorem:

Theorem 3 (Floquet Parameter Reduction)**.** *Consider the general problem of the form*

$$\mathcal{L}_1 v = \lambda v,$$

where $\mathcal{L}_1$ *is of the form*

$$\mathcal{L} = \sum_{j=0}^{M} f_j(u_0) \left(\partial_x + i\mu\right)^j,$$

and $f_j(u_0)$ *is purely real. Then, by symmetry, if* (λ, v) *is an eigenvalue/eigenfunction pair for the Floquet parameter* $\mu = \mu_1$*, then* (λ^*, v^*) *is an eigenvalue/eigenfunction pair for the Floquet parameter* $\mu = -\mu_1$*.*

Proof. Without loss of generality, we assume that $L = 2\pi$. If λ is an eigenvalue when $\mu = \mu_1$, then λ satisfies

$$\lambda v = \sum_{j=0}^{M} f_j(u_0) \left(\partial_x + i\mu_1\right)^j v.$$

By taking the complex conjugate of both sides, we see that

$$\begin{aligned} \lambda^* v^* &= \sum_{j=0}^{M} f_j(u_0) \left(\partial_x - i\mu_1\right)^j v^* \\ &= \sum_{j=0}^{M} f_j(u_0) \left(\partial_x + i(-\mu_1)\right)^j v^*. \end{aligned}$$

Thus it is easy to see that if (λ, v) is an eigenvalue/eigenfunction pair for the Floquet parameter $\mu = \mu_1$, then (λ^*, v^*) is an eigenvalue/eigenfunction pair for the Floquet parameter $\mu = -\mu_1$. □

The benefit of this theorem is that for the general problem of the form indicated above, we know that instead of investigating all values of μ inside the interval from $\left(\frac{-\pi}{L}, \frac{\pi}{L}\right]$, we only need to investigate the interval $\mu \in \left[0, \frac{\pi}{L}\right]$, as the remaining eigenvalues/eigenfunction resulting from the negative half of the original interval will simply be the complex conjugate of the eigenvalues/eigenfunctions obtained from the half interval.

5.3 Hill's Method Applied to the AFM Formulation

One of the major objectives of this dissertation is to determine the spectral stability of periodic traveling wave solutions to Euler's equations using the AFM formulation discussed in the second chapter. However, application of Hill's method to AFM requires some careful consideration when dealing with perturbations inside the integral. The next few sections address some of these complications and derive the numerical formulation for Hill's method applied to AFM. We conclude with numerical results for the spectra of periodic traveling wave solutions to Euler's equations.

5.3.1 Linearization

We start the application of Hill's method in the same manner that we did in the general evolution equation case by considering a traveling wave solution

$$\mathcal{F} = (\eta_0(x-ct), q_0(x-ct), c)\,,$$

that solves the equations given in Chapter 3[2]. In the same traveling coordinate frame, we add a small perturbation of the form

$$\begin{aligned} q(x-ct,t) &= q_0(x-ct,t) + \epsilon q_1(x-ct,t) + \mathcal{O}(\epsilon^2), \\ \eta(x-ct,t) &= \eta_0(x-ct,t) + \epsilon \eta_1(x-ct,t) + \mathcal{O}(\epsilon^2), \end{aligned}$$

where ϵ is a small parameter. The perturbations η_1 and q_1 are moving at the same speed and in the same direction as the original traveling wave solution. Our goal is to determine the time dependence of the perturbation in order to determine how the deviation from the original solution evolves.

For simplicity, we replace $x - ct$ with x where η and q are periodic in the new variable x with period 2π. When referring to x in the stationary frame, a specific note will be made. Since we are linearizing about a solution, the terms at $\mathcal{O}(\epsilon^0)$ reduce to zero. and the leading order terms of the equation at $\mathcal{O}(\epsilon)$ are

$$\begin{aligned} q_{1,t} - f_1(\eta_0, q_0)\eta_{1,t} = cq_{1,x} - q_{0,x}q_{1,x} - g\eta_1 - f_2(\eta_0, q_0)\eta_{1,x} \\ + f_1(\eta_0, q_0)\left(-c\eta_{1,x} + q_{0,x}\eta_{1,x} + \eta_{0,x}q_{1,x}\right), \end{aligned}$$

$$\int_0^{2\pi} e^{-ikx} i\eta_{1,t}\mathcal{C}_k dx = \int_0^{2\pi} e^{-ikx}\Big(ic\eta_{1,x}\mathcal{C}_k + ick\eta_{0,x}\eta_1\mathcal{S}_k + q_{1,x}\mathcal{S}_k + q_{0,x}k\eta_1\mathcal{C}_k\Big)dx \qquad k \in \Lambda,$$

where for simplicity and brevity

$$f_1(\eta_0, q_0) = \frac{\eta_{0,x}\,(q_{0,x} - c)}{1 + \eta_{0,x}^2}, \quad f_2(\eta_0, q_0) = f_1^2(\eta_0, q_0),$$

$$\mathcal{S}_k = \sinh(k(\eta_0 + h)), \text{ and } \mathcal{C}_k = \cosh(k(\eta + h)).$$

5.3.2 Separation of Variables

Since the linearization about a solution (η_0, q_0, c) does not specifically depend on time t, we can use separation of variables to isolate the time dependent part of the solution. Let

$$q_1(x,t) = e^{\lambda t}\tilde{q}_1(x), \text{ and } \eta_1(x,t) = e^{\lambda t}\tilde{\eta}_1(x).$$

---

[2]We continue working under the assumption that our traveling wave solution is 2π-periodic

Substituting the separated solution into the linearized equations yields the following generalized eigenvalue problem:

$$\begin{aligned}\lambda\left(\tilde{q}_1 - f_1(\eta_0, q_0)\tilde{\eta}1\right) = c\tilde{q}_{1,x} - q_{0,x}\tilde{q}_{1,x} - g\tilde{\eta}_1 - f_2(\eta_0, q_0)\tilde{\eta}_{1,x} \\ + f_1(\eta_0, q_0)\left(-c\eta_{1,x} + q_{0,x}\eta_{1,x} + \eta_{0,x}q_{1,x}\right),\end{aligned}$$

$$i\lambda\int_0^L e^{-ikx}\tilde{\eta}_1\mathcal{C}_k dx = \int_0^L e^{-ikx}\Big(ic\tilde{\eta}_{1,x}\mathcal{C}_k + ick\eta_{0,x}\tilde{\eta}_1\mathcal{S}_k + \tilde{q}_{1,x}\mathcal{S}_k + q_{0,x}k\tilde{\eta}_1\mathcal{C}_k\Big)dx \quad k \in \Lambda.$$

5.3.3 Floquet Decomposition

Since all of the coefficients in the linear problem are periodic in x with the same fundamental period 2π, we can use Floquet's Theorem as outlined in the previous section. We can justify the use of the theorem inside an integral equation simply by noting the equivalence between the DNO and AFM formulation. As such, we proceed by obtaining all possible bounded perturbations with the following decomposition:

$$\tilde{q}_1(x) = e^{i\mu x}\bar{q}_1(x), \text{ and } \tilde{\eta}_1(x) = e^{i\mu x}\bar{\eta}_1(x),$$

where $\bar{q}_1(x)$ and $\bar{\eta}_1(x)$ are periodic with period 2π. However, in order to proceed with Floquet's Theorem, the original non-local equation needs to be reformulated to allow for perturbations that have a different period than that of the fundamental solution[3]. We break down the Floquet decomposition into two steps: (i) the Floquet decomposition of the local equation, and (ii) Floquet decomposition of the non-local equation.

Local Equation Floquet Decomposition

Substituting the new Floquet decomposition directly into the separation of variable formulation of the local equation, we obtain

$$\begin{aligned}\lambda\left(\bar{q}_1 - f_1(\eta_0, q_0)\bar{\eta}_1\right) = (c - q_{0,x})\left(i\mu + \partial_x\right)\bar{q}_1 - g\bar{\eta}_1 - f_2(\eta_0, q_0)\left(i\mu + \partial_x\right)\bar{\eta}_1 \\ + f_1(\eta_0, q_0)\left(-c\left(i\mu + \partial_x\right)\bar{\eta}_1 + q_{0,x}\left(i\mu + \partial_x\right)\bar{\eta}_1 + \eta_{0,x}\left(i\mu + \partial_x\right)\bar{q}_1\right).\end{aligned} \tag{5.7}$$

Non-local Equation Floquet Decomposition

In order to perturb the non-local equation with periodic perturbations of arbitrary period, we reformulate the integral from one over a fundamental period cell to an average value on the whole line. This allows us to eliminate the integration over a fixed period that would be related (in a complicated way) to the parameter μ. It should be noted that if the solution is periodic and satisfies

[3]In a typical linear differential equation, when a Floquet decomposition is introduced ($f(x) = e^{i\mu x}g(x)$ where $g(x)$ is periodic with the same period as the coefficients) the exponential term $e^{i\mu x}$ cancels out of the equation and can be ignored. However, the Floquet exponential will play a role in the lattice we use in our integral equation.

the non-local spectral equation, it will also satisfy the average value equation over the full line for any k. Let

$$\langle f(x)\rangle = \lim_{M\to\infty}\frac{1}{M}\int_{-M/2}^{M/2} f(x)dx$$

Upon reformulating the problem as an average value over the whole line, we find

$$\begin{aligned}\left\langle e^{-i(k-\mu)x}\mathcal{S}_k\bar{\eta}_1\right\rangle &= \Big\langle e^{-i(k-\mu)x}\big(ic\left(i\mu+\partial_x\right)\bar{\eta}_1\mathcal{C}_k \\ &\quad +ick\eta_{0,x}\bar{\eta}_1\mathcal{S}_k+\left(i\mu+\partial_x\right)\bar{q}_1\mathcal{S}_k+q_{0,x}k\bar{\eta}_1\mathcal{C}_k\big)\Big\rangle. \end{aligned} \tag{5.8}$$

5.3.4 Fourier Decomposition

Using the previous decomposition, we represent the 2π-periodic eigenfunctions $\bar{q}_1$ and $\bar{\eta}_1$ by their Fourier series. In other words, let

$$\bar{q}_1(x)=\sum_{m=-\infty}^{\infty}\hat{Q}_m e^{imx},\text{ and }\bar{\eta}_1(x)=\sum_{m=-\infty}^{\infty}\hat{N}_m e^{imx}.$$

We represent the periodic variable coefficient functions by their Fourier Series as well. Substituting these expressions into the Floquet decomposition given in 5.7 and 5.8, we are able to determine a bi-infinite matrix eigenvalue problem, where the eigenvectors are the Fourier coefficients $\hat{Q}_j$ and $\hat{N}_j$ for $j\in\{0,\pm1,\pm2,\ldots\}$. Obtaining the Fourier decomposition for the local problem is straight forward, however the decomposition for the non-local equation requires some care. We separate the decomposition into two separate sections.

Fourier Decomposition of the Local Equation

The local equation becomes

$$\begin{aligned}&-g\hat{N}_n+\sum_{m=-\infty}^{\infty}\left(i\mu+im\right)\hat{F}_{1,n-m}\hat{N}_m+\sum_{m=-\infty}^{\infty}\hat{F}_{2,n-m}\left(i\mu+im\right)\hat{Q}_m \\ &\quad=\lambda\left(\sum_{m=-\infty}^{\infty}\hat{F}_{3,n-m}\hat{N}_m-\hat{Q}_n\right).\end{aligned} \tag{5.9}$$

where the coefficients $\hat{F}_{j,n}$ are given by the following expressions

$$\begin{aligned}\hat{F}_{1,n} &= \int_0^L e^{-\frac{2in\pi x}{L}}f_1(\eta_0,q_0)\left(q_{0,x}-c-\eta_{0,x}f_1(\eta_0,q_0)\right)dx,\\ \hat{F}_{2,n} &= \int_0^L e^{-\frac{2in\pi x}{L}}\left(q_{0,x}-c-\eta_{0,x}f_1(\eta_0,q_0)\right)dx,\\ \hat{F}_{3,n} &= \int_0^L e^{-\frac{2in\pi x}{L}}f_1(\eta_0,q_0)dx.\end{aligned}$$

Fourier Decomposition of the Non-local Equation

Substituting the Fourier Series into the non-local equation and representing all variable coefficients by their Fourier series representation as well, we have

$$\Big[\sum_{j=-\infty}^{\infty}\sum_{m=-\infty}^{\infty}\left(\hat{G}_{1,j}^{(k)}+ic(i\mu+im)\hat{G}_{2,j}^{(k)}\right)\hat{N}_m+\sum_{j=-\infty}^{\infty}\sum_{m=-\infty}^{\infty}(i\mu+im)\hat{G}_{3,j}^{(k)}\hat{Q}_m\Big]\langle E\rangle$$
$$=i\lambda\sum_{j=-\infty}^{\infty}\sum_{m=-\infty}^{\infty}\hat{G}_{2,j}^{(k)}\hat{N}_m\langle E\rangle \tag{5.10}$$

where

$$\begin{aligned}\hat{G}_{1,n}^{(k)} &= \int_0^L e^{-\frac{2in\pi x}{L}}\left(kq_{0,x}\mathcal{C}_k+ickη_{0,x}\mathcal{S}_k\right)dx,\\ \hat{G}_{2,n}^{(k)} &= \int_0^L e^{-\frac{2in\pi x}{L}}\left(\mathcal{C}_k\right)dx,\\ \hat{G}_{3,n}^{(k)} &= \int_0^L e^{-\frac{2in\pi x}{L}}\left(ic\mathcal{S}_k\right)dx,\end{aligned}$$

and $\mathcal{S}_k$ and $\mathcal{C}_k$ are given earlier.

Each term in the doubly-infinite sum contains the average value of E defined above. The average value of this integral is identically zero unless the exponent is a multiple of 2π. In other words, the contribution from the integral is identically zero unless

$$k=\mu+n \qquad ,\forall n\in\mathbb{Z}.$$

Thus, we see that the only contribution in the integral equation occurs when k is a shift of the original dual lattice. Substituting this relationship into the exponent, we are left with the integral

$$\int_{-M/2}^{M/2}\exp\left[ix\left(j+m-n\right)\right]dx.$$

As before, this integral is identically zero unless $j+m-n=0$ and one otherwise. This allows us to collapse the double infinite sum to a single infinite sum given by

$$\begin{aligned}&\sum_{m=-\infty}^{\infty}\left(\hat{G}_{1,n-m}^{(k(\mu))}+ic(i\mu+im)\hat{G}_{2,n-m}^{(k(\mu))}\right)\hat{N}_m\\ &\quad+\sum_{m=-\infty}^{\infty}(i\mu+im)\hat{G}^{(k(\mu))}(\mu+n)_{3,n-m}\hat{Q}_m\\ &\quad=i\lambda\sum_{m=-\infty}^{\infty}\hat{G}_{2,n-m}^{(k(\mu))}\hat{N}_m,\end{aligned} \tag{5.11}$$

which is true for all $n\in\mathbb{Z}$.

Combining the above equation with (6.6) yields a generalized bi-infinite eigenvalue problem for determining the spectrum of the linearized operator about the stationary traveling wave solutions.

We define the quantity $\hat{\mathbf{X}}$ as a bi-infinite vector of the Fourier coefficients $\hat{Q}_j$ and $\hat{N}_j$ for all $j \in \mathbb{Z}$ such that $\hat{\mathbf{X}} = \left[\ldots, \hat{N}_{-1}, \hat{N}_0, \hat{N}_1, \ldots \hat{Q}_{-1}, \hat{Q}_0, \hat{Q}_1, \ldots\right]^T$. With this notoation, we can rewrite the Fourier decomposition in the following matrix form:

$$\begin{bmatrix} A(\mu) & B(\mu) \\ C(\mu) & D(\mu) \end{bmatrix} \hat{\mathbf{X}} = \lambda \begin{bmatrix} 0 & S(\mu) \\ -I & V(\mu) \end{bmatrix} \hat{\mathbf{X}},$$

where

$$A(\mu)_{n,m} = -g\delta(n-m) + (i\mu + im)\,\hat{F}_{1,n-m}, \quad B(\mu)_{n,m} = \hat{F}_{2,n-m}\,(i\mu + im)\,,$$

$$C(\mu)_{n,m} = \hat{G}^{(k(\mu))}_{1,n-m} + ic(i\mu + im)\hat{G}^{(k(\mu))}_{2,n-m}, \quad D(\mu)_{n,m} = (i\mu + im)\hat{G}^{(k(\mu))}_{3,n-m}$$

$$S(\mu)_{n,m} = \hat{F}_{3,n-m}, \quad \text{and} \quad V(\mu)_{n,m} = i\hat{G}^{(k(\mu)}_{2,n-m}.$$

Since the time dependence of the surface evolution showing up in a nonlinear way in the equation for the evolution of the velocity potential at the surface, we are not solving a typical eigenvalue problem of the form $\lambda u = Mu$. Instead, we must solve a generalized eigenvalue problem of the form $\lambda N u = Mu$. We can solve the generalized eigenvalue problem numerically by truncating the Fourier series representation from $\mathbb{Z}$ to $\{0, \pm 1, \pm 2, \ldots \pm N\}$. Thus, we obtain $2(2N+1)$ equations for the $2(2N+1)$ unknown Fourier coefficients $\hat{Q}_n$ and $\hat{N}_n$.

Remark 16. *At this point, we should note that there is a singularity at $\mu = 0$. From before, we know that the non-local equation is as long as $k \neq 0$. For the problem posed over the whole line, the same holds as an average value. Since $k = \mu + m$, the only case where $k = 0$ is when both μ and n are equal to zero (the equation for the zeroth Fourier mode of the non-local equation when $\mu = 0$). In this situation, there is one less equation from the non-local equation, yet we still have $2(2N+1)$ unknowns. If we examine the zeroth mode of the local equation corresponding to $\mu = 0$, it is obvious that $\lambda = 0$ is a double eigenvalue corresponding to these two equations. Thus, we can eliminate the zeroth Fourier mode equation for both the local and non-local equation when $\mu = 0$. This reduces the number of equations to $2N$. We can also add in the assumption that the average value of the perturbation is zero which results in both being zero. This reduces the number of unknowns to $2N$. At this point, for the case of $\mu = 0$ we proceed as normal to determine the remaining $2N$ eigenvalues.*

Remark 17. *Since we are solving a generalized eigenvalue problem of the form $\mathbf{MX} = \lambda\mathbf{NX}$, we must worry about the invertability of the matrix $\mathbf{N}$. For the AFM formulation, the matrix $\mathbf{N}$ is in block form and can be written as upper triangular. This implies that the determinant of the matrix is given by the product of the block diagonal matrices modulo a sign change due to interchanging rows. Since one of the diagonal matrices is the identity, the determinant of the matrix in question is given by $\det(S(\mu))$ where $S(\mu)$ is defined earlier. For our problem, we numerically determined that the determinant is non-zero for $\mu \neq 0$.*

5.4 Numerical Stability Results

With the Hill's method formulation applied to AFM, we develop a numerical scheme to determine the spectra for the periodic traveling wave solutions in the previous chapter. We begin by making use of the underlying symmetry of our problem to reduce the size of the interval of μ values we need to consider. Then we proceed to outline the numerical implementation, validate our formulation, and present our results on the stability of periodic traveling wave solutions to Euler's equations.

5.4.1 Numerical Simplifications

During the general derivation of Hill's method, it was proved that if all of the linearized coefficient functions were real-valued, the computational domain in μ could be halved. While the coefficient functions for this problem are not strictly real-valued, they do posess a symmetry which allows us to again, reduce the computational domain of μ in half.

Theorem 4 (Floquet Parameter Reduction, AFM)**.** *Consider the Floquet decomposition of AFM, where $\mathcal{F} = (\eta_0, q_0, c)$ is a real valued solution set to the nonlinear traveling wave problem given in the previous chapter. If $(\lambda, \bar{\eta}_1, \bar{q}_1)$ is an eigenvalue/eigenfunction pair for $\mu = \mu_1$, then $(\lambda^*, \bar{\eta}_1^*, \bar{q}_1^*)$ is an eigenvalue/eigenfunction pair for $\mu = -\mu_1$.*

Proof. We prove this for the case where $h = \infty$. The proof for finite depth is identical.

If λ is an eigenvalue when $\mu = \mu_1$, we have

$$\begin{aligned}
\lambda\left(\bar{q}_1 + g_1\bar{\eta}_1\right) &= f_1\left(\partial_x + i\mu_1\right)\bar{q} \\
&\quad + \Big(h_0 + h_1\left(\partial_x + i\mu_1\right) + h_2\left(\partial_x + i\mu_1\right)^2\Big)\bar{\eta}_1, \\
i\lambda\int_0^{2\pi} e^{-imx}e^{|m+\mu_1|\eta_0}\bar{\eta}_1 dx &= \int_0^{2\pi} e^{-imx}e^{|m+\mu_1|\eta_0}\Big(\operatorname{sign}(m+\mu_1)\left(\partial_x + i\mu_1\right)\bar{q}_1 \\
&\quad + i|m+\mu_1|c\eta_{0,x}\bar{\eta}_1 + (m+\mu_1)\,q_{0,x}\bar{\eta}_1 + ci\left(\partial_x + i\mu_1\right)\bar{\eta}_1\Big)dx.
\end{aligned}$$

Taking the complex conjugate of both sides of the equations yields

$$\begin{aligned}
\lambda^*\left(\bar{q}_1^* + g_1\bar{\eta}_1^*\right) &= f_1\left(\partial_x - i\mu_1\right)\bar{q}_1^* \\
&\quad + \Big(h_0 + h_1\left(\partial_x - i\mu_1\right) + h_2\left(\partial_x - i\mu_1\right)^2\Big)\bar{\eta}_1^*, \\
-i\lambda^*\int_0^{2\pi} e^{imx}e^{|m+\mu_1|\eta_0}\bar{\eta}_1^* dx &= \int_0^{2\pi} e^{imx}e^{|m+\mu|\eta_0}\Big(\operatorname{sign}(m+\mu)\left(\partial_x - i\mu_1\right)\bar{q}_1^* \\
&\quad - i|m+\mu_1|c\eta_{0,x}\bar{\eta}_1^* + (m+\mu_1)\,q_{0,x}\bar{\eta}_1^* - ci\left(\partial_x - i\mu_1\right)\bar{\eta}_1^*\Big)dx.
\end{aligned}$$

Focusing specifically on the non-local equation, we multiply through by -1. Additionally, since this equation is valid for all $m \in \mathbb{Z}$, we can replace m with $-m$. This yields

$$i\lambda^* \int_0^{2\pi} e^{-imx} e^{|-m+\mu_1|\eta_0} \bar{\eta}_1^* dx = \int_0^{2\pi} e^{-imx} e^{|-m+\mu_1|\eta_0} \Big(-\text{sign}(-m+\mu_1)\,(\partial_x - i\mu_1)\,\bar{q}_1^* + i\big|-m+\mu_1\big| c\eta_{0,x}\bar{\eta}_1^* - (-m+\mu_1)\,q_{0,x}\bar{\eta}_1^* + ci\,(\partial_x - i\mu_1)\,\bar{\eta}_1^* \Big) dx.$$

Using the fact that $|-m+\mu_1| = |m-\mu_1|$ and $-\text{sign}(-m+\mu_1) = \text{sign}(m-\mu_1)$, we have

$$i\lambda^* \int_0^{2\pi} e^{-imx} e^{|m-\mu_1|\eta_0} \bar{\eta}_1^* dx = \int_0^{2\pi} e^{-imx} e^{|m-\mu_1|\eta_0} \Big(\text{sign}(m-\mu_1)\,(\partial_x - i\mu_1)\,\bar{q}_1^* + i\big|m-\mu_1\big| c\eta_{0,x}\bar{\eta}_1^* + (m-\mu_1)\,q_{0,x}\bar{\eta}_1^* + ci\,(\partial_x - i\mu_1)\,\bar{\eta}_1^* \Big) dx.$$

Combining the above equation with the conjugate of the local equation, we have

$$\lambda^* \left(\bar{q}_1^* + g_1\bar{\eta}_1^*\right) = f_1\,(\partial_x - i\mu_1)\,\bar{q}_1^* + \Big(h_0 + h_1\,(\partial_x - i\mu_1) + h_2\,(\partial_x - i\mu_1)^2\Big)\,\bar{\eta}_1^*,$$

$$i\lambda^* \int_0^{2\pi} e^{-imx} e^{|m-\mu_1|\eta_0} \bar{\eta}_1^* dx = \int_0^{2\pi} e^{-imx} e^{|m-\mu_1|\eta_0} \Big(\text{sign}(m-\mu_1)\,(\partial_x - i\mu_1)\,\bar{q}_1^* + i\big|m-\mu_1\big| c\eta_{0,x}\bar{\eta}_1^* + (m-\mu_1)\,q_{0,x}\bar{\eta}_1^* + ci\,(\partial_x - i\mu_1)\,\bar{\eta}_1^* \Big) dx.$$

This is the same eigenvalue problem for $\mu = -\mu_1$ and thus, if $(\lambda, \bar{\eta}_1, \bar{q}_1)$ is an eigenvalue/eigenfunction pair for $\mu = \mu_1$, then $(\lambda^*, \bar{\eta}_1^*, \bar{q}_1^*)$ is an eigenvalue/eigenfunction pair for $\mu = -\mu_1$. □

The benefit of this theorem is that it again allows us to reduce the interval of μ values we investigate when examining the stability of stationary periodic solutions from $(-.5, .5]$ to $[0, .5]$ as before, even though we do not have a formulation that falls under the general theorem proved in the previous section. Thus the amount of numerical computations is cut in half.

Thus far, we have linearized the AFM formulation about a stationary periodic traveling wave solution. Using separation of variables, we are examining those solutions that behave exponentially. We have introduced a growth rate λ yielding an eigenvalue problem for the determiniation of the spectrum. Using Floquet's theorem, we decomposed all bounded periodic solutions into a 2π-periodic linear differential equation parameterized by the parameter μ which varies over the range $[-.5, .5)$. Using the symmetry in our problem, we only need to examine the parameter values $\mu \in [0, .5]$. At this point, we are left with an eigenvalue problem with 2π-periodic boundary conditions for each μ in our interval. To determine the spectrum, we use a Fourier decomposition to turn the differential equation into a bi-infinite matrix problem that can be truncated and solved numerically. We repeat this process for all μ in our discretized interval $\mu \in [0, .5]$. The collection of all eigenvalues is our numerical approximation to the spectrum. As before, all multiplications are carried out in the physical domain, and all differentiation is carried out in the Fourier domain.

5.4.2 Numerical Convergence and Accuracy

As previously mentioned, before we discuss the stability results, we need to establish confidence in our numerical scheme and approach. While convergence is guaranteed for the class of operators defined in [20], we have re-worked the method and applied it to a different class of operators. We shall not try to establish analytic convergence results for our setting. However, confidence would be increased with knowledge of how the approximation of a particular eigenvalue changes as we increase the size of the truncated problem. In other words, if our method is Cauchy convergent, we would have strong indicators of the consistency and accuracy of our method.

Let λ_N represent a particular eigenvalue corresponding to a truncation size N (which corresponds to $2N+1$ Fourier coefficients). We define the Cauchy error as

$$e_N = ||\lambda_N - \lambda_{N-1}||.$$

Recalling the definition of Cauchy convergence given in the previous chapter, our hope is that we can choose any $\epsilon > \epsilon_{\text{tol}}$ (our allowable tolorance) and show that as we take the size of our truncation large enough, the difference in the approximation of the eigenvalues converges to ϵ_{tol}. For several scenarios, we tracked the approximation of the eigenvalues with the largest real part as a function of truncation size. The Cauchy errors are given in Table 5.4.2.

Table 5.1: Cauchy error for the calculation of the eigenvalue with largest real part for $h = .5$, and two eigenvalues with real parts for $h = 1.5$.

N	$h = .5$	$h = 1.5$	$h = 1.5$
3	5.1036e-05	7.3966e-06	2.9912e-06
4	3.7838e-07	7.9354e-12	7.6283e-10
5	4.6025e-11	2.401e-15	2.1943e-15
6	3.6857e-13	1.7606e-16	1.4463e-16
7	1.8532e-15	1.2409e-15	1.2286e-16
8	3.1619e-16	6.0266e-16	7.2879e-16

As can be seen clearly in the Figures 5.1, and 5.2, the Cauchy error decreases linearly on a logarithmic scale which hints at spectral accuracy. Additionally the figures show that it is not necessary to consider large truncation values. Thus, in general, we can start with a small number of Fourier modes. As the nonlinearity of the traveling wave solution increases (the amplitude a), a larger number of Fourier modes is necessary.

In the case of multiple local maximum eigenvalues, we still demonstrate Cauchy convergence for the dominant growth rates as seen in Figure 5.2.

We note that in general, we only need a small number of Fourier modes to determine the spectrum to high degrees of accuracy. However, for long wave length perturbations, the convergence is much

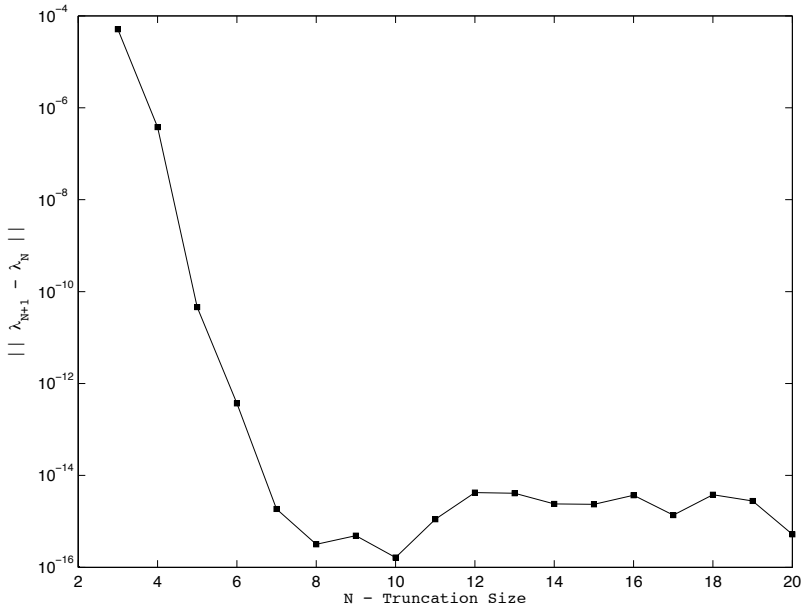

Figure 5.1: Cauchy error for the maximal eigenvalue corresponding to a solution with depth $h = .5$ and amplitude $a = .01$

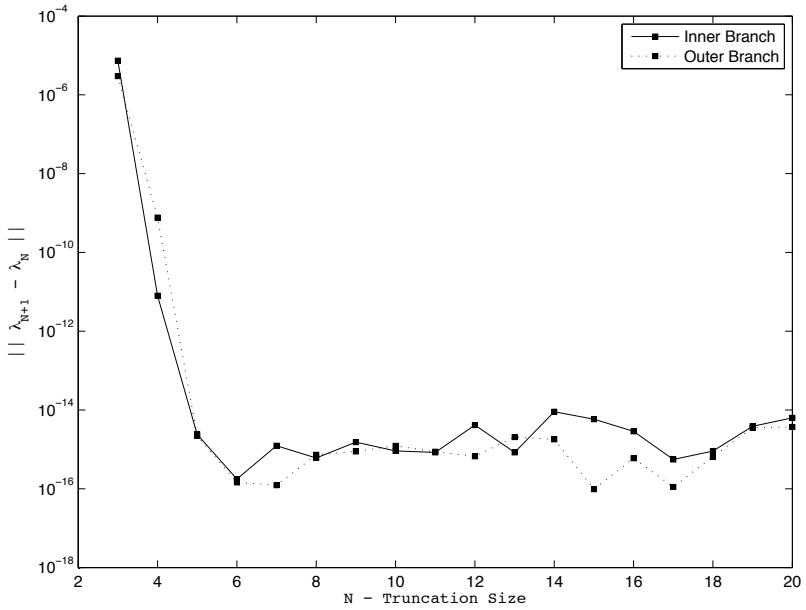

Figure 5.2: Cauchy error for the two local maximum eigenvalues corresponding to a solution with depth $h = 1.5$ and amplitude $a = .01$

slower when there is no instability for μ near zero. Specifically, we consider the case with amplitude $a = .01$ and $h = .5$. For $\mu << 1$, the sequence never quite converges in a Cauchy sense as seen in Figure 5.3 for reasonable error tolerances. Heuristically, this is specific to small μ values when the corresponding eigenvalues near the origin do not have positive real parts. However, for depths $h > 1.363$ when modulational instabilities are present, the convergence rate for small μ values is similar to those shown in Figures 5.1 and 5.2.

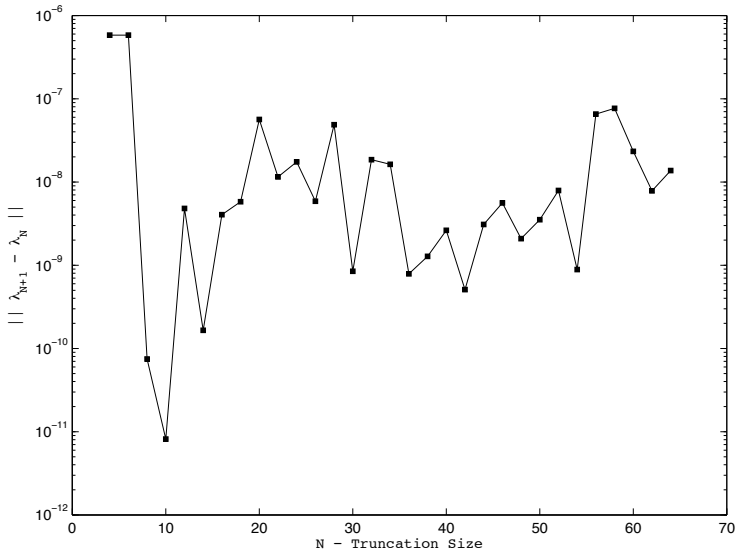

Figure 5.3: Cauchy Error for the largest eigenvalue when $\mu = 10^{-7}$ for $h = .5$ and $a = .01$.

5.5 Full Spectra for Various Depths and Amplitudes

In this section, we present the numerical results on stability, and investigate their properties. We begin by looking at the full spectra for several parameter choices in depth h and amplitude a. We specifically choose to investigate three depths: $h = .5$, $h = 1.5$ and $h = \infty$. These choices give us two depths above and one depth below the critical Benjamin-Feir threshold instability discussed in the introduction.

5.6 Spectra for various depths

We begin the exploration of the spectra by starting with infinite depth since the instabilities in deep water are well known. As mentioned in the introduction, the Nonlinear Schrödinger (NLS) equation was demonstrated to be a valid approximation for waves in deep water. Additionally, one can show that the NLS equation demonstrates the same modulational instability as the full Euler equations for

surface gravity waves (for a summary of these calculations, see [26]). The Benjamin-Feir modulational instability implies that the waves are unstable to long-wave perturbations. Furthermore, analysis for the Nonlinear Schrödinger equation shows that the modulational instabilities emanate from the origin in the complex plane. In other words, the unstable eigenvalues due to long-wave perturbations will be near the origin. Using Hill's method, the spectrum for NLS associated with periodic traveling wave solutions is given in Figure 5.4.

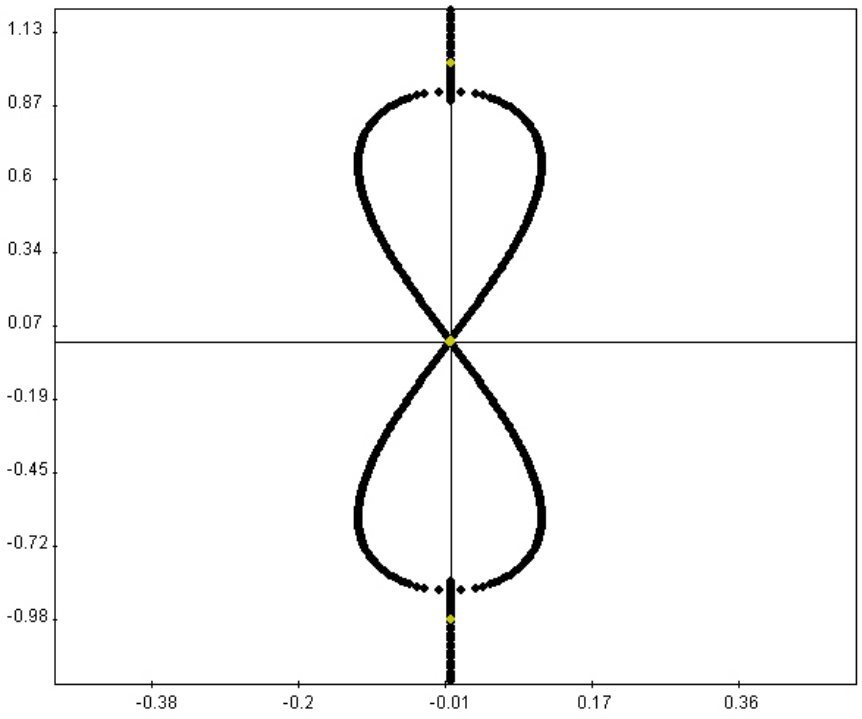

Figure 5.4: Spectrum for the Nonlinear Schrödinger Equation associated with a periodic traveling wave solution. The points in gold correspond to growth rates associated with perturbations of the same wavelength as the original solution ($\mu = 0$).

Calculating the spectrum for a fluid of infinite depth for a solution corresponding to amplitude $a = .01$ yields a remarkably similar spectrum as shown in Figure 5.5. Heuristically, the two spectra are very similar with the exception that the entire imaginary axis remains as part of the spectra for Euler's equations and not for NLS. We also calculate the spectra for $h = 1.5$ which is still above the Benjamin-Feir threshold, so we might expect to see a similar figure-eight spectrum as seen in NLS and Euler's equation in infinite depth. Calculating the spectrum with 32 Fourier modes and $20,000$ different μ slices, we generate the spectrum given in Figure 5.6. There are two main instabilities shown in Figure 5.6. The dominant instability is near the origin. Zooming in on this instability

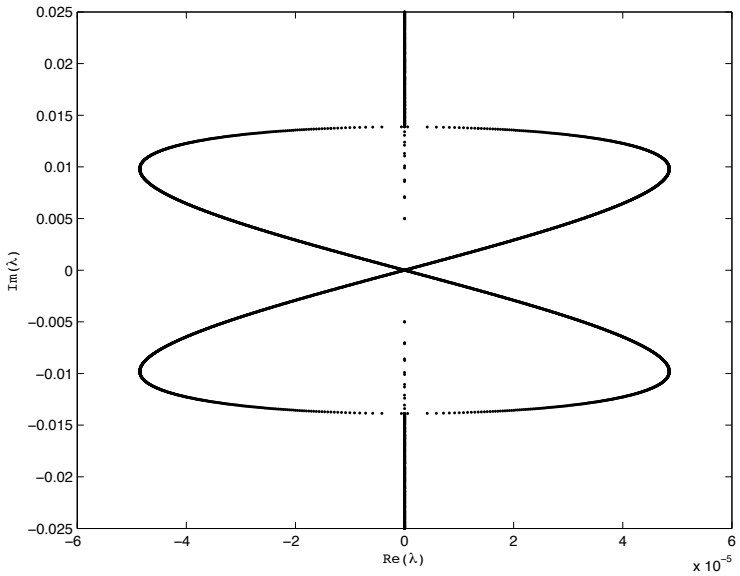

Figure 5.5: Spectrum for $h = \infty$ and $a = .01$

shows that it is the same sort of modulational instability seen in deep water as seen in Figure 5.7. The other instability occurs for shorter wave-length perturbations and is also shown enlarged in Figure 5.7. We refer to this instability and other similar instabilites as "high-frequency instabilities" since the frequency of the growth rate in time (the imaginary part of λ) is larger than that of the modulational instabilities. Finally, we generate the spectrum for $h = .5$ and $a = .01$, which is below the Benjamin-Feir threshold. According to the theory, we should not see modulational instability for small amplitude waves. As seen in Figure 5.8, this is indeed the case. However, even though the solution is stable to long wave perturbations, the solution demonstrates the same high-frequency instabilities that were seen in the case of $h = 1.5$. The more dominant instability can be compared with the instabilities mentioned by McLean and Francius & Kharif [25, 42][4]. However, to our knowledge, the second band of instabilities has not been presented in the literature.

[4]We make a note that the shallow water high-frequency instabilities that we have found do not seem to be explicitly stated in the literature. Several investigations of instability in shallow water explicitly limited to two-dimensions seem to be restricted to (i) long wave perturbations or (ii) highly nonlinear waves near the limiting Stokes wave. The only reference to shallow water instabilities that we have found are limits of transverse perturbations [10,25,42].

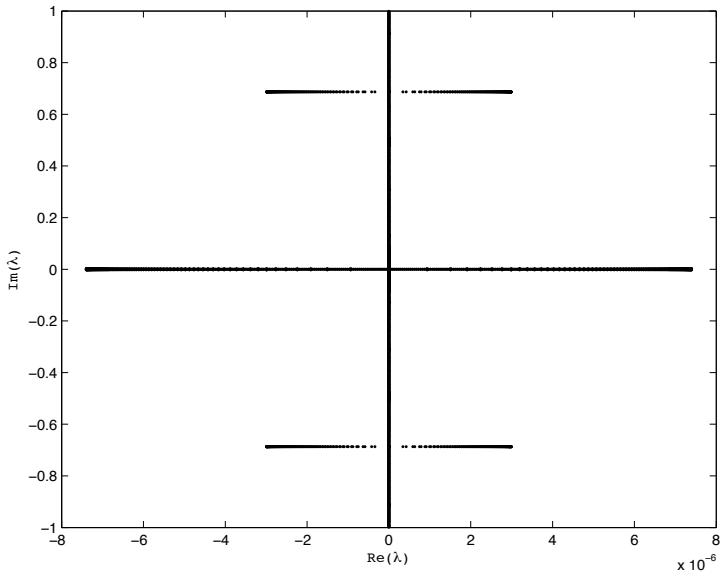

Figure 5.6: Spectrum for $h = 1.5$ and $a = .01$.

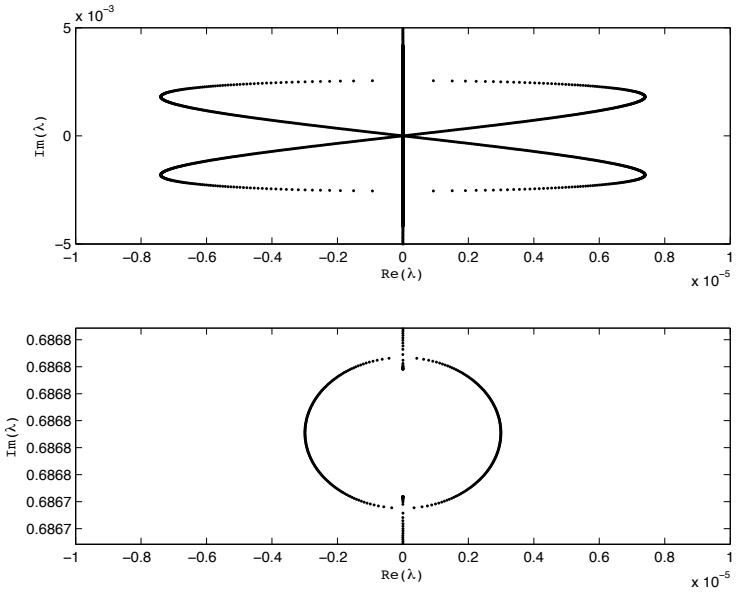

Figure 5.7: Spectrum for $h = 1.5$ and $a = .01$ enlarged near the modulational (top) and high-frequency (bottom) instabilities.

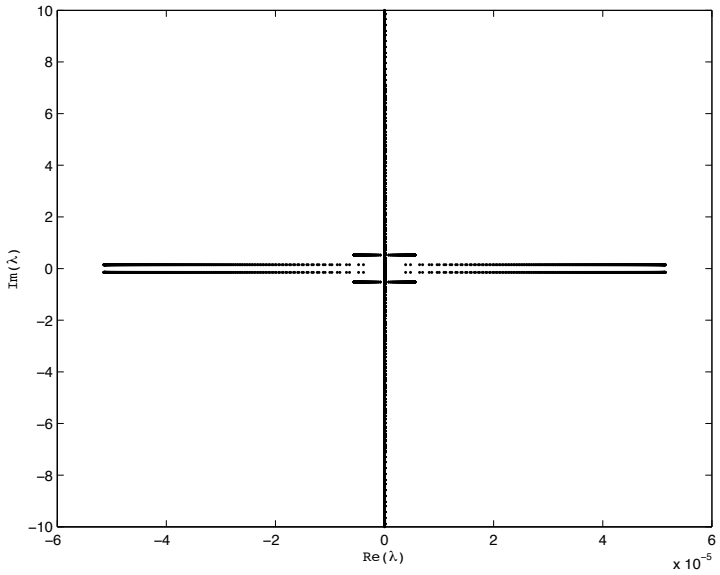

Figure 5.8: Spectrum for $h = .5$ and $a = .01$

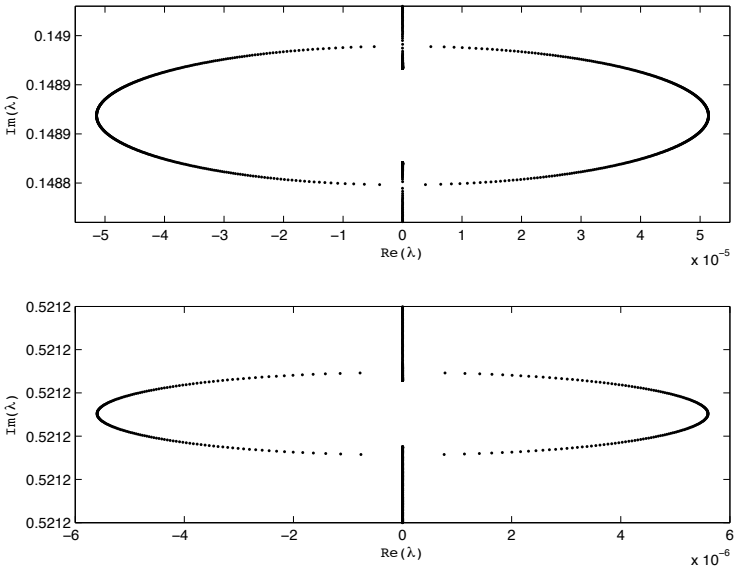

Figure 5.9: Enlargement of the spectrum for $h = .5$ and $a = .01$

We only present sample spectra for three depth categories as the spectra for other parameters within these categories look similar. This is not a suprising fact since Nicholls proved that the

spectrum is analytically dependent on the amplitude of the traveling wave solution. However, investigations into how the spectrum varies as a function of problem parameter are insightful. In the next sections, we address the qualitative behavior of the spectrum as several parameters are varied including the amplitude of the solution and the depth of the fluid.

5.7 Instability as a Function of Amplitude

The individual spectra given in Figures 5.5, 5.6, and 5.8 are interesting and yield information regarding the magnitude of the instability. However, it is sometimes useful to have summarization of the data for a given parameter. For example, in Figure 5.10, we plot the spectra for $h = 1.5$ corresponding to various amplitudes. It is evident from this plot that the amplitude of the instability is growing with the nonlinearity of the solution.

Another useful plot is information regarding the class of perturbations to which the solution is unstable. For example, the spectrum associated with the traveling wave solution with depth $h = .5$ and amplitude $a = .01$, is spectrally unstable as seen in Figures 5.8 and 5.9. However, it would be interesting to see which Floquet exponents give rise to the instability. Furthermore, it is fruitful to determine how the stability changes as the amplitude changes. In Figures 5.11 and 5.12, we demonstrate the instability region as a function of μ vs. a. We note that for $h = .5$ and $a > .038$, there are instabilities associated with μ near zero as seen in Figures 5.11 and 5.12. At first glance, this might seem inconsistent with the Benjamin-Feir result that for depths less than $h_c = 1.363$, solutions do not exhibit instability to long-wave perturbations. However, the Benjamin-Feir instability result is only valid for small-amplitude solutions, which our numerics validate. Thus, since the instability occurs for moderate amplitude solutions, the result is consistent. Furthermore, these results are consistent with the instabilities presented in [9, 10, 25, 42].

5.8 Instability as a Function of Depth

A second litmus test for the validity of our reformulation is the capture of the Benjamin-Feir instability. As mentioned in the introduction, the observation of the Benjamin-Feir instability sparked interest in the stability of Stokes waves. Since the work of the late 1960's, there have been numerous experimental, analytical and numerical investigations to support the instability of Stokes waves when the depth is greater than a critical depth. This instability arises when Stokes wave solutions in dimensionless depths $kh > 1.363$ are perturbed with long wavelength perturbations ($\mu << 1$). For all kh smaller than this critical threshold, the Stokes waves remain stable to modulational perturbations. It is important to realize that this statement is only valid for small μ, so while we can conclude instability of waves in depths greater than the critical threshold, we can make no conclusions regarding the stability of Stokes waves in more shallow fluids.

Our initial goal when investigating the instability as a function of kh was to show that as kh was increased, the eigenvalues corresponding to long wavelength perturbations become unstable when kh crosses the critical threshold $kh = 1.363$. Choosing an arbitrary wave amplitude $a = .01$ and a

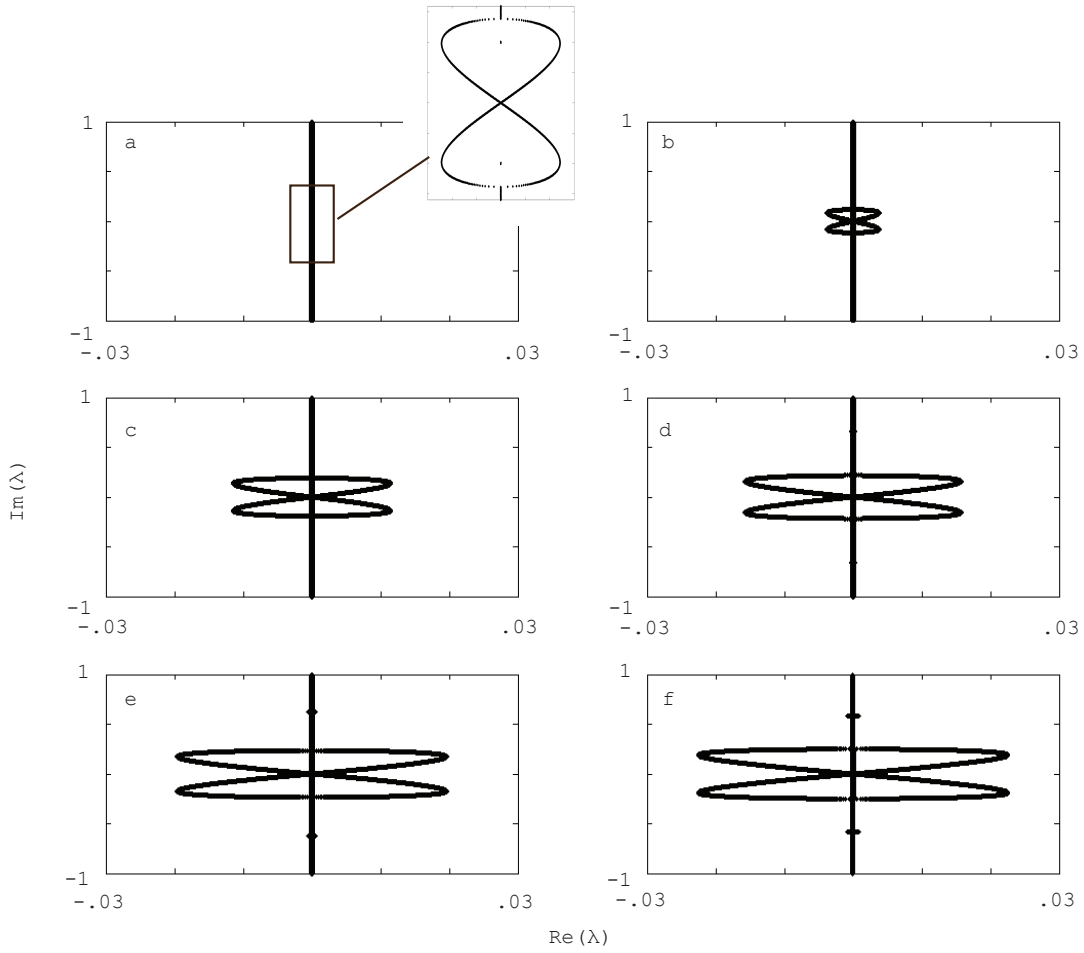

Figure 5.10: Various spectra for $h = \infty$ with different amplitudes. (a) $a = .01$, (b) $a = .1$, (c) $a = .2$, (d) $a = .25$ (e)$h = .3$ (f) $h = .35$

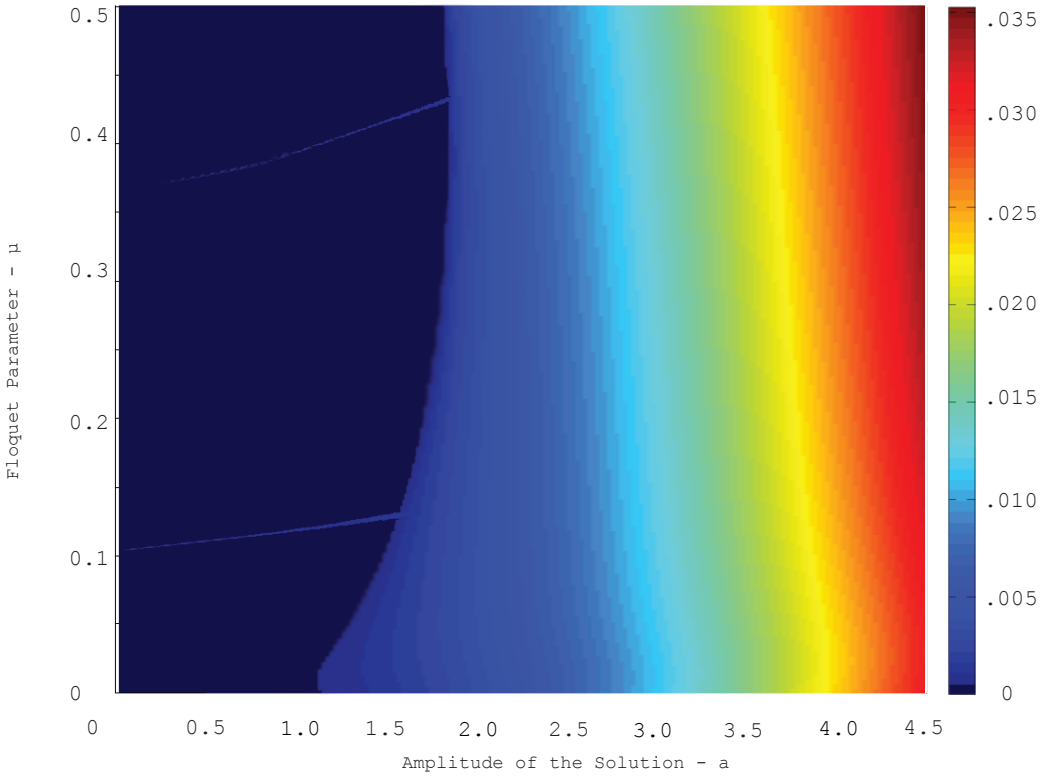

Figure 5.11: Stability regions for $h = .5$. The brighter regions represent regions of larger instability.

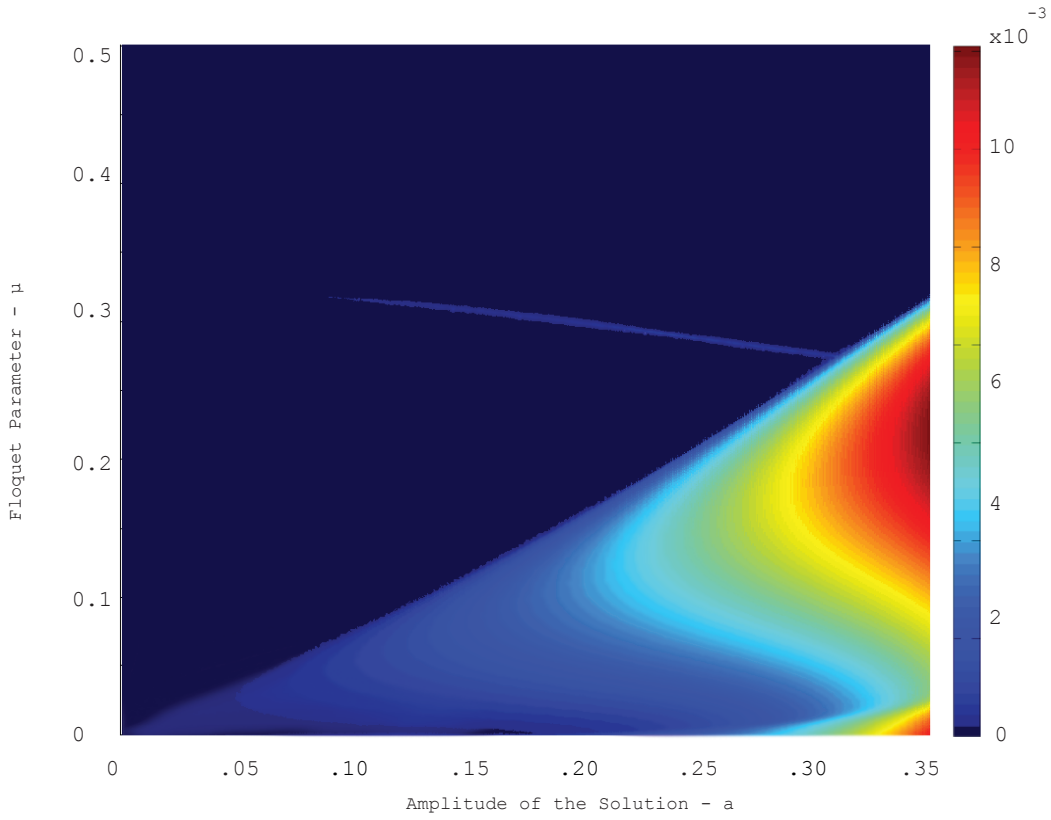

Figure 5.12: Stability regions for $h = 1.5$. The brighter regions represent regions of larger instability.

wave number $k = 1$, we found the corresponding traveling wave solution for a range of depths from $h = .5$ to $h = 2$. Next, we calculate the spectrum for small μ values $\mu \in [0, .01]$ and plotted the real part of the most unstable eigenvalue, as well as the corresponding eigenfunction[5]. This replication of known results increases the confidence in our numerical results.

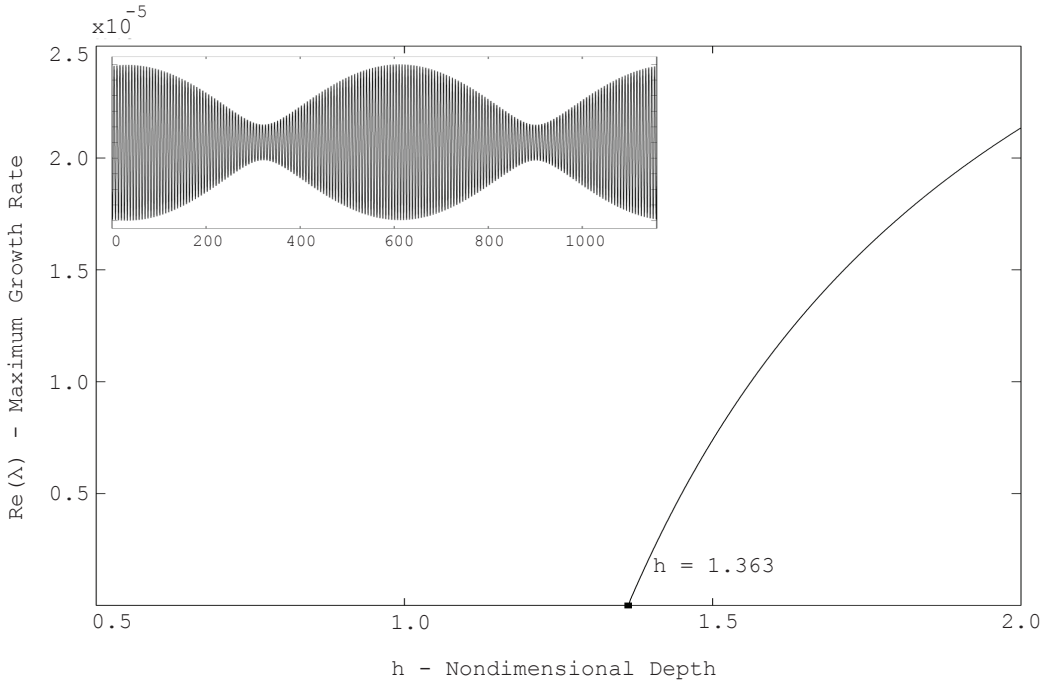

Figure 5.13: Maximal growth rates due to long wave perturbations ($\mu << 1$) as a function of dimensionless depth for $a = .01$. The growth rate becomes non-zero when $h > 1.363$ as predicted by the theory. The inset figure demonstrates the eigenfunction corresponding to the most unstable eigenvalue for $h = 1.5$, where the Floquet parameter $\mu \approx .00542$

As is seen in Figure 5.13, the most unstable eigenvalue due to long wave perturbations remains undetectable until h is increased above the critical threshold $h = 1.363$. Additionally, we show the eigenfunction corresponding to the instability for $h = 1.5$ which is above the critical depth. However, as is demonstrated in the above full spectrum diagrams, for $kh < 1.363$, periodic solutions are also unstable.

A surprising result that we found is that once the depth of the fluid is increased beyond the critical depth $h = 1.363$, the Benjamin-Feir instability is not necessarily dominant. The high-

[5]Because the system is Hamiltonian, there is a quadra-fold symmetry of the spectrum about the origin in the complex plane. Thus, for any eigenvalue λ, there are three additional eigenvalues λ^*, $-\lambda$ and $-\lambda^*$, and their associated eigenfunctions. When we present an eigenfunction, we take the linear combination of the four eigenfunctions corresponding to the symmetric eigenvalues

frequency instabilities, while decreasing in magnitude as a function of h, yield a larger effect on the solution than the modulational instability initially. This role is eventually taken over by the moduational instability for $h > 1.4306$ as seen in Figure 5.14. Additionally, these instabilities (as seen in Figure **??**) occur for shorter wavelength perturbations.

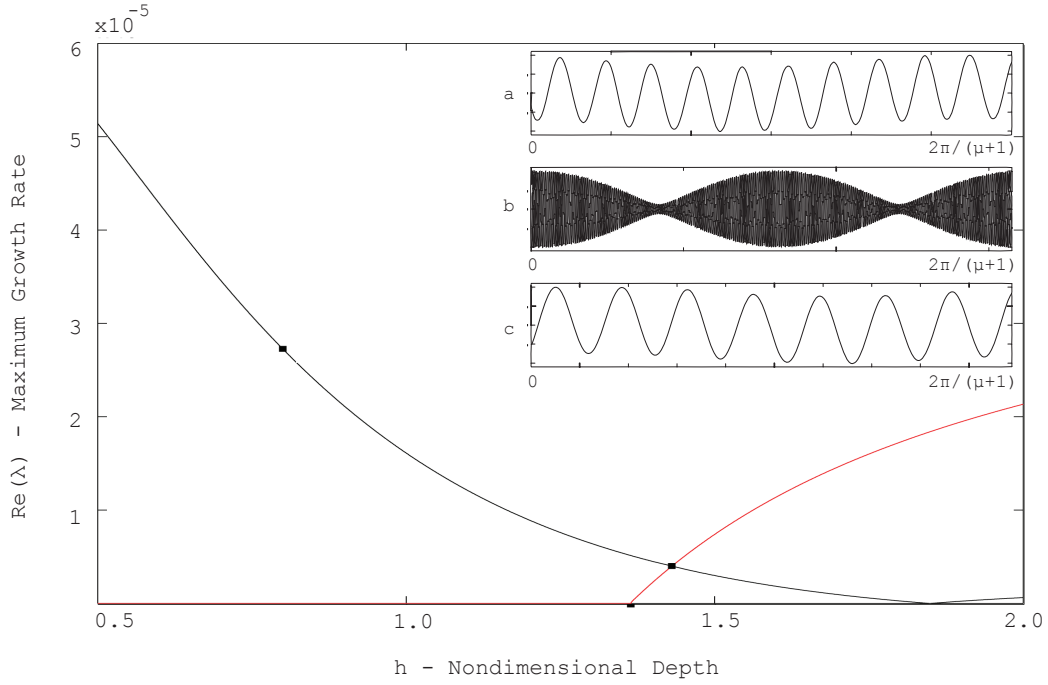

Figure 5.14: Maximal growth rates as a function of dimensionless depth for $a = .01$ where the high-frequency instability is shown in red and compared with the Benjamin-Feir Instability. The inset figure demonstrates the eigenfunctions corresponding to (a) $h = .8$ and $\mu = .2092$, (b) $h = 1.4603$ and $\mu \approx .00468$ due to the modulational perturbation, and (c) $h = 1.4603$ and $\mu \approx .3199$ due to the high-frequency instability.

Another interesting investigation is the time propagation of the linear dynamics of the traveling wave solution perturbed by the most unstable eigenfunction. For example, we consider the traveling wave solutions corresponding to $a = .01$, at the depths indicated in Figure 5.14. Recalling that our original perturbed solution was of the form

$$\eta(x,t) = \eta_0(x) + \epsilon e^{\lambda t} e^{i\mu x} \eta_1(x),$$

we explicitly calculate the linear perturbation for multiple times t. The time steps are shown in Figures 5.15, 5.16, and 5.17. Since the eigenvalues are unstable, the amplitude of the solutions should grow as demonstrated in each of the figures. Since we are using the lineearization, we expect

that these approximations are only valid for very small times. However, the initial transition of the instability can give useful insight into the short-term behavior of the solution.

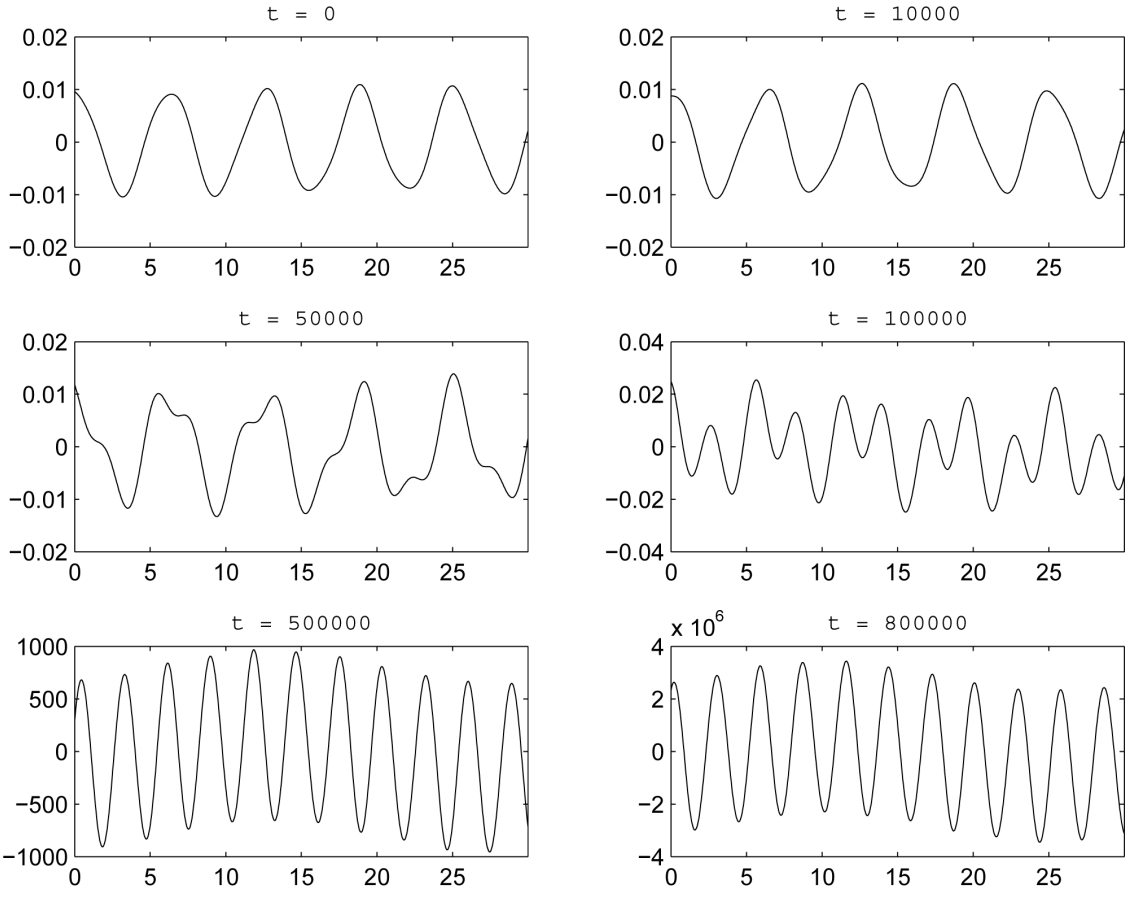

Figure 5.15: Time evolution of the linear approximation $\eta = \eta_0 + \epsilon e^{i\mu x + \lambda t}\eta_1(x)$ where η_0 is the traveling wave solution corresponding to $a = .01$ and $h = .8$, $\epsilon = .001$, μ is the Floquet exponent corresponding to the most unstable perturbation, and λ and $\eta_1(x)$ are the eigenvalue/eigenfunction pair corresponding to the largest growth rate as determined by Hill's method. Linear approximations are shown at various time-steps.

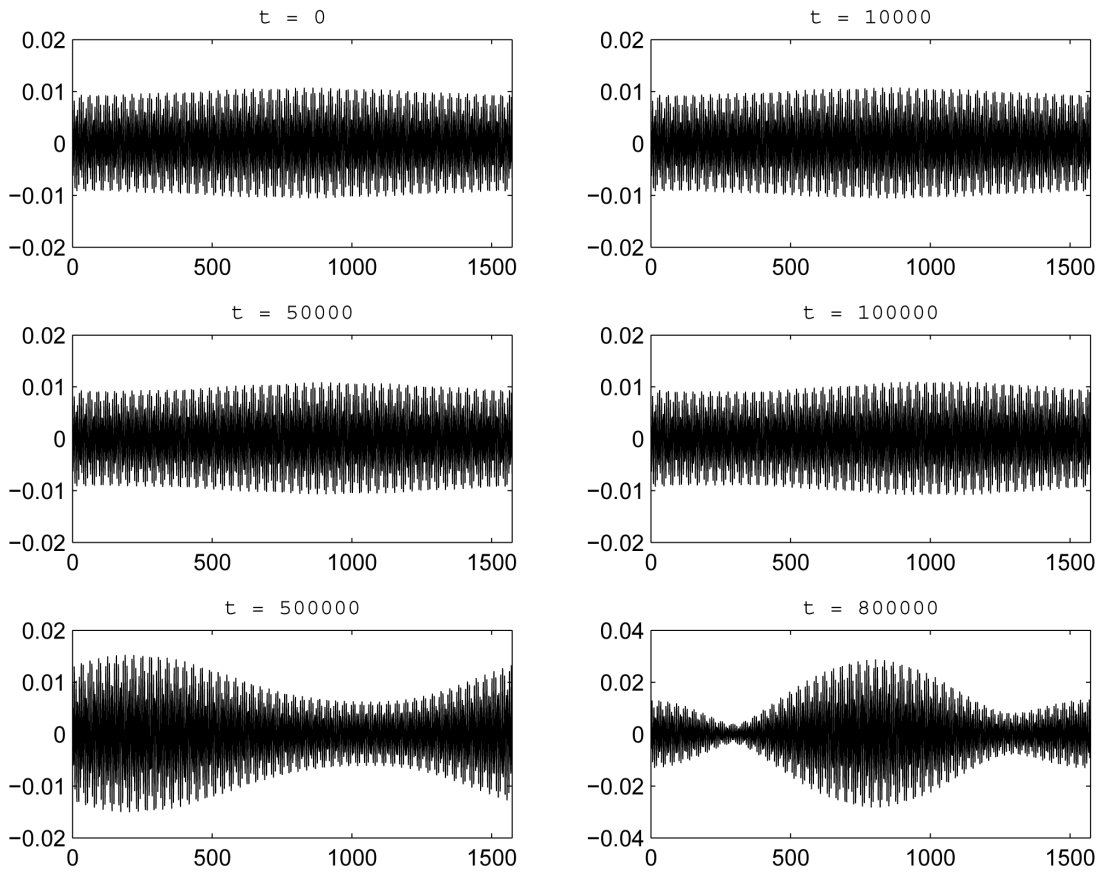

Figure 5.16: Time evolution of the linear approximation $\eta = \eta_0 + \epsilon e^{i\mu x+\lambda t}\eta_1(x)$ where η_0 is the traveling wave solution corresponding to $a = .01$ and $h = 1.4306$, $\epsilon = .001$, μ is the Floquet exponent corresponding to the most unstable perturbation as as result of Benjamin-Feir, and λ and $\eta_1(x)$ are the eigenvalue/eigenfunction pair corresponding to the largest growth rate as determined by Hill's method. Linear approximations are shown at various time-steps.

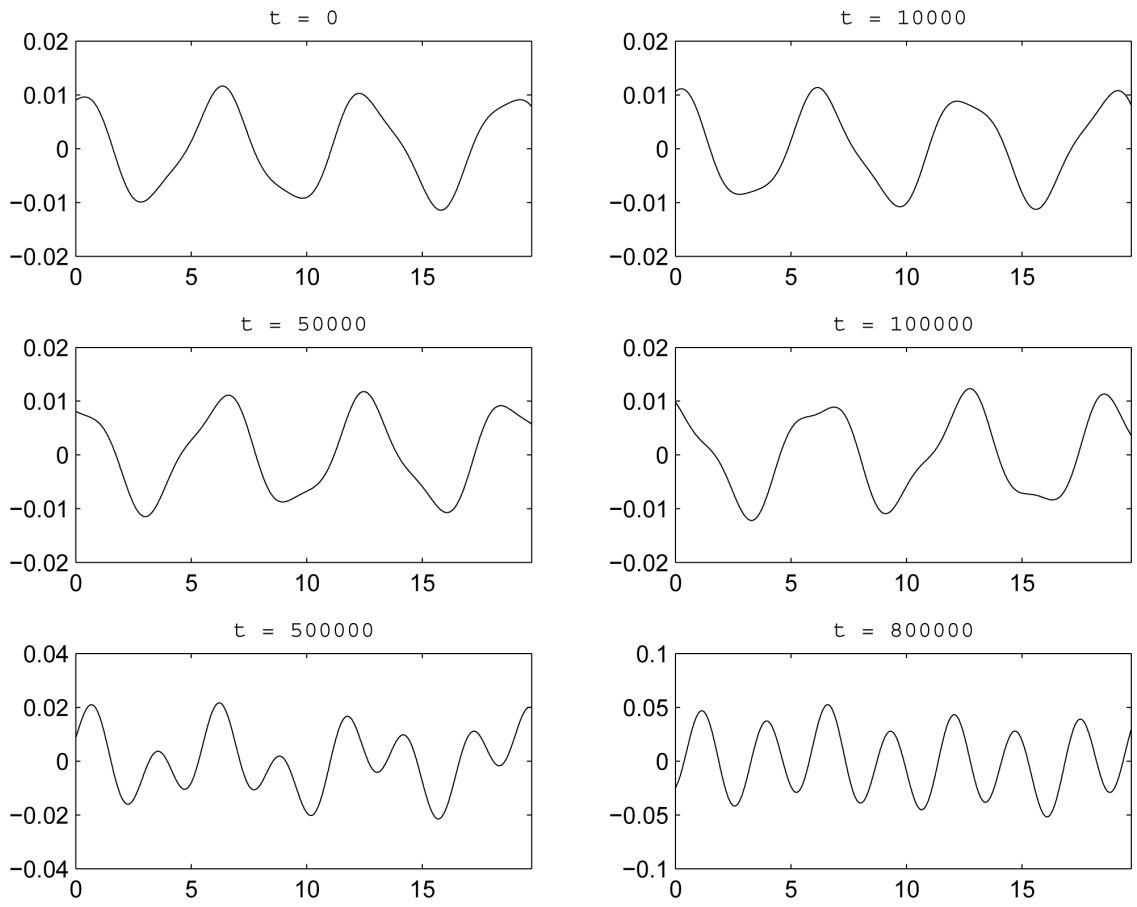

Figure 5.17: Time evolution of the linear approximation $\eta = \eta_0 + \epsilon e^{i\mu x + \lambda t}\eta_1(x)$ where η_0 is the traveling wave solution corresponding to $a = .01$ and $h = 1.4306$, $\epsilon = .001$, μ is the Floquet exponent corresponding to the most unstable perturbation due to the new instabilities, and λ and $\eta_1(x)$ are the eigenvalue/eigenfunction pair corresponding to the largest growth rate as determined by Hill's method. Linear approximations are shown at various time-steps.

Chapter 6

Stability of Two-Dimensional Solutions to Three-Dimensional Perturbations

Waves traveling in the deep ocean are subjected to effects from multiple directions. By understanding the effects of three-dimensional perturbations, we gain a better understanding of the effects of perturbation on the ocean surface. In this chapter, we investigate the stability of two-dimensional traveling wave solutions to three-dimensional perturbations. We begin by considering the three-dimenstional extension of the AFM formulation. Using the two-dimensional solutions of (3.7), we perturb the solutions in three dimensions, and linearize the three-dimensional equations about this perturbation. As in the previous chapter, we use separation of variables to introduce a time-dependent growth rate, which results in an eigenvalue problem. Since our solution does not depend on the second surface dimension, we can further reduce our problem before we apply Hill's method to determine the spectrum associated with our solution.

6.1 Equations of Motion in Three Dimensions

In Chapter 2 of this dissertation, we recalled Euler's equations in two dimensions. We do not repeat the derivation for the three-dimensional problem here. However, it should be noted that the derivation for the original formulation and the AFM formulation is a trivial extension of the two-dimensional derivation. The AFM formulation for the water-wave problem in three dimensions is given by a similar set of local and non-local equations. In a traveling coordinate frame where $\mathbf{x} = (x, y)$ is moving at a speed $\bar{c} = (c_x, c_y)$, the non-local equation is

$$\int_0^{L_2} \int_0^{L_1} e^{-i\bar{k}\cdot\mathbf{x}} \left((\eta_t - \bar{c}\cdot\nabla\eta)\cosh(\kappa(h+\eta)) - \frac{\bar{k}\cdot\nabla q}{\kappa}\sinh(\kappa(h+\eta)) \right) dxdy = 0, \tag{6.1}$$

for all $\bar{k} \in \Lambda$, where

$$\bar{k} = (k_x, k_y), \quad \mathbf{x} = (x, y), \quad \kappa = ||\bar{k}||_2$$
$$\nabla = (\partial_x, \partial_u), \text{ and } \Lambda = \{a(k_x, k_y) | k_x = \frac{2m\pi}{L_1}, k_y = \frac{2n\pi}{L_2}, (m, n) \in \mathbb{Z} - \{0\}\}.$$

Similarly, the local equation is given by

$$q_t - \bar{c} \cdot \nabla q + \frac{1}{2} |\nabla q|^2 + g\eta - \frac{1}{2} \cdot \frac{(\eta_t + \nabla q \cdot \nabla \eta)^2}{1 + |\nabla \eta|^2} = 0. \tag{6.2}$$

The above equations will serve as the equations of motion. It should be noted that two-dimensional solutions of (3.7) also solve the above equations since the y dependence drops out explicitly.

6.2 Linearization of the Equations of Motion about a Two-Dimensional Stationary Solution

Since our goal is to apply Hill's Method to determine the spectra, we begin by linearizing (6.1) and (6.2) about a two-dimensional traveling wave solution. Our perturbed solution is of the form

$$\eta(x, y, t) = \eta_0(x) + \epsilon \eta_1(x, y, t) + \ldots, \qquad q(x, y, t) = q_0(x) + \epsilon q_1(x, y, t) + \ldots,$$

where $\mathcal{F} = (\eta_0, q_0, c_x)$ is a solution to the two-dimensional problem given in Chapter 3, and $\mathbf{x}$ is moving in a traveling reference frame with speed $\bar{c} = (c_x, 0)$.

We begin with the local equation. Substituting this perturbation into equation (6.2) and keeping only terms to order ϵ, we obtain

$$q_{1,t} - c_x q_{1,x} + q_{0,x} q_{1,x} + g\eta_1 - f(\eta_0, q_0)\Big(\eta_{1,t} + \eta_{1,x}(q_{0,x} - c_x) + \eta_{0,x} q_{1,x} - \eta_{0,x} f(\eta_0, q_0) eta_{1,x}\Big) = 0, \tag{6.3}$$

where

$$f(\eta_0, q_0) = \frac{\eta_{0,x}(q_{0,x} - c_x)}{1 + \eta_{0,x}^2}.$$

Since the problem does not depend on t or y explicitly (since the functions η_0 and q_0 are both independent of y and t), we can use separation of variables to decompose $\eta_1(x, y, t)$ and $q_1(x, y, t)$ into the following form

$$\eta_1(x, y, t) = e^{\lambda t} e^{i\rho y} \tilde{\eta_1}(x) + c.c., \text{ and } q_1(x, y, t) = e^{\lambda t} e^{i\rho y} \tilde{q_1}(x) + c.c.,$$

where ρ is the wave number of the perturbation. Substituting this into (6.3), we have

$$\lambda \tilde{q_1} - c_x \tilde{q}_{1,x} + q_{0,x} \tilde{q}_{1,x} + g\tilde{\eta_1} - f\Big(\lambda \tilde{\eta_1} + \tilde{\eta}_{1,x}(q_{0,x} - c_x) + \eta_{0,x} \tilde{q}_{1,x} - \eta_{0,x} f \tilde{\eta}_{1,x}\Big) = 0, \tag{6.4}$$

which is the same equation that we obtained in the previous chapter for the stability of two dimensional solutions with respect to two dimensional perturbations. At this point, the local equation

is ready for the Fourier-Floquet decomposition. We first address the non-local equation before we proceed to the stability analysis.

For the non-local equation (6.1), we have to again consider the average value over the domain in both x and y since the perturbations are not necessarily periodic with the same period as the fundamental traveling wave solution. In other words, we begin with the spectral equation written in the form

$$\lim_{M_1,M_2\to\infty}\frac{1}{M_1M_2}\int_{-M_2/2}^{M_2/2}\int_{-M_1/2}^{M_1/2}e^{-i\bar{k}\cdot\mathbf{x}}\Big(i(\eta_t-\bar{c}\cdot\nabla\eta)\cosh(\kappa(h+\eta))\\ -\frac{\bar{k}\cdot\nabla q}{\kappa}\sinh(\kappa(h+\eta))\Big)dxdy=0.$$

Substituting the perturbation into the above equation yields

$$\lim_{M_1,M_2\to\infty}\frac{1}{M_1M_2}\int_{-M_2/2}^{M_2/2}\int_{-M_1/2}^{M_1/2}e^{-i\bar{k}\cdot\mathbf{x}}\Big(i\eta_{1,t}\mathcal{C}_\kappa-ic_x\eta_{0,x}\kappa\eta_1\mathcal{S}_\kappa-ic_x\eta_{1,x}\mathcal{C}_\kappa\\ -\frac{1}{\kappa}\left(\bar{k}\cdot q_1\right)\mathcal{S}_\kappa-kq_{0,x}\eta_1\mathcal{C}_\kappa\Big)dxdy=0,$$

where

$$\mathcal{S}_\kappa=\sinh(\kappa(\eta_0+h)\text{ and }\mathcal{C}_\kappa=\cosh(\kappa(\eta_0+h)).$$

As before, since the problem does not depend on t or y explicitly, we can use separation of variables to decompose $\eta_1(x,y,t)$ and $q_1(x,y,t)$. Using the same decomposition as before, we obtain

$$\lim_{M_1,M_2\to\infty}\frac{1}{M_1M_2}\int_{-M_2/2}^{M_2/2}\int_{-M_1/2}^{M_1/2}e^{-i\bar{k}\cdot\mathbf{x}}e^{i\rho y}\Big(i\tilde{\eta}_{1,t}\mathcal{C}_\kappa-ic_x\tilde{\eta}_{1,x}\mathcal{C}_\kappa-\eta_{0,x}c_x\kappa\tilde{\eta}_1\mathcal{S}_\kappa\\ -\frac{1}{\kappa}\left(k_x\tilde{q}_{1,x}+i\rho k_y\tilde{q}_1\right)\mathcal{S}_\kappa-kq_{0,x}\tilde{\eta}_1\mathcal{C}_\kappa\Big)dxdy=0.$$

Since our new integrand only depends on y through the term $e^{-i(k_y-\rho)y}$, we can eliminate the integration with respect to y completely. Calculating the average value along the y direction results in the following integral

$$\lim_{M_2\to\infty}\frac{1}{M_2}\int_{-M_2/2}^{M_2/2}e^{-i(k_y-\rho)y}dy=\lim_{M_2\to\infty}\frac{2}{M_2(k_y-\rho)}\sin\left(\frac{M_2(k_y-\rho)}{2}\right).$$

Taking the limit as $M_2\to\infty$, the contribution is identically zero if $k_y\neq\rho$. Otherwise, if $k_y=\rho$, the contribution from the integral is unity. Thus, the lineariziation of the non-local equation simplifies to

$$\lim_{M_1\to\infty}\frac{1}{M_1}\int_{-M_1/2}^{M_1/2}e^{-ik_xx}\Big(i\lambda\tilde{\eta}_1\mathcal{C}_\kappa-ic_x\tilde{\eta}_{1,x}\mathcal{C}_\kappa-\eta_{0,x}c_x\kappa\tilde{\eta}_1\mathcal{S}_\kappa\\ -\frac{1}{\kappa}\left(k_x\tilde{q}_{1,x}+i\rho^2\tilde{q}_1\right)\mathcal{S}_\kappa-kq_{0,x}\tilde{\eta}_1\mathcal{C}_\kappa\Big)dx=0, \tag{6.5}$$

where $\kappa=\sqrt{k_x^2+\rho^2}$.

Remark 18. *It should be noted that if we set $\rho = 0$, the above equation reduces to the same expression for the two-dimensional case presented in the previous chapter as we expect.*

6.3 Hill's Method Implementation

Now that we have linearized the equations about the traveling wave solution and introduced the exponential growth/decay rate in time, we have the following generalized eigenvalue problem

$$\lambda\left(\tilde{q}_1 - f\tilde{\eta}_1\right) = c_x\tilde{q}_{1,x} - q_{0,x}\tilde{q}_{1,x} + f\Big(+ \tilde{\eta}_{1,x}(q_{0,x} - c_x) + \eta_{0,x}\tilde{q}_{1,x} - \eta_{0,x}f\tilde{\eta}_{1,x}\Big) = 0,$$

$$\lim_{M_1\to\infty}\frac{\lambda}{M_1}\int_{-M_1/2}^{M_1/2} e^{-ik_x x}\Big(i\tilde{\eta}_1\mathcal{C}_\kappa\Big)dx = \lim_{M_1\to\infty}\frac{1}{M_1}\int_{-M_1/2}^{M_1/2} e^{-ik_x x}\Big(ic_x\tilde{\eta}_{1,x}\mathcal{C}_\kappa + i\eta_{0,x}c_x\kappa\tilde{\eta}_1\mathcal{S}_\kappa + \frac{1}{\kappa}\left(k_x\tilde{q}_{1,x} + i\rho^2\tilde{q}_1\right)\mathcal{S}_\kappa + kq_{0,x}\tilde{\eta}_1\mathcal{C}_\kappa\Big)dx = 0.$$

6.3.1 Floquet Decomposition

This eigenvalue problem is valid for all ρ since our y dependence is based on solutions of the form $\eta_1 = e^{\lambda t + i\rho y}\tilde{\eta}_1(x)$ and $q_1 = e^{\lambda t + i\rho y}\tilde{q}_1(x)$. To determine the spectra, we use Hill's method as defined in the previous chapter. Thie first step is to recall that the spectra is the set of all λ values such that the above equations have bounded solutions for $\tilde{q}_1$ and $\tilde{\eta}_1$. Since all of the coefficient functions are periodic with period 2π, we can use Floquet's Theorem to show that all bounded solutions are of the form

$$\tilde{\eta}_1(x) = e^{-i\mu x}\bar{\eta}_1(x), \text{ and } \tilde{q}_1(x) = e^{-i\mu x}\bar{q}(x),$$

where $\mu \in [-1/2, 1/2)$ and $\bar{q}_1$ and $\bar{\eta}_1$ are 2π periodic functions[1]. Substituting the Floquet decomposition into the eigenvalue problem yields

$$\lambda\left(\tilde{q}_1 - f\tilde{\eta}_1\right) = c_x(i\mu + \partial_x)\bar{q}_1 - q_{0,x}(i\mu + \partial_x)\bar{q}_1 - g\bar{\eta}_1 + f\Big((q_{0,x} - c_x)(i\mu + \partial_x)\bar{\eta}_1 + \eta_{0,x}(i\mu + \partial_x)\bar{q}_1 - \eta_{0,x}f(i\mu + \partial_x)\bar{\eta}_1\Big),$$

$$\lim_{M_1\to\infty}\frac{\lambda}{M_1}\int_{-M_1/2}^{M_1/2} e^{-i(k_x-\mu)x}\Big(i\tilde{\eta}_1\mathcal{C}_\kappa\Big)dx = \lim_{M_1\to\infty}\frac{1}{M_1}\int_{-M_1/2}^{M_1/2} e^{-ik_x x}\Big(ic_x\mathcal{C}_\kappa(i\mu + \partial_x)\bar{\eta}_1 + i\eta_{0,x}c_x\kappa\bar{\eta}_1\mathcal{S}_\kappa + \frac{1}{\kappa}\left(k_x(i\mu + \partial_x) + i\rho^2\right)\bar{q}_1\mathcal{S}_\kappa + k_xq_{0,x}\bar{\eta}_1\mathcal{C}_\kappa\Big)dx = 0.$$

6.3.2 Fourier Decomposition

Using the previous decomposition, we represent the 2π-periodic eigenfunctions $\bar{q}_1$ and $\bar{\eta}_1$ by their Fourier series. In other words, let

$$\bar{q}_1(x) = \sum_{m=-\infty}^{\infty}\hat{Q}_m e^{imx}, \text{ and } \bar{\eta}_1(x) = \sum_{m=-\infty}^{\infty}\hat{N}_m e^{imx}.$$

[1] As in the previous chapter, we consider traveling wave solutions that are periodic with period 2π.

Additionally, we represent the periodic variable coefficient functions by their Fourier series as well. Substituting the series representations into the Floquet decomposition, we are able to determine a bi-infinite matrix eigenvalue problem, where the eigenvectors are the Fourier coefficients $\hat{Q}_j$ and $\hat{N}_j$ for $j \in \{0, \pm 1, \pm 2, \ldots\}$. The Fourier decomposition proceeds exactly as in the previous chapter for the local equation. We obtain the set of equations

$$\begin{aligned} -g\hat{N}_n + \sum_{m=-\infty}^{\infty} (i\mu + im)\, \hat{F}_{1,n-m}\hat{N}_m + \sum_{m=-\infty}^{\infty} \hat{F}_{2,n-m}\, (i\mu + im)\, \hat{Q}_m \\ = \lambda \left(\sum_{m=-\infty}^{\infty} \hat{F}_{3,n-m}\hat{N}_m - \hat{Q}_n \right), n \in \mathbb{Z} - \{0\}. \end{aligned} \tag{6.6}$$

The coefficients $\hat{F}_{j,n}$ are given by the following expressions

$$\begin{aligned} \hat{F}_{1,n} &= \int_0^L e^{-\frac{2in\pi x}{L}} f_1(\eta_0, q_0)\, (q_{0,x} - c - \eta_{0,x} f_1(\eta_0, q_0))\, dx, \\ \hat{F}_{2,n} &= \int_0^L e^{-\frac{2in\pi x}{L}}\, (q_{0,x} - c - \eta_{0,x} f_1(\eta_0, q_0))\, dx, \\ \hat{F}_{3,n} &= \int_0^L e^{-\frac{2in\pi x}{L}} f_1(\eta_0, q_0) dx. \end{aligned}$$

The non-local equation is similar to the Fourier decomposition in the previous chapter. However, there are two differences. The first difference is that the hyperbolic sine and cosine terms now depend on $\kappa = \sqrt{k_x^2 + \rho^2}$ instead of k_x directly. The second difference is the addition of a new term dependent on the perturbation of the velocity potential and ρ. Substituting the Fourier series into the non-local equation and representing all variable coefficients by their Fourier series representation as well, we have

$$\begin{aligned} \Big[\sum_{j=-\infty}^{\infty} \sum_{m=-\infty}^{\infty} \left(\hat{G}_{1,j}^{(k)} + ic(i\mu + im)\hat{G}_{2,j}^{(k)} \right) \hat{N}_m + \sum_{j=-\infty}^{\infty} \sum_{m=-\infty}^{\infty} \left(\frac{k_x}{\kappa}(i\mu + im) + \frac{i\rho^2}{\kappa} \right) \hat{G}_{3,j}^{(k)} \hat{Q}_m \Big] \langle E \rangle \\ = i\lambda \sum_{j=-\infty}^{\infty} \sum_{m=-\infty}^{\infty} \hat{G}_{2,j}^{(k)} \hat{N}_m \langle E \rangle \end{aligned} \tag{6.7}$$

where

$$\begin{aligned} \hat{G}_{1,n}^{(k)} &= \int_0^L e^{-\frac{2in\pi x}{L}}\, (kq_{0,x}\mathcal{C}_k + ick\eta_{0,x}\mathcal{S}_k)\, dx, \\ \hat{G}_{2,n}^{(k)} &= \int_0^L e^{-\frac{2in\pi x}{L}}\, (\mathcal{C}_k)\, dx, \\ \hat{G}_{3,n}^{(k)} &= \int_0^L e^{-\frac{2in\pi x}{L}}\, (\mathcal{S}_k)\, dx, \end{aligned}$$

and $\mathcal{S}_k$ and $\mathcal{C}_k$ are given earlier.

Each term in the double infinite sum contains the average value of E as defined above. The average value of this integral is identically zero unless the exponent is a multiple of 2π. In other

words the contribution from the integral is identically zero unless

$$k_x = \mu + n, \qquad \forall n \in \mathbb{Z}.$$

Thus, we see that the only contribution in the integral equation occurs when k is a shift of the original dual lattice. Substituting this relationship into the exponent, we are left with the integral

$$\int_{-M/2}^{M/2} \exp\left[ix\left(j+m-n\right)\right] dx.$$

As before, this integral is identically zero unless $j+m-n=0$ and one otherwise. This allows us to collapse the double infinite sum to a single infinite sum given by

$$\begin{aligned}
&\sum_{m=-\infty}^{\infty} \left(\hat{G}^{(k(\mu))}_{1,n-m} + ic(i\mu+im)\hat{G}^{(k(\mu))}_{2,n-m} \right) \hat{N}_m \\
&\quad + \sum_{j=-\infty}^{\infty} \sum_{m=-\infty}^{\infty} (i\mu+im)\hat{G}^{(k(\mu))}(\mu+n)_{3,n-m}\hat{Q}_m \Big] \\
&\quad = i\lambda \sum_{m=-\infty}^{\infty} \hat{G}^{(k(\mu))}_{2,n-m}\hat{N}_m, \qquad (6.8)
\end{aligned}$$

which holds for all $n \in \mathbb{Z}$.

Combining the above equation with (6.6) yields a generalized bi-infinite eigenvalue problem for determining the spectrum of the linearized operator about the stationary traveling wave solutions. We define the quantity $\hat{\mathbf{X}}$ as a bi-infinite vector of the Fourier coefficients $\hat{Q}_j$ and $\hat{N}_j$ for all $j \in \mathbb{Z}$ such that $\hat{V} = \Big[\ldots, \hat{N}_{-1}, \hat{N}_0, \hat{N}_1, \ldots \hat{Q}_{-1}, \hat{Q}_0, \hat{Q}_1, \ldots\Big]^T$. With this notation, we can rewrite the Fourier decomposition in the following matrix form:

$$\begin{bmatrix} A(\mu,\rho) & B(\mu,\rho) \\ C(\mu,\rho) & D(\mu,\rho) \end{bmatrix} \hat{\mathbf{X}} = \lambda \begin{bmatrix} 0 & S(\mu,\rho) \\ -I & V(\mu,\rho) \end{bmatrix} \hat{\mathbf{X}},$$

where

$$A(\mu)_{n,m} = -g\delta(n-m) + (i\mu+im)\,\hat{F}_{1,n-m}, \quad B(\mu)_{n,m} = \hat{F}_{2,n-m}\,(i\mu+im)\,,$$

$$C(\mu)_{n,m} = \hat{G}^{(k(\mu))}_{1,n-m} + ic(i\mu+im)\hat{G}^{(k(\mu))}_{2,n-m}, \quad D(\mu)_{n,m} = (i\mu+im)\hat{G}^{(k(\mu))}_{3,n-m}$$

$$S(\mu)_{n,m} = \hat{F}_{3,n-m}, \quad \text{and} \quad V(\mu)_{n,m} = i\hat{G}^{(k(\mu)}_{2,n-m}.$$

6.4 Numerical Simplifications and Convergence

6.4.1 Numerical Simplifications

As in the previous chapter, we are able to reduce the interval of μ values from $\mu \in [-1/2, 1/2)$ to the interval $\mu \in [0, 1/2]$. This proof is identical to the one given in Chapter 5. We repeat it here for completeness.

Theorem 5 (Floquet Parameter Reduction, AFM)**.** *Consider the Floquet decomposition of AFM due to three-dimensional perturbations of a two-dimensional solution. This solution, $\mathcal{F} = (\eta_0, q_0, c)$, is a real valued solution set to the nonlinear traveling wave problem given in the Chapter 4. If $(\lambda, \bar{\eta}_1, \bar{q}_1)$ is an eigenvalue/eigenfunction pair for $\mu = \mu_1$, then $(\lambda^*, \bar{\eta}_1^*, \bar{q}_1^*)$ is an eigenvalue/eigenfunction pair for $\mu = -\mu_1$.*

Proof. We prove this for the case where h is finite. The proof for infinite depth is identical.

If λ is an eigenvalue when $\mu = \mu_1$, we have

$$\begin{aligned}
\lambda\left(\bar{q}_1 + g_1\bar{\eta}_1\right) &= f_1\left(\partial_x + i\mu_1\right)\bar{q} \\
&\quad + \Big(h_0 + h_1\left(\partial_x + i\mu_1\right) + h_2\left(\partial_x + i\mu_1\right)^2\Big)\bar{\eta}_1, \\
i\lambda\int_0^{2\pi} e^{-imx}\tilde{\eta}_1\mathcal{C}_\kappa dx &= \int_0^{2\pi} e^{-imx}\Big(ic_x\mathcal{C}_\kappa(i\mu_1 + \partial_x)\bar{\eta}_1 + i\eta_{0,x}c_x\kappa\bar{\eta}_1\mathcal{S}_\kappa \\
&\quad + \frac{1}{\kappa}\mathcal{S}_\kappa\left((\mu_1 + m)(i\mu_1 + \partial) + i\rho^2\right)\bar{q}_1 + (\mu_1 + m)q_{0,x}\bar{\eta}_1\mathcal{C}_\kappa\Big)dx = 0.
\end{aligned}$$

where $\kappa = \sqrt{\rho^2 + (\mu + m)^2}$.

The local equation is identical to the local equation given in Chapter 5 for all ρ, so all we need to worry about is the non-local equation. If we proceed as we did in the previous chapter, all we need to do is take the complex-conjugate of the non-local equation and replace m with $-m$. This results in the equation

$$\begin{aligned}
i\lambda^*\int_0^{2\pi} e^{-imx}\bar{\eta}_1^*\mathcal{C}_{\kappa_-}dx &= \int_0^{2\pi} e^{-imx}\Big(ic_x\mathcal{C}_{\kappa_-}(-i\mu_1 + \partial_x)\bar{\eta}_1^* + i\eta_{0,x}c_x\kappa_-\bar{\eta}_1^*\mathcal{S}_{\kappa_-} \\
&\quad + \frac{1}{\kappa_-}\mathcal{S}_{\kappa_-}\left((m - \mu_1)(-i\mu_1 + \partial) + i\rho^2\right)\bar{q}_1^* + (m - \mu_1)q_{0,x}\bar{\eta}_1^*\mathcal{C}_{\kappa_-}\Big)dx,
\end{aligned}$$

where $\kappa_- = \sqrt{\rho^2 + (\mu_1 - m)^2}$. The local equation is the same as the one given in proof of the theorem for two-dimensional perturbations. This is the same eigenvalue problem for $\mu = -\mu_1$ and thus, if $(\lambda, \bar{\eta}_1, \bar{q}_1)$ is an eigenvalue/eigenfunction pair for $\mu = \mu_1$, then $(\lambda^*, \bar{\eta}_1^*, \bar{q}_1^*)$ is an eigenvalue/eigenfunction pair for $\mu = -\mu_1$. □

Again, this demonstrates that the spectrum as a function of μ is symmetric about $\mu = 0$. Furthermore, we note that the problem is symmetric in ρ as well. This is easily seen since ρ only appears in the form ρ^2. Again, we have cut the interval in half. Furthermore, it is again useful to note that since Euler's equations are Hamiltonian, there is a quadra-fold symmetry of the spectra in the complex plane. Hence, if λ is an eigenvalue for some μ value, then $-\lambda^*$ is an eigenvalue for the same μ value, and likewise for $-\mu$, if λ^* is an eigenvalue then $-\lambda$ is also an eigenvalue. Thus, we have the following four eigenvalue pairs: (λ, μ), $(-\lambda^*, \mu)$, $(\lambda^*, -\mu)$, and $(-\lambda, -\mu)$.

6.4.2 Numerical Convergence and Accuracy

As discussed in the previous chapter, before we discuss the stability results, we need to establish confidence in our numerical scheme and approach. Again, we shall not try to establish analytic convergence results for our setting; instead, investigate the Cauchy convergence of our numerical method. Let λ_N represent a particular eigenvalue corresponding to a truncation size N (which corresponds to $2N+1$ Fourier coefficients). As before, the Cauchy error is defined as

$$e_N = ||\lambda_N - \lambda_{N-1}||.$$

For three different depths, we tracked the approximation of the eigenvalues with the largest real part as a function of truncation size. The Cauchy errors are given in Table 6.1. As can be see in

Table 6.1: Cauchy error for the calculation of the eigenvalue with largest real part for $h = .5$, $h = 1.5$, and $h = \infty$ with $a = .1$

N	$h = .5$	$h = 1.5$	$h = \infty$
5	3.11e-03	1.19e-07	2.03e-08
6	3.24e-04	2.93e-09	3.27e-10
7	7.45e-05	7.15e-11	5.17e-12
8	1.75e-05	1.70e-12	7.89e-14
9	3.95e-06	3.98e-14	6.66e-16
10	8.66e-07	1.21e-17	6.75e-16
11	1.88e-07	3.95e-16	1.88e-16
12	4.08e-08	6.44e-16	1.22e-15
13	8.89e-09	5.07e-16	1.31e-15
14	1.95e-09	5.73e-16	2.11e-15
15	4.27e-10	2.38e-15	2.75e-15
16	9.30e-11	3.48e-15	2.95e-15
17	2.01e-11	6.96e-16	2.18e-15
18	4.32e-12	3.38e-15	4.02e-15
19	9.21e-13	6.64e-16	3.12e-15
20	1.94e-13	1.20e-15	8.11e-17

Figure 6.1, the adjustment to the maximal eigenvalue decays to ϵ_{mach} as N increases. It should also be noted that the decay rate for $h = .5$ is significantly slower than the decay rate for the other depths $h = 1.5$ and $h = \infty$ with the same amplitude. This is not suprising when we take into account that $a = .1$ corresponds to a significantly more nonlinear wave when $h = .5$ than for the other depths. Thus, we have confidence that our method converges in a Cauchy sense.

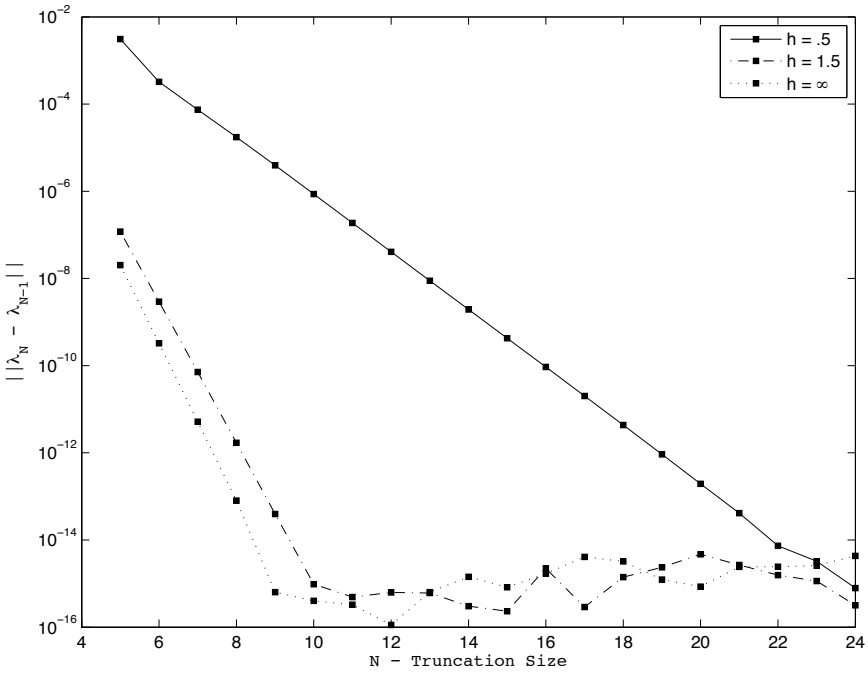

Figure 6.1: Cauchy error for the maximal eigenvalue corresponding to a solution with depth $h = .5$ and amplitude $a = .01$

6.5 Results

Transverse stability of traveling wave solutions has been examined by several researchers. The earliest notable work on transverse stability of the fully nonlinear equations was conducted by Bryant [10]. Using a set of truncated nonlinear approximations to Euler's equation on finite depth, he explored the instabilities using a smaller number of wave interactions. In 1982, McLean presented the first results regarding the transverse instabilities of two-dimensional solutions to Euler's equations for finite depth. Using the original formulation, McLean considered perturbations of the form

$$\eta_1 = e^{-\sigma t}e^{ipx+iqy}\sum_{-\infty}^{\infty} a_j e^{ijx} \text{ and } \phi_1 = e^{-\sigma t}e^{ipx+iqy}\sum_{-\infty}^{\infty} b_j e^{ijx}\frac{\cosh(\kappa_j(z+h))}{\cosh(\kappa_j h)},$$

In this section, we present the numerical results on stability to our numerical scheme. We begin by looking at the full spectra for several parameter choices in depth h and a fixed amplitude $a = .1$. We specifically choose to investigate three depths: $h = .5$, $h = 1.5$ and $h = \infty$. These choices give us two depths above and one depth below the critical Benjamin-Feir threshold instability discussed in the introduction. The results are then compared and related back to results obtained in the literature.

We begin our investigation with $h = .5$ and $a = .1$. This choice is a moderated amplitude wave. As expected, this wave is unstable as demonstrated in the full spectrum given in Figure 6.2. Likewise, we show the full spectrum for $h = 1.5$ in Figure 6.3. It is important to note that the magnitude of the largest real part of the spectra in both cases is much larger than the dominant instability when perturbed with two-dimensional perturbations (see Chapter 5 for reference). This demonstrates that the dominant instabilities for these waves are the instabilities that arise from transverse or fully three dimensional perturbations. This is not always the case. For $h = \infty$ and $a = .3$, we found that the dominant instabilities are two-dimensional.

6.5.1 Maximum Growth Rates as a Function of μ and ρ

Additionally, while the full spectra demonstrated in Figures 6.2 and 6.3 give good visualizations of the growth rate and frequency of the instabilities, looking at the instabilities as a function of μ and ρ can be more useful. This allows us to visualize the stability regions in parameter space and read off values of μ and ρ corresponding to instabilities. We begin with the spectra as a function of μ. In Figures 6.9 and 6.5, we demonstrate the real part of the spectrum for $h = .5$ and $h = 1$. Additionally, we demonstrate the same plots in Figures 6.6 and 6.7 as a function of ρ.

Remark 19. *We note that as there are instability bands that consistently appear as we increase the wave number ρ as seen in Figure 6.9 near $\rho = .6$ and $\rho = 1.25$. As these bands continue to appear, the magnitude of the instability decreases limiting towards zero.*

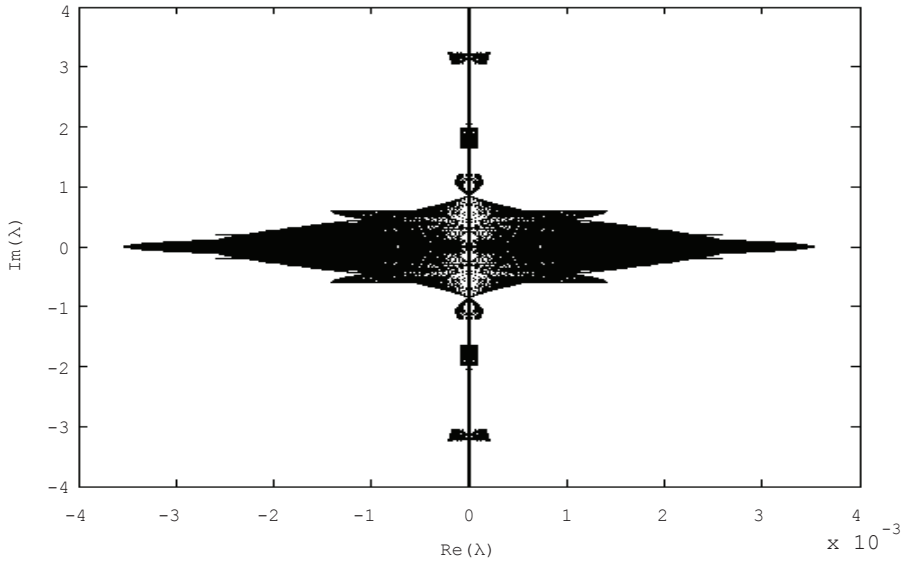

Figure 6.2: The real part of the spectra as a function of Floquet parameter μ for $h = .5$ and amplitude $a = .1$. Calculated with $N = 16$ Fourier modes, 1000 μ values, and 300 ρ values.

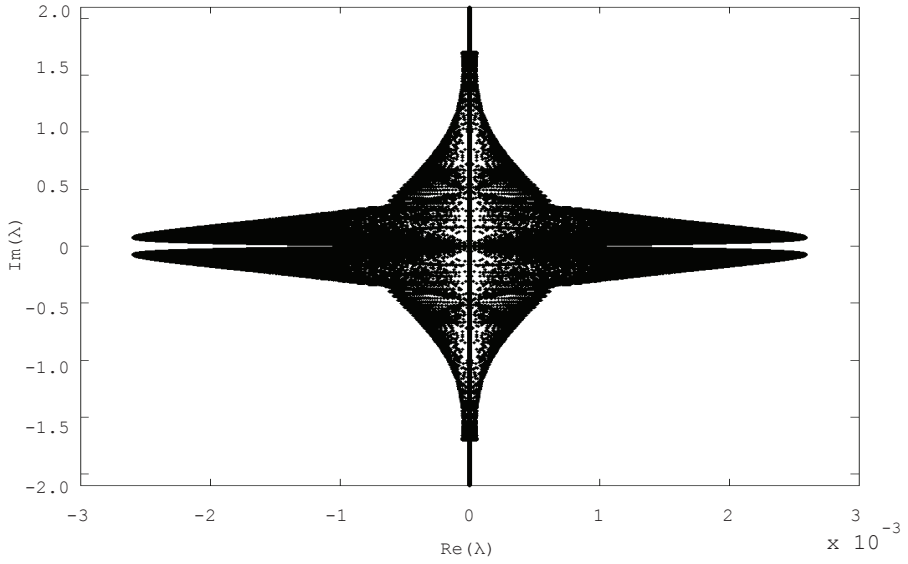

Figure 6.3: The real part of the spectra as a function of Floquet parameter μ for $h = 1.5$ and amplitude $a = .1$. Calculated with $N = 16$ Fourier modes, 1000 μ values, and 300 ρ values.

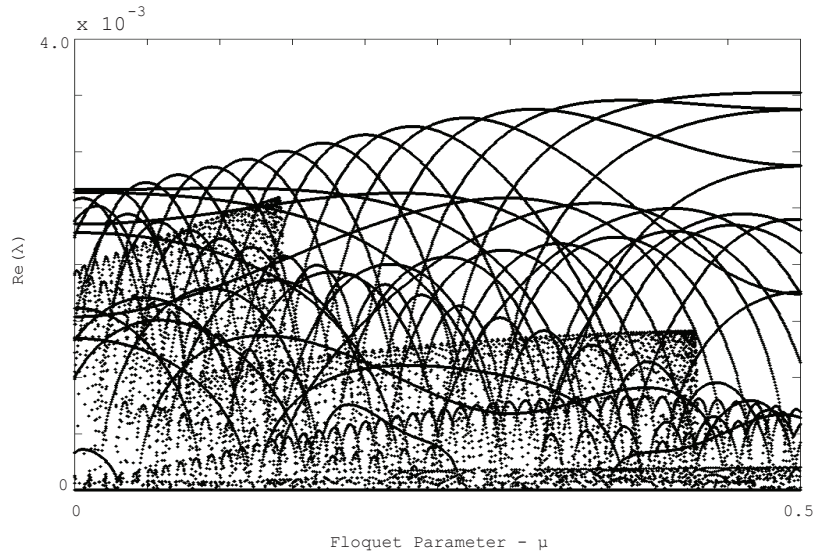

Figure 6.4: The real part of the spectra as a function of Floquet parameter μ for $h = .5$ and amplitude $a = .1$. Calculated with $N = 16$ Fourier modes, 1000 μ values, and 300 ρ values.

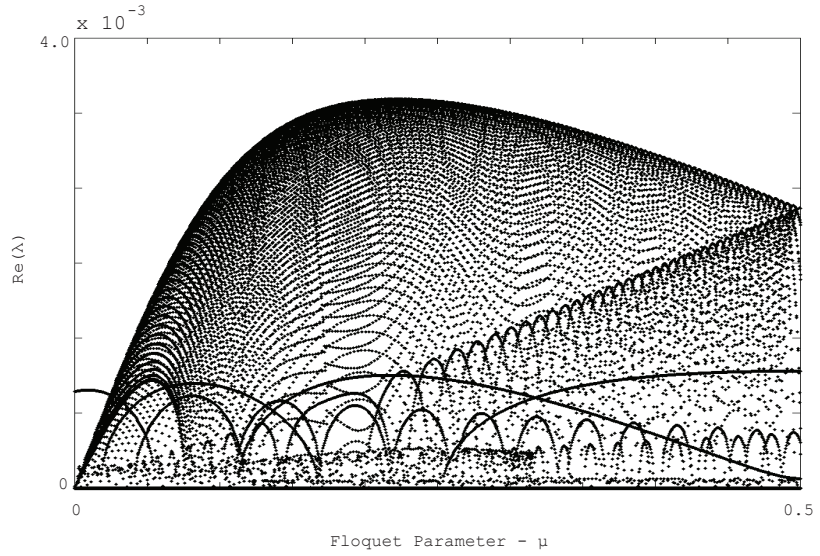

Figure 6.5: The real part of the spectra as a function of Floquet parameter μ for $h = 1.5$ and amplitude $a = .1$. Calculated with $N = 16$ Fourier modes, 1000 μ values, and 300 ρ values.

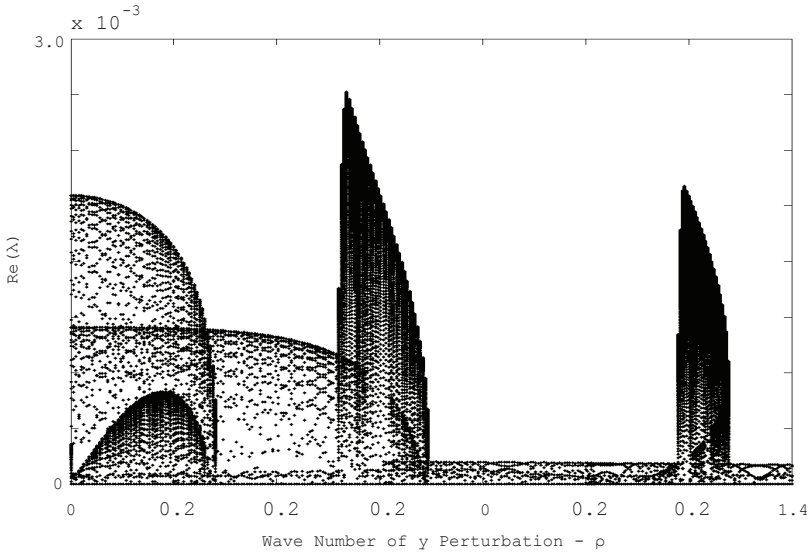

Figure 6.6: The real part of the spectrum as a function of the wave number of the y perturbation ρ for $h = 1.5$ and amplitude $a = .1$. Calculated with $N = 16$ Fourier modes, 1000 μ values, and 300 ρ values.

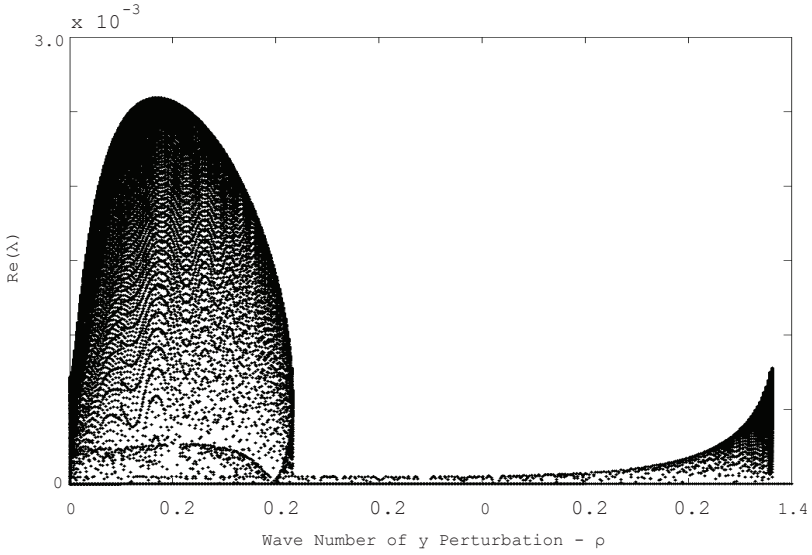

Figure 6.7: The real part of the spectrum as a function of the wave number of the y perturbation ρ for $h = 1.5$ and amplitude $a = .1$. Calculated with $N = 16$ Fourier modes, 1000 μ values, and 300 ρ values.

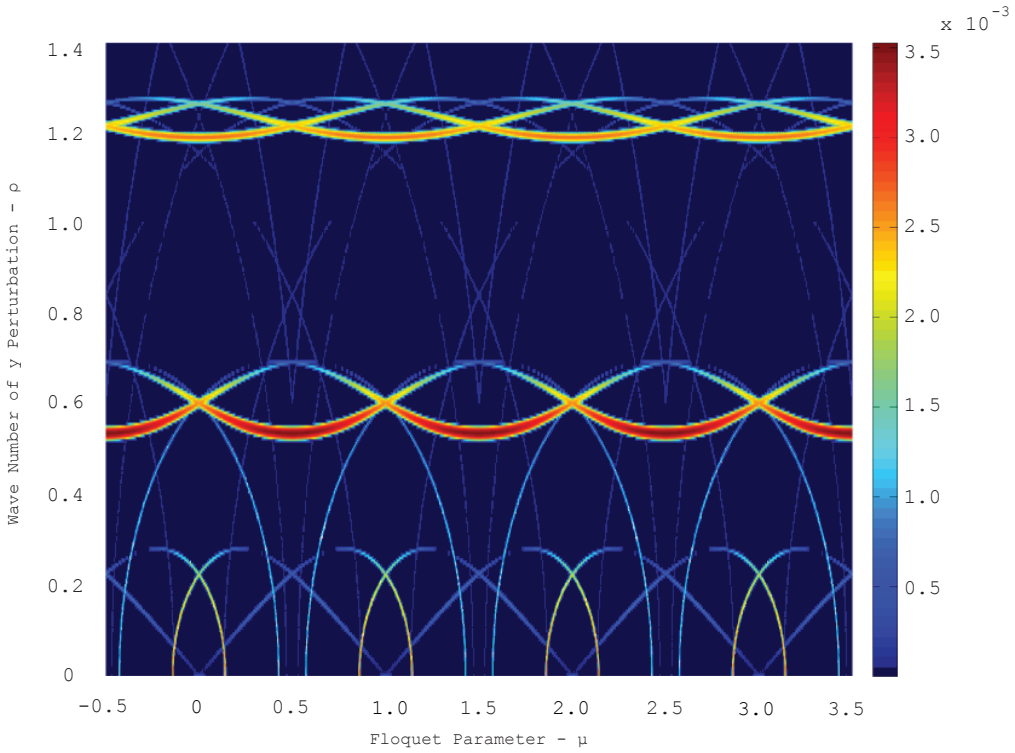

Figure 6.8: The maximum real part of the spectra as a function of Floquet parameter μ and wave number ρ for $h = .5$ and amplitude $a = .1$. Calculated with $N = 16$ Fourier modes, 1000 μ values, and 300 ρ values.

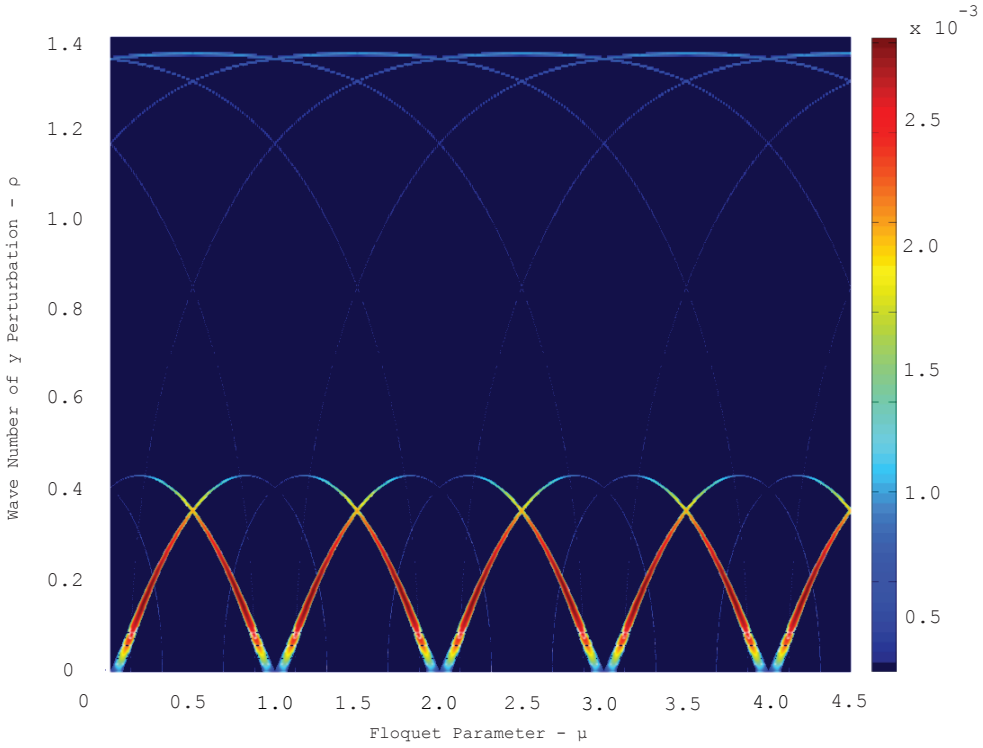

Figure 6.9: The maximum real part of the spectra as a function of Floquet parameter μ and wave number ρ for $h = .5$ and amplitude $a = .1$. Calculated with $N = 16$ Fourier modes, 1000 μ values, and 300 ρ values.

6.5.2 Eigenfunction Corresponding to the Most Unstable Eigenvalue

Yet another interesting investigations is to examine the eigenfunctions corresponding to the most unstable perturbations. For $h = .5$ and $h = 1.5$, we calculate the sum of the eigenfunctions corresponding to the quadra-fold pairs of eigenvalues with the largest real part. Adding the appropriate eigenfunctions and normalizing the amplitude to one, we obtain the surfaces given in Figures 6.10 and 6.11.

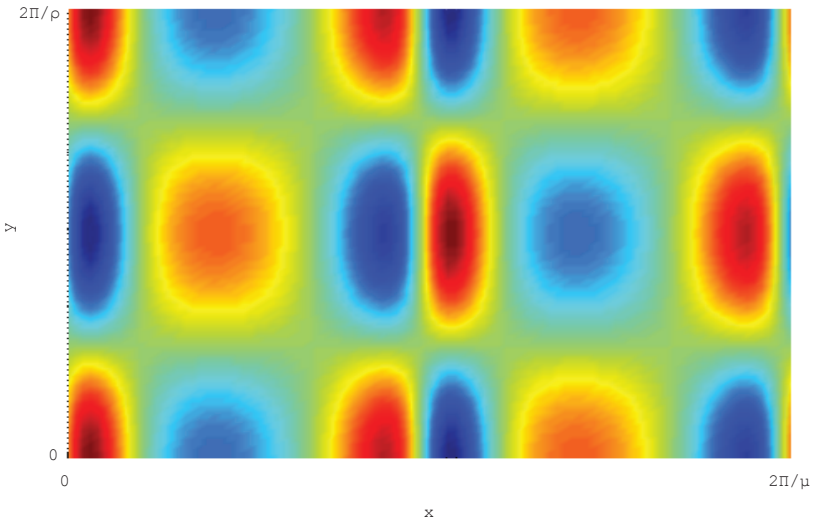

Figure 6.10: The combined eigenfunction corresponding to the most unstable eigenvalue and its complex conjugate pairs for $h = .5$ and $a = .1$.

As in the previous chapter, we recall that our original perturbation was of the form

$$\eta(x, y, t) = \eta_0(x) + \epsilon e^{\lambda t} e^{i\rho y} e^{i\mu x} \eta_1(x).$$

We again explicitly calculate the solution to the linear problem for multiple times t. The time steps are shown in Figures 6.12 and 6.13. Since the eigenvalues are unstable, the amplitude of the solutions should grow as demonstrated in each of the figures. Since we are using the linearization, we expect that these approximations are only valid for very small times. However, the initial transition of the instability can give useful insight into the short-term behavior of the solution.

6.6 Discussion of the Results

Throughout this chapter, we have presented the instabilities of two-dimensional traveling wave solutions to three-dimensional perturbations applied to the new AFM equations. By using the non-local formulation in combination with Hill's method, we have determined various spectra numerically with

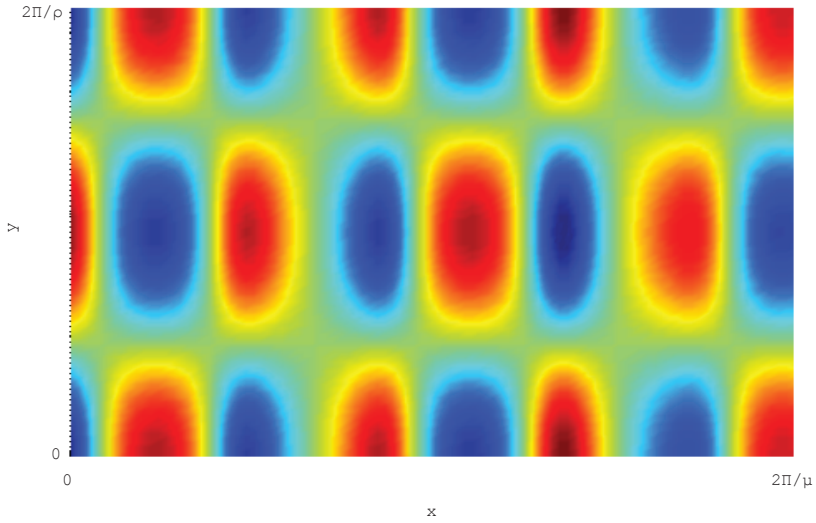

Figure 6.11: The combined eigenfunction corresponding to the most unstable eigenvalue and its complex conjugate pairs for $h = 1.5$ and $a = .1$.

high degree of accuracy. Additionally, as demonstrated in Figure 6.1, the error of the approximation of the most unstable eigenvalue converges rapidly as a function of the number of Fourier modes used in the truncation. In fact, in comparison to the method presented by Francius and Kharif, our method converges much faster. To quantify this, where they need 60 Fourier modes to obtain the eigenvalue with Cauchy error of order 10^{-8}, we only need 32 modes to obtain a Cauchy error of ϵ_{mach} (Data obtained from the appendix of [25], available online only).

We have obtained the same general results as those of Francius and Kharif for $h = .5$. However, we have noticed that our stability regions are smaller than those presented in [25]. For example, in the following figure we demonstrate the stability regions obtained in [25] along with our own stability regions calculated for $h = .5$ and $a = .160$. As shown in the Figure 6.14, the general shape is consistent, but our instability regions are much thinner[2]. To determine if this is a numerical artifact, we increased the number of Fourier modes in our calculation. However, we found that this was not the case, and the convergence rates near the maximum growth rate converged at a similar rate to that shown in Figure 6.1 for $h = .5$. We still have confidence in our method.

In general, we found that for small amplitude waves, the dominant instability was transverse (occured when $\rho \neq 0$) noting that the magnitude of the dominant three-dimensional instability was sometimes multiple orders of magnitude greater than the dominant two-dimensional instability. The same results were found by Bryant [10]. For $h = .5$, he found that for four-wave interactions, the

[2]It is important to note that since we incorporated the periodicity into our calculations of the spectrum, our results are essentially tiled versions of the results presented in [25]. This is akin to thinking of our instability regions in the (μ, ρ)-plane as being on a cylinder which is periodic in μ.

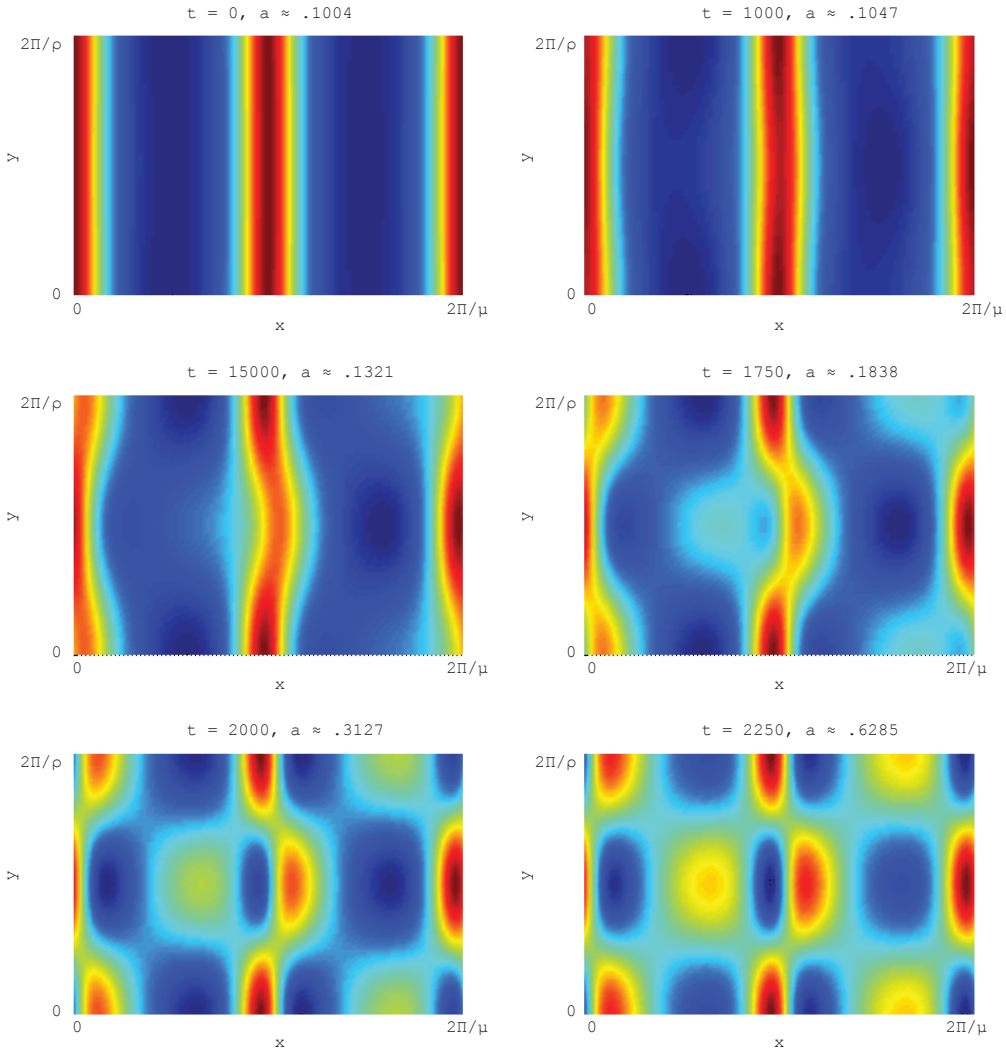

Figure 6.12: The solution to the linear problem for $h = .5$ and $a = .1$ corresponding to the most unstable perturbation.

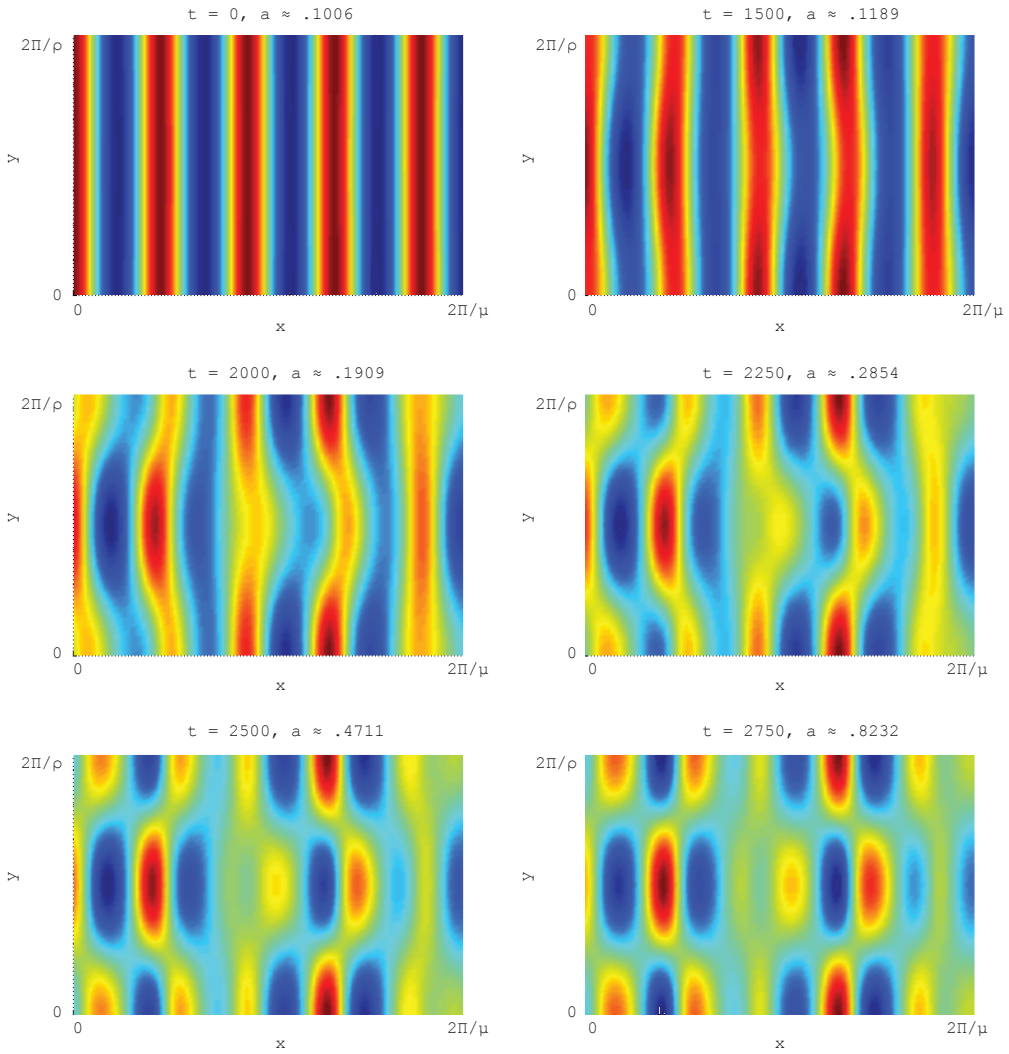

Figure 6.13: The solution to the linear problem when $h = 1.5$ and $a = .1$ corresponding to the most unstable perturbation.

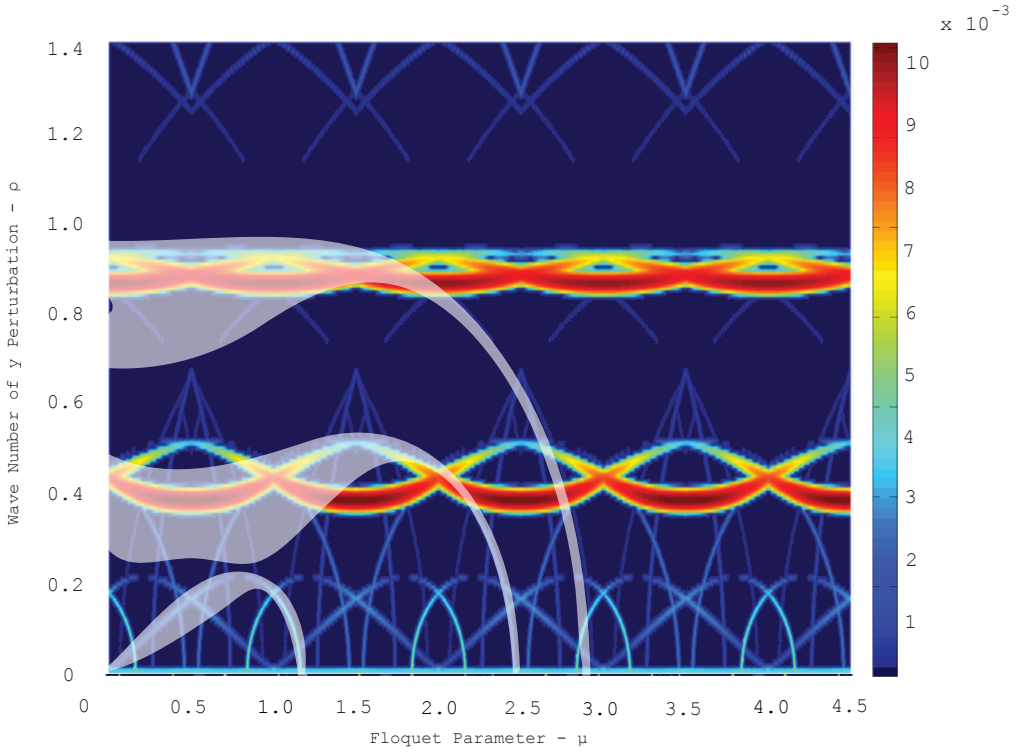

Figure 6.14: The solution to the linear problem when $h = 1.5$ and $a = .1$ corresponding to the most unstable perturbation.

dominant instability was fully three-dimensional. However, as the perturbations were time-evolved in his truncated equations, the two-dimensional instabilities dominated. As mentioned in Kharif and Francius, it would be interesting to explore the time evolution of a traveling wave perturbed with both of the dominant two- and three-dimensional instabilities to determine how each effected the long time dynamics. This would be an interesting avenue for future work since little is know about the time propagation of perturbations in shallow water in the fully nonlinear equations. Another interesting results is that for $h = .5$, the dominant instability corresponds to $\mu = 1/2$, which is also noted in [25]. This implies that the dominant instability is phase-locked with the original solution expanded over twice the original period.

Chapter 7

Conclusion

The main goal of this dissertation is to investigate the stability of traveling wave solutions using a periodic extension of the AFM formulation as given in [1]. There are several new contributions to the field of surface gravity waves obtained through this dissertation. First, we demonstrate the equivalence of a non-local formulation of the periodic water waves problem to the original set of Euler's equations. While it is obvious that solutions to the original formulation solve the AFM formulation, the opposite is not so clear. Our proof of the equivalence was a minor extension of the results obtained by Ablowitz and Haut [2] obtained for decaying solutions on the whole line. Without the statement of equivalence, we would not have been able justify the use of the AFM formulation to determine the stability of traveling wave solutions.

The next new contribution is a new single equation for the surface elevation in a traveling coordinate frame. To the best of our knowledge, all descriptions of surface gravity waves in physical variables are a system of coupled partial differential equations with two unknowns; the surface elevation and the velocity potential. Solving for the surface profile requires solving for an extra unknown. Using the non-local formulation for the periodic problem in a traveling coordinate frame, we reduce the traveling wave problem from a system of two equations for two unknowns (the surface elevation and the velocity potential at the surface) to a single equation for the surface elevation. This new equation for the surface elevation in finite depth is

$$\sum_{k\in\Lambda} e^{ikx} \int_0^L e^{-ikx} \Big(\sqrt{(1+\eta_x^2)(c^2-2g\eta)} sinh(k(\eta+h)) \Big) dx = 0.$$

Similarly, for infinite depth, the surface elevation satisfies

$$\sum_{k\in\Lambda} e^{ikx} \int_0^L e^{-ikx} e^{|k|\eta} \Big(\sqrt{(1+\eta_x^2)(c^2-2g\eta)} \Big) dx = 0.$$

The new traveling wave equation for the surface elevation is the basis of a numerical scheme we present to determine the surface elevation. Using a pseudo-continuation approach, we develop an iterative method to determine the traveling wave solutions based on a combination of the Poincaré-Lindstedt perturbation method and spectral renormalization. This numerical scheme is a useful iterative approach that we believe has important implications for future research when Newton's method fails. These cases include high-resolutions solutions, and extensions to the case of the two-dimensional surface (three-dimensional waves).

Finally, by applying a Fourier-Floquet decomposition to the non-local formulation, we present the full spectra for traveling wave solutions with respect to two- and three-dimensional perturbations. To the best of our knowledge, this is the first time that the full spectrum for Euler's equations have been presented. Previous results were limited to few wave interactions, or dominant eigenvalues. Our new contribution is that we have obtained a numerical approximation to the full spectra with respect to all bounded perturbations of our traveling wave solutions. We compare our dominant instabilities to those presented by Bryant, McLean, and Kharif and Francius [9, 10, 25, 42] where we have found that our results are more accurate and less computationally expensive. Our results are in general agreement with previously found results. However, with respect to transverse perturbations, our instability regions are much narrower than those defined in the previous literature. We believe that due to the demonstrated accuracy of our method, our results are more precise and detailed.

Bibliography

[1] M. J. Ablowitz, A. S. Fokas, and Z. H. Musslimani. On a new non-local formulation of water waves. *Journal of Fluid Mechanics*, 562:313–343, 2006.

[2] M. J. Ablowitz and T. S. Haut. Spectral formulation of the two fluid Euler equations with a free interface and long wave reduction. *Analysis and Applications*, 6:323–348, 2008.

[3] Mark J. Ablowitz and Ziad H. Musslimani. Spectral renormalization method for computing self-localized solutions to nonlinear systems. *Optics Letters*, 30:2140–2142, 2005.

[4] D. J. Acheson. *Elementary Fluid Dynamics*. Oxford University Press, Oxford, 1990.

[5] C. Amick and J. Toland. On solitary water-waves of finite amplitude. *Arch. Rational Mech. Anal.*, 76:9–95, 1981.

[6] T.B. Benjamin. Instability of periodic wave trains in nonlinear dispersive systems. *Proceedings, Royal Society of London, A*, 299:59–79, 1967.

[7] T.B. Benjamin and Feir J. E. The disintegration of wave trains on deep water. part i. theory. *Journal of Fluid Mechanics*, 27:417–430, 1967.

[8] T. H. Bridges and A. Mielke. A proof of the Benjamin-Feir instability. *Archive for Rational Mechanics and Analysis*, 133:145–198, 1995.

[9] P. J. Bryant. Stability of periodic waves in shallow water. *Journal of Fluid Mechanics*, 66:81–96, 1974.

[10] P. J. Bryant. Oblique instability of periodic waves in shallow water. *Journal of Fluid Mechanics*, 86:783–792, 1978.

[11] B. Buffoni, E.N. Dancer, and J.F. Toland. The regularity and local bifurcation of steady periodic water waves. *Arch. Rational Mech. Anal.*, 152:207–240, 2000.

[12] B. Buffoni, E.N. Dancer, and J.F. Toland. The sub-harmonic bifurcation of stokes waves. *Arch. Rational Mech. Anal.*, 152:241–271, 2000.

[13] B. Chen and P. G. Saffman. Numerical evidence for the existence of new types of gravity waves of permanent form on deep water. *Stud. Appl. Math.*, 62:1–21, 1980.

[14] T. Colin, F. Dias, and J. M. Ghidaglia. On rotational effects in the modulation of weakly nonlinear waves over finite depth. *European Journal of Mechanics B/Fluids*, 14:775–793, 1995.

[15] T. Colin, F. Dias, and J. M. Ghidaglia. On modulation of weakly nonlinear water waves. *Contemp. Math.*, 200:47–56, 1996.

[16] W. Craig, P. Guyenne, D. P. Nicholls, and C. Sulem. Hamiltonian long wave expansions for water waves over a rough bottom. *Proceedings, Royal Society of London, A*, 461:839–873, 2005.

[17] W. Craig and D. P. Nicholls. Traveling gravity water waves in two and three dimensions. *European Journal of Mechanics B/Fluids*, 21:615–641, 2002.

[18] W. Craig and C. Sulem. Numerical simulation of gravity waves. *Journal of Computational Physics*, 108:73–83, 1993.

[19] A. D. D. Craik. The origins of water wave theory. *Annual Review of Fluid Mechanics*, 36:1–28, 2004.

[20] C. W. Curtis and B. Deconinck. On the convergence of Hill's method. *Mathematics of Computation, To Appear.*

[21] L. Debnath. *Nonlinear Water Waves.* Academic Press, Boston, 1994.

[22] B. Deconinck and J. N. Kutz. Computing spectra of linear operators using Hill's method. *Journal of Computational Physics*, 219:296–321, 2006.

[23] F. Dias and C. Kharif. Nonlinear gravity and capillary-gravity waves. *Annual Review of Fluid Mechanics*, 32:301–346, 1999.

[24] Bernard Epstein. *Partial Differential Equations: An Introduction.* Krieger Pub Co, New York, 1975.

[25] M. Francius and C. Kharif. Three-dimensional instabilities of periodic gravity waves in shallow water. *Journal of Fluid Mechanics*, 561:417–437, 2006.

[26] R. Grimshaw. *Nonlinear Waves in Fluids: Recent Advances and Modern Applications.* Springer, Wein, 2005.

[27] K. L. Henderson, D. H. Peregrine, and H. W. Dold. Unsteady water wave modulations: fully nonlinear solutions and comparisons with the nonlinear Schrödinger equation. *Wave Motion*, 29:341–361, 1999.

[28] J. C. R. Hunt. Nonlinear wave theory and the contributions of T. Brooke Benjamin (1929 - 1995). *Annual Review of Fluid Mechanics*, 38:1–25, 2006.

[29] M. Ioualalen, C. Kharif, and A. J. Roberts. Stability regimes of finite depth short-crested water waves. *Journal of Physical Oceanography*, 29:2318–2331, 1999.

[30] R. S. Johnson. *Modern Introduction to the Mathematical Theory of Water Waves*. Cambridge University Press, Cambridge, 2001.

[31] C. Kharif and A. Ramamonjiarisoa. On the stability of gravity waves on deep water. *Journal of Fluid Mechanics*, 218:163–170, 1990.

[32] P. K. Kundu and I. M. Cohen. *Fluid Mechanics*. Academic Press, San Diego, 2002.

[33] T. Levi-Civita. Determination rigoureuse des ondes permanentes dampleur finie. *Math. Ann.*, 93:264–314, 1925.

[34] M. S. Longuet-Higgins. On the nonlinear transfer of energy in the peak gravity-wave spectrum: a simplified model. *Proceedings, Royal Society of London, A*, 347:311–328, 1976.

[35] M. S. Longuet-Higgins. The instabilities of gravity waves of finite amplitued in deep water I. superharmonics. *Proceedings, Royal Society of London, A*, 360:471–488, 1978.

[36] M. S. Longuet-Higgins. The instabilities of gravity waves of finite amplitued in deep water II. subharmonics. *Proceedings, Royal Society of London, A*, 360:489–505, 1978.

[37] M. S. Longuet-Higgins. On the stability of steep gravity waves. *Proceedings, Royal Society of London, A*, 396:269–280, 1984.

[38] M. S. Longuet-Higgins. Bifurcation and instability in gravity waves. *Proceedings, Royal Society of London, A*, 403:167–187, 1986.

[39] M. S. Longuet-Higgins and D. G. Dommermuth. Crest instabilities of gravity waves. part 3. nonlinear development and breaking. *Journal of Fluid Mechanics*, 336:33–50, 1997.

[40] M. S. Longuet-Higgins and M. Tanaka. On the crest instability of steep surface waves. *Journal of Fluid Mechanics*, 336:51–68, 1997.

[41] R. S. MacKay and P.G. Saffman. Stability of water waves. *Proceedings, Royal Society of London, A*, 406:115–125, 1986.

[42] J. W. McLean. Instabilities of finite-amplitude gravity waves on water of finite depth. *Journal of Fluid Mechanics*, 114:331–341, 1982.

[43] R. Miche. Mouvements ondulatoires de la mer en profondeur constante ou décroissante. *Annales des Ponts et Chausses*, 114:25–78, 131–164, 270–292, 369–406, 1944.

[44] A. I. Nekrasov. On steady waves. *Izv. Ivanovo-Voznesensk. Politekhn. In-ta*, 3, 1921.

[45] D. P. Nicholls. *Traveling Gravity Water Waves in Two and Three Dimensions*. PhD thesis, Brown University, May 1998.

[46] D. P. Nicholls. Spectral stability of traveling water waves: Analytic dependence of the spectrum. *Journal of Nonlinear Science*, 17:369–397, 2007.

[47] D. P. Nicholls. Spectral data for travelling water waves: singularities and stability. *Journal of Fluid Mechanics*, 625:339–360, 2009.

[48] H. Okamoto and M. Shoji. *The Mathematical Theory of Permanent Progressive Water-Waves*. World Scientific Publishing Co. Pte. Ltd., Singapore, 2001.

[49] M. Onorato, A. R. Osborne, M. Serio, and S. Bertone. Freak waves in random oceanic sea states. *Physical Review Letters*, 86:5831–5834, 2001.

[50] C. E. Pearson. *Numerical Methods in Engineering and Science*. Van Nostrand Reinhold Compan Inc., New York, 1986.

[51] D. E. Pelinovsky and Y. A. Stepanyant. Convergence of Petviashvili's iteration method for numerical approximations of stationary solutions of nonlinear wave equations. *SIAM Journal on Numerical Analysis*, 42:1110–1127, 2004.

[52] Lawrence Perko. *Differential Equations and Dynamical Systems*. Springer-Verlag, New York, 1975.

[53] V. I. Petviashvili. Equation of an extraordinary soliton. *Fizika Plazmy*, 2:469–472, 1976.

[54] Shen S. S. *A course on Nonlinear Waves*. Springer, Dordrecht, 1993.

[55] J. J. Stoker. *Water Waves: The Mathematical Theory with Applications*. Wiley-Interscience, New York, 1992.

[56] G. G. Stokes. On the theory of oscillatory waves. *Trans. Camb. Phil. Soc*, 8:441–455, 1847.

[57] D. Struik. Determination rigoureuse des ondes irrotationnelles periodiques dans un canal 'a profondeur finie. *Math. Ann.*, 95:595–634, 1926.

[58] M. Tanaka. The stability of steep gravity waves. *Journal of the physical society of Japan*, 52:3047–3055, 1983.

[59] F. Verhulst. *Methods and Applications of Singular Perturbations: Boundary Layers and Multiple Timescale Dynamics*. Springer, New York, 2005.

[60] D. Viswanath. The Lindstedt-Poincaré technique as an algorithm for computing periodic orbits. *SIAM Review*, 43:497–495, 2001.

[61] G. B. Whitham. Non-linear dispersion of water waves. *Journal of Fluid Mechanics*, 27:399–412, 1967.

[62] G. B. Whitham. *Linear and Nonlinear Waves*. Wiley-Interscience, New York, 1974.

[63] J. M. Williams. Limiting gravity waves in water of finite depth. *Philosophical Transactions, Royal Society of London, A*, 302:139–188, 1981.

[64] J. Yang and T. I. Lakoba. Universally-convergent squared-operator iteration methods for solitary waves in general nonlinear wave equations. *Stud. Appl. Math.*, 118:153–197, 2007.

[65] H. C. Yuen and B. M. Lake. Instabilities of waves in deep water. *Annual Review of Fluid Mechanics*, 12:303–334, 1980.

[66] V. E. Zakharov. Stability of periodic waves of finite amplitude on the surface of a deep fluid. *J. Appl. Mech. Tech. Phys.*, 9:190–194, 1968.

APPENDIX A

Poincaré-Lindstedt Numerical Method

As mentioned in Chapter 4, the Poincaré-Lindstedt method applied to Euler's equations was not as robust as Newton's method. However, we were able to successfully follow a bifurcation branch for solutions in parameter space. In this appendix, we illustrate the Poincaré-Lindstedt method for the traveling wave equation in detail and present some results.

A.1 Problem Formulation

Recall from earlier that traveling wave solutions to Euler's equations belong to a two parameter family of solutions for three physical parameters; amplitude, wave length, and wave speed. When using the Poincaré-Lindstedt numerical method, we fix the amplitude and wave speed of the solution in order to determine the corresponding wave length. This is acheived by normalizing the spatial scale so that the periodic solutions is periodic with period 2π by rescaling x.

We begin with the spectral traveling wave equation for a periodic wave of arbitrary wave length given in (3.7), and rescale x such that $x \to \omega x$ and $2\pi = \omega L$. Substituting this rescaled variable into the spectral non-local equation, we have

$$\int_0^{2\pi} e^{-inx}\sqrt{(1+\omega^2\eta_x^2)\,(c^2-2g\eta)}\sinh\left(\omega n(\eta+h)\right)dx = 0, \quad n \in \mathbb{Z}-\{0\},$$

where we have used the relationship between k and ω given by

$$k = \frac{2n\pi}{L} = \frac{2n\pi}{2\pi/\omega} = n\omega.$$

As described earlier, we perturb both ω and the surface elevation η to set up our iterative scheme by considering approximate solutions ω_0 and η_0, and their first order corrections ω_1 and η_1

respectively. In other words, we let $\eta = \eta_0 + \epsilon\eta_1 + \mathcal{O}(\epsilon^2)$ and $\omega = \omega_0 + \epsilon\omega_1 + \mathcal{O}(\epsilon^2)$. Substituting these expansions into the above equation and keeping terms to order ϵ results in the linear equation for the correction terms (ω_1,η_1):

$$\begin{aligned}\Big(\omega_0 n\mathcal{C}_n f(\eta_0,\omega_0) - \frac{\mathcal{S}_n}{f(\eta_0,\omega_0)} g(1+\omega_0^2\eta_{0,x}^2) + \frac{\mathcal{S}_n\omega_0^2\eta_{0,x}}{f(\eta_0,\omega_0)}(c^2-2g\eta_0)\partial_x\Big)\eta_1 \\ = -f(\eta_0,\omega_0)\mathcal{S}_n - \Big(f(\eta_0,\omega_0)n\omega_0\mathcal{C}_n - \tfrac{\mathcal{S}_n}{f(\eta_0,\omega_0)}(c^2-2g\eta_0)\omega_0\eta_{0,x}^2\Big)\omega_1\end{aligned}$$

where

$$\begin{aligned} f(\eta_0,\omega_0) &= \sqrt{(c^2-2g\eta_0)(1+\omega_0^2\eta_{0,x}^2)}, \\ \mathcal{S}_n &= \sinh(\omega_0 n(\eta_0+h)), \text{ and} \\ \mathcal{C}_n &= \cosh(\omega_0 n(\eta_0+h)). \end{aligned}$$

For simplicity, we have set $\epsilon = 1$. We represent both η_0 and η_1 by their Fourier series representation, where $\eta_1 = \sum_{n=-\infty}^{\infty} e^{inx}\hat{\eta}_{1,n}$. Furthermore, we rewrite the equations as the infinite dimensional linear system for the Fourier coefficients of η_1 in the following form:

$$\hat{A}(\omega_0,\eta_0)\hat{\mathbf{N}} = \hat{B}(\omega_0,\eta_0) + \omega_1\hat{C}(\omega_0,\eta_0),$$

where

$$\hat{A}_{m,n} = \int_0^{2\pi} e^{-i(m-n)x} Big(\omega_0 n\mathcal{C}_n f(\eta_0,\omega_0) - \frac{\mathcal{S}_n}{f(\eta_0,\omega_0)} g(1+\omega_0^2\eta_{0,x}^2) + \frac{\mathcal{S}_n\omega_0^2\eta_{0,x}}{f(\eta_0,\omega_0)}(c^2-2g\eta_0)\partial_x\Big)dx,$$

and

$$\begin{aligned} \hat{B}_m &= \int_0^{2\pi} e^{-imx} f(\omega_0,\eta_0)\mathcal{S}_n dx, \\ \hat{C}_m &= \int_0^{2\pi} e^{-imx}\Big(f(\eta_0,\omega_0)n\omega_0\mathcal{C}_n - \frac{\mathcal{S}_n}{f(\eta_0,\omega_0)}(c^2-2g\eta_0)\omega_0\eta_{0,x}^2\Big)dx. \end{aligned}$$

We truncate the bi-infinite linear system for the unknown Fourier coefficients $\hat{\mathbf{N}}$ so that we solve for N Fourier coefficients ($2N+1$ unknowns). As described in Chapter 4, we only obtain $2N$ equations from the non-local spectral equation. Without loss of generality, we can assume that our solutions (and their corrections) maintain zero average, and thus the zeroth Fourier mode is zero. This reduces the number of unknowns to $2N$ and allows us to achieve the solution for η_1 by rewriting the Fourier coefficients $\hat{\mathbf{N}}$ as the sum two parts: $\hat{\mathbf{N}} = \hat{\mathbf{N}}_1 + \omega_1\hat{\mathbf{N}}_2$. Decomposing the solution in this manner, we can solve for $\hat{\mathbf{N}}_1$ and $\hat{\mathbf{N}}_2$ by considering the equation

$$\hat{A}(\omega_0,\eta_0)\Big(\hat{\mathbf{N}}_1 + \omega_1\hat{\mathbf{N}}_2\Big) = \hat{B}(\omega_0,\eta_0) + \omega_1\hat{C}(\omega_0,\eta_0),$$

when $\omega_1 = 0$ and $\omega_1 = 1$. This gives us the following two vector equations for the two unknown vectors $\hat{\mathbf{N}}_1$ and $\hat{\mathbf{N}}_2$

$$\hat{\mathbf{N}}_1 = \hat{A}^{-1}\hat{B}, \text{ and } \hat{\mathbf{N}}_2 = \hat{A}^{-1}\Big(\hat{B}+\hat{C}\Big) - \hat{\mathbf{N}}_1.$$

However, we still need to determine the correction to the period. We solve for ω_1 by requiring that the new updated solution is perpendicular to the residual of the uncorrected solution. In other words, $\langle \eta_{1,1}(x) + \omega_1 \eta_{1,2}, \mathcal{N}(\eta_0) \rangle = 0$ where $\eta_{1,j}$ corresponds to the solution obtained from the Fourier coefficients in $\hat{\mathbf{N}}_j$ for $j = 1, 2$. Once we determine ω_1 from this constraint, we obtain the correction for the solution and repeat this process until the two-norm of the correction converges to ϵ_{tol}. In other words, the corrections to our solution become negligible.

To determine the wave length of the solution as a function of amplitude, we renormalize the solution at each iteration so that the infinity-norm of the solution is a desired amplitude 'a'. This allows us to follow a branch in parameter space by increasing the amplitude of the solution while determining the corresponding wave length for any fixed wave length c.

A.2 Numerical Implementation

To begin the implementation of this numerical scheme, we must begin with an initial guess η_0 and ω_0 to determine corrections η_1 and ω_1. As discussed in Chapter 3, the bifurcation of non-trivial solutions begins where the null-space of the linearization about the trivial solution is non-zero. Thus, if we choose an initial c, we know that the appropriate wave numbers are given by

$$c^2 k - g \tanh kh = 0. \tag{A.1}$$

Using a nonlinear solver, we can determine the wave number k corresponding to a fixed c value. Since the wave length is related to the wave number by the relationship $L = \frac{2\pi}{k}$, and $L = \frac{2\pi}{\omega}$, ω is identically k. For our initial guess, we choose

$$\omega_0 = k \qquad \eta_0 = \epsilon cos(x)$$

where k satisfies (A.1) for the selected wave speed c. Since we start with a small amplitude solution, our goal is to continue up the bifurcation branch to determine larger amplitude solutions. We follow the same procedure outline in Chapter 4, however, we outline it here again for completeness.

- For a given wave speed c, start with a small amplitude initial guess η_0 and an appropriate corresponding initial speed ω_0 where

$$\eta_0 = a_1 \cos(x), \qquad c^2 k - g \tanh kh = 0 \qquad a_1 << 1.$$

- Use the Poincaré-Lindstedt method outline in the previous section to determine the solution with the given amplitude a_1 and corresponding wave length $2\pi/\omega$. This determines a new small amplitude solution set $(\eta, 2\pi/\omega)$ with amplitude a_1.

- Proceed to calculate higher amplitude solutions by rescaling η_1 to a new amplitude a_2 slightly larger than a_1. Estimate a new initial guess for ω based on the previously solved for value of ω. The rescaled surface elevation and estimated wave length will serve as the new initial guess.

- Solve the nonlinear equations numerically again to determine a new solution set (η, ω) with amplitude a_2.

- Repeat this process, increasing the amplitude each time until the critical wave height is reached.

The general process is identical to the method outlined in Chapter 4 except the nonlinear solver is replaced by the Poincaré-Lindstedt method.

A.3 Numerical Convergence and Stability

As discussed for the general method in Chapter 4, before we present results, we briefly discuss convergence and stability of the Poincaré-Lindstedt algorithm. We ask the same questions as with the Newton's method solver: *given the current numerical scheme, can we can demonstrate that as we increase the number of Fourier modes used to approximate the surface elevation, the Fourier coefficients of each successive approximation converge towards the same solution.*

Figure A.1 and Table A.1 give the Cauchy error (as defined in Chapter 4) for the surface elevation $\eta(x)$ and the frequency ω as a function of the truncation size. As the truncation size N increases, the norm of the correction decreases linearly on a logarithmic scale. Additionally, we calculated the residual error to confirm that our method was converging point wise to an actual solution of the problem (see Table A.2 for residual error data). As with our implementation in Chapter 4, this is a strong indicator of the stability and accuracy of the Poincaré-Lindstedt method applied to our spectral traveling wave equation.

Table A.1: The Cauchy error corresponding to the solution obtained using the Poincaré-Lindstedt method when $h = .5$, $c \approx .67980$ and $a \approx .04621$.

N	$\|\|\eta_N - \eta_{N-1}\|\|_2$	$\|\|\omega_N - \omega_{N-1}\|\|_2$	N	$\|\|\eta_N - \eta_{N-1}\|\|_2$	$\|\|\omega_N - \omega_{N-1}\|\|_2$
9	6.43e-07	5.66e-07	21	1.27e-13	3.50e-13
10	1.57e-07	1.36e-07	22	9.84e-14	6.12e-13
11	3.94e-08	3.42e-08	23	1.58e-13	1.19e-12
12	1.02e-08	8.86e-09	24	1.44e-13	1.07e-12
13	2.72e-09	2.36e-09	25	1.59e-14	4.37e-14
14	7.39e-10	6.43e-10	26	2.75e-14	8.48e-14
15	2.06e-10	1.79e-10	27	6.04e-14	8.37e-14
16	5.84e-11	5.01e-11	28	7.07e-14	2.29e-14
17	1.68e-11	1.36e-11	29	8.80e-15	1.35e-14
18	4.96e-12	4.81e-12	30	2.37e-14	1.91e-13
19	1.49e-12	1.53e-12	31	2.85e-14	1.99e-13
20	4.39e-13	2.10e-13	32	1.53e-14	1.24e-13

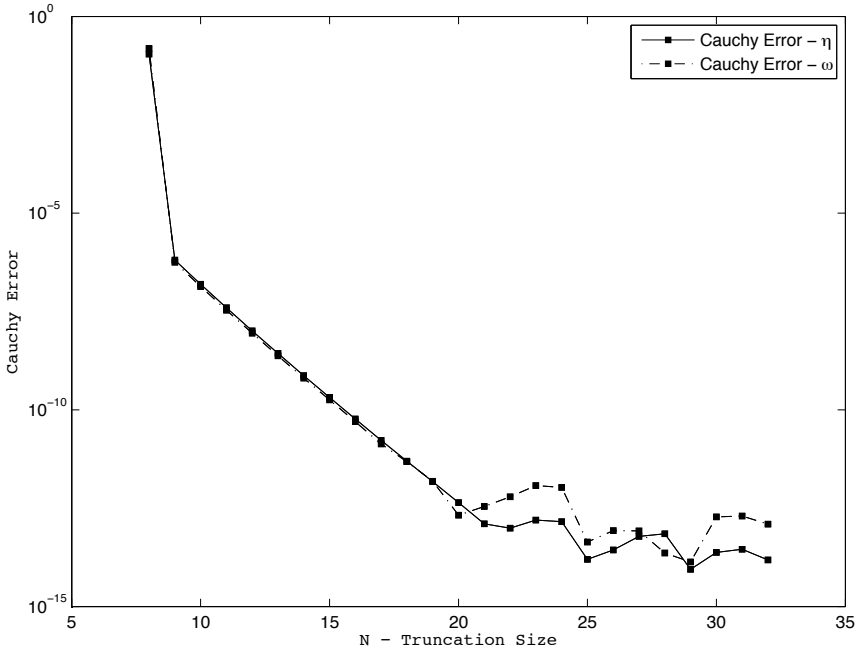

Figure A.1: Cauchy error of the solution η and parameter ω for $h = .5$, $c \approx .67980$ and $a \approx .04621$. The error tolarence for the iteration method was set at $\epsilon_{tol} = 10^{-15}$.

Table A.2: The Cauchy error corresponding to the solution obtained using the Poincaré-Lindstedt method when $h = .5$, $c \approx .67980$ and $a \approx .04621$.

N	e_N	N	e_N	N	e_N	N	e_N	N	e_N
8	1.29e-11	13	1.09e-15	18	7.84e-15	23	8.50e-15	28	1.08e-15
9	7.78e-13	14	2.14e-15	19	1.20e-15	24	2.15e-15	29	6.68e-16
10	4.94e-14	15	2.25e-15	20	1.70e-16	25	2.46e-16	30	4.14e-15
11	7.07e-15	16	1.90e-16	21	3.70e-15	26	9.21e-16	31	9.19e-16
12	2.79e-16	17	7.91e-15	22	1.12e-15	27	1.18e-14	32	3.00e-16

A.3.1 Numerical Results

Solutions were calculated for using the Poincaré-Lindstedt numerical scheme. We include on example of our periodic solutions at depth $h = .5$. Additionally, we show the bifurcation curve in parameter space and an indicator of where the displayed solutions lie on the curve.

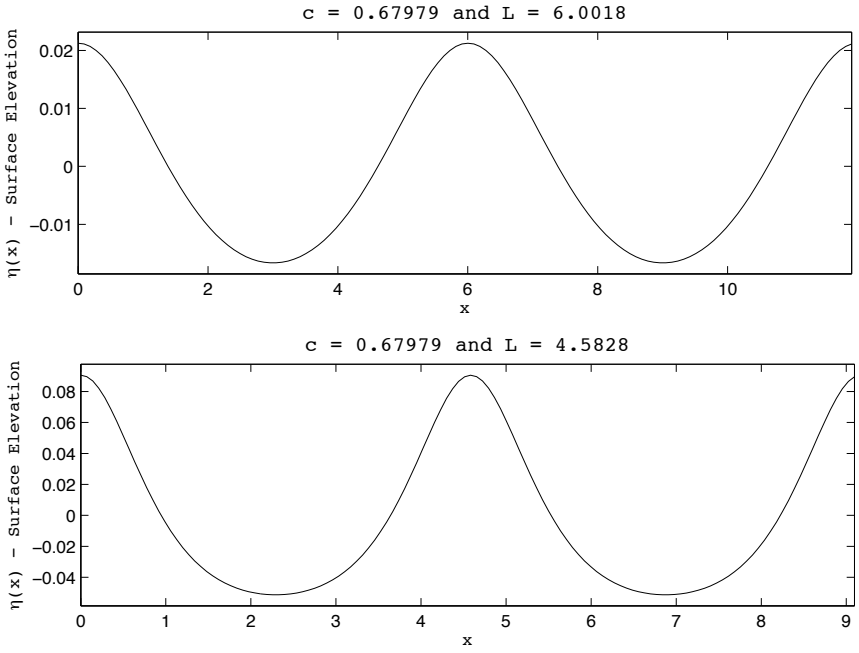

Figure A.2: Solutions for $h = .5$ with amplitudes $a \approx .021257$ (top) and $a \approx .0905750$ (bottom). Both solutions are calculated with $N = 64$ Fourier modes. The residual error for both approximations was less than 10^{-14}. Corresponding periods and norms are marked on the bifurcation curve shown in Figure A.3

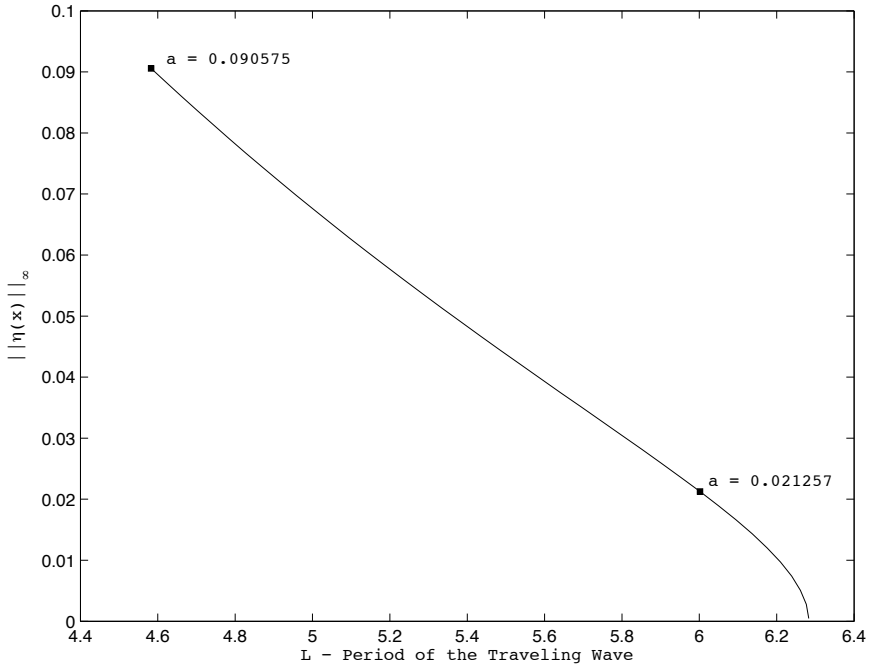

Figure A.3: Bifurcation of amplitude vs. period of the solution for $h = .5$.